The Philosophical Magazine

UNIVERSITY OF HAWAII
LIBRARY
OCT 25 '61

FIRST PUBLISHED IN 1798

A Journal of Theoretical Experimental and Applied Physics

Vol. 6 February 1961 No. 62
Eighth Series

25s. 0d., plus postage
Annual Subscription £13 10s. 0d., payable in advance

ALERE FLAMMAM

Printed and Published by
TAYLOR & FRANCIS LTD
RED LION COURT, FLEET STREET, LONDON, E.C.4

THE PHILOSOPHICAL MAGAZINE

Editor

Professor N. F. Mott, M.A., D.Sc., F.R.S.

Editorial Board

Sir Lawrence Bragg, O.B.E., M.C., M.A., D.Sc., F.R.S.
Sir George Thomson, M.A., D.Sc., F.R.S.
Professor A. M. Tyndall, C.B.E., D.Sc., F.R.S.

Authors wishing to submit papers for publication in the Journal should send manuscripts directly to the Publishers.

Manuscripts should be typed in *double* spacing on one side of quarto (8 × 10 in.) paper, and authors are urged to aim at absolute clarity of meaning and an attractive presentation of their texts.

References should be listed at the end in alphabetical order of authors and should be cited in the text in terms of author's name and date. Diagrams should normally be in Indian ink on white card, with lettering in soft pencil, the captions being typed on a separate sheet.

A leaflet giving detailed instructions to authors on the preparation of papers is available on request from the Publishers.

Authors are entitled to receive 25 offprints of a paper in the Journal free of charge, and additional offprints can be obtained from the Publishers.

The *Philosophical Magazine* and its companion journal, *Advances in Physics*, will accept papers for publication in experimental and theoretical physics. The *Philosophical Magazine* publishes contributions describing new results, letters to the editor and book reviews. *Advances in Physics* publishes articles surveying the present state of knowledge in any branch of the science in which recent progress has been made. The editors welcome contributions from overseas as well as from the United Kingdom, and papers may be published in English, French and German.

Thermally-activated Glide in Magnesium Crystals from 4·2° to 420°K†

By H. Conrad‡, R. Armstrong, H. Wiedersich and G. Schoeck
Westinghouse Research Laboratories, Pittsburgh 35, Pennsylvania

[Received June 21, 1960; and in revised form October 10, 1960]

Abstract

The effect of changes in strain rate and temperature on the flow stress of Mg single crystals was determined in the range of 4·2° to 420°K. The present data, along with those obtained previously, indicate that the intersection of dislocations is the controlling mechanism. Cottrell's original model must, however, be modified to include an effect of stress on the activation volume. This effect appears to be due primarily to the fact that the force between two intersecting dislocations varies with their distance of separation rather than a change in the effective forest spacing.

§ 1. Introduction

The deformation of metal crystals is in many cases governed by thermally-activated dislocation mechanisms. If a single activation process controls the deformation, the strain rate $\dot{\gamma}$ is given by

$$\dot{\gamma}=\nu \exp(-G/kT) \qquad \ldots\ldots\ldots \quad (1)$$

where ν is a frequency factor which includes essentially the frequency of vibration, the number of places where the activation can take place, and the strain per successful fluctuation. $G=H-TS$ is the Gibbs free energy of activation where H is the enthalpy of activation (commonly termed the 'activation energy') and S is the entropy of activation. Conrad and Wiedersich (1960) have shown that the value of H can be obtained from flow stress data by the following equation:

$$H=-kT^2\left[\frac{\left(\dfrac{\partial\tau}{\partial T}\right)_{\dot{\gamma}}-\dfrac{\tau_\mu}{\mu}\dfrac{d\mu}{dT}}{\left(\dfrac{\partial\tau}{\partial\ln\dot{\gamma}/\nu}\right)_T}\right]=-kT^2\left[\frac{\left(\dfrac{\partial\tau^*}{\partial T}\right)_{\dot{\gamma}}}{\left(\dfrac{\partial\tau}{\partial\ln\dot{\gamma}/\nu}\right)_T}\right] \qquad \ldots \quad (2)$$

where τ is the applied shear stress and τ_μ is the long-range internal stress which is proportional to the shear modulus μ. $\tau^*=\tau-\tau_\mu$ is the excess of the applied stress over the internal stress. It is called the effective stress or thermal component of the flow stress.

Two mechanisms have been proposed which control the movement of dislocations in their glide plane in metal crystals with a close-packed structure (c.p.h. and f.c.c.): (*a*) the mutual intersection of dislocations (Cottrell 1952, Nabarro 1952, Seeger 1954) and (*b*) the overcoming of the Peierls stress (Conrad 1958, Lytton *et al.* 1958, Weertman 1958). One major difference between these two mechanisms is the effect of stress on the activation energy H. For the intersection mechanism Cottrell (1952) and Seeger (1954) have suggested that the activation energy is decreased linearly by the effective stress, i.e.

---

† Communicated by the Authors.
‡ Now at Atomics International, P.O. Box 309, Canoga Park, California.

$$H=H_0-v_0\tau^* \quad . \quad . \quad . \quad . \quad . \quad . \quad . \quad . \quad . \quad (3)$$

where v_0 is termed the 'activation volume'. $v_0=d_0l_0\mathbf{b}$ where d_0 is the intersecting width (approximately twice the width of the gliding dislocation); l_0 is the average spacing between the dislocations threading the glide plane (termed the 'forest'); and $\mathbf{b}$ is the Burgers vector. Modifications of eqn. (3) have been proposed which consider that the activation volume is itself a function of stress (Friedel 1956, Basinski 1959) and temperature (Thornton and Hirsch 1958). For the Peierls mechanism Seeger (1956) has calculated the activation energy to be

$$H=H_{\mathrm{K}}\left(1+\tfrac{1}{4}\log\frac{16\tau_p{}^{\circ}}{\pi\tau^*}\right) \quad . \quad . \quad . \quad . \quad . \quad . \quad . \quad (4)$$

for the limit $\tau^*\ll\tau_p{}^{\circ}$. H_{K} is the energy of a kink and $\tau_p{}^{\circ}$ is the value of the Peierls stress at 0°K.

For the deformation of f.c.c. metal crystals in Stages II and III (multiple glide) there is now considerable evidence to support the intersection of dislocations as the rate-controlling mechanism at low temperatures (Friedel 1956, Seeger 1957, Thornton and Hirsch 1958, Basinski 1959). For Stage I deformation of f.c.c. crystals or the deformation of c.p.h. crystals (single glide or so-called easy-glide), the determination of the rate-controlling mechanism has been somewhat more elusive. The major problem has been that the experimentally determined flow parameter $B=(\partial\ln\dot{\gamma}/\partial\tau)_T$ is independent of temperature (Conrad and Robertson 1957, 1958, Conrad 1958) rather than proportional to the reciprocal of the temperature as required for the intersection mechanism when eqn. (3) describes the activation energy. More recent work on Mg crystals by Conrad *et al.* (1960) has, however, indicated that this apparent discrepancy is probably a reflection of the fact that the activation volume is itself a function of the stress and that in order to obtain a constant strain rate the stress must increase with decrease in temperature.

Since this latter investigation (Conrad *et al.* 1960) was limited in the temperature range covered (78° to 364°K) and in the number of temperatures considered (four), it appeared that additional work over a larger temperature range should be conducted to positively identify the controlling mechanism during single-glide (easy-glide). Consequently, in the present investigation the deformation behaviour of Mg single crystals was investigated in considerable detail over the range of 4·2° to 420°K. Of special interest was the determination of the effect of temperature on the flow parameters

τ^* and B. From such measurements the effect of temperature and stress on the activation energy H and the activation volume v was determined.

§ 2. EXPERIMENTAL PROCEDURE

The Mg crystals employed in the present study were approximately 1 cm diameter and 15 cm long. They were grown from the melt in a graphite mould under a static atmosphere of He from redistilled Mg of $< 0{\cdot}02\%$ impurities. Their orientations were determined by the Laue back-reflection technique and are given in the table. Previous to testing, they were immersed in 25% by volume HCl to remove a surface layer about 0·1 cm thick, and then chemically polished in 20% by volume nitric acid. Following polishing, the specimens were rinsed successively in tap water, distilled water, and acetone, and then allowed to dry in air.

Initial orientation and critical resolved shear stress τ_0 of Mg crystals

Crystal	χ_0 (1)	λ_0 (2)	T°K	$\dot{\gamma}$ (3) $\text{min}^{-1} \times 10^2$	τ_0 g/mm^2
2	28	40	377	1·35	39
6	23	34	78	1·44	109
12	43	51	85	1·15	68
15	50	50	78	1·14	70
16	29	38	300	1·70	47
21	18	32	4·2	2·50	134

(1) χ_0 = Angle between specimen axis and basal plane.
(2) λ_0 = Angle between specimen axis and $\langle 100 \rangle$.
(3) $\dot{\gamma}$ = Resolved shear strain rate.

The experimental parameters of eqn. (2) must be obtained for a constant structure. This was accomplished by employing so-called differential tests, i.e. tests where the strain-rate or temperature are changed during the deformation. Two testing machines were employed: an Instron Model TT-B and a special screw machine built by Arcweld Mfg. Co.†. In general, the Instron machine was used for tests above 78°K while the Arcweld machine was employed for tests between 78° and 4·2°K. Several tests were also conducted on the latter machine in the range above 78°K to obtain an overlap of data. Only the Arcweld machine was employed for tests below 78°K because of the larger space between cross-heads, which permitted the insertion of the helium cryostat.

A 1000 lb SR-4 load cell connected to the X-axis of an Instron X–Y recorder was employed to measure the load in both machines. This gave a stress accuracy of approximately 2%. The cross-head movement was measured by a clip gauge employing SR–4 resistance wire gauges connected to the Y-axis of the recorder, giving a resolved shear strain sensitivity of approximately 5×10^{-5}. The strain rate in both machines could be rapidly changed by factors up to 1 : 2000 over the range of resolved shear strain rate of $10^{-4}\,\text{min}^{-1}$ to $10\,\text{min}^{-1}$.

---

† Arcweld Manufacturing Co., Grove City, Pa.

Temperatures between room temperature and 78°K were obtained by the method described previously (Conrad 1958), which employs a nitrogen vapour spray on the specimen as the refrigerant. To obtain temperatures above room temperature, resistance heating elements were installed in the low-temperature container. In all cases the temperature was measured and controlled by a previously calibrated copper–constantan couple attached to the specimen and connected to a L and N Speedomax Type G recorder-controller with a D.A.T. anticipatory control. The temperature was controlled within ± 1°K over the length of the specimen from 78° to 420°K.

Fig. 1

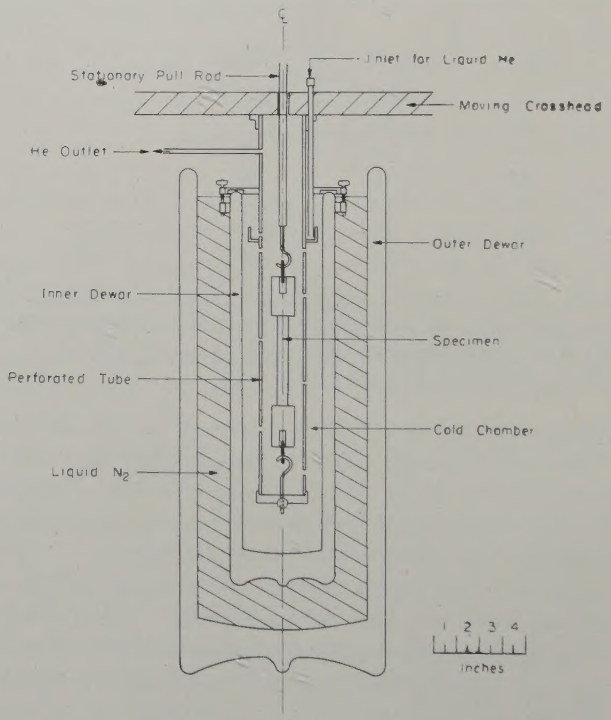

Schematic of helium cryostat.

Temperatures between 78° and 4·2°K were obtained by the cryostat shown in fig. 1. A temperature of 4·2°K was obtained by filling the inner chamber with liquid He, while temperatures between 78° and 4·2°K were obtained by controlling the flow of He into the cryostat from a large He dewar in the manner described by Wessel (1956). By this method the temperature was maintained constant to within ± 1°K.

To make a temperature change, the specimen was always unloaded to about 50% of the flow stress, to prevent creep from occurring during the change. A decrease in temperature generally required about 2 min, while an increase required about 5–10 min. In all cases, the test was continued only after the temperature, indicated by the couple attached to the specimen, had remained constant for at least 5 min. An indication that thermal equilibrium had been established was also provided by the fact that no further change in dimensions associated with thermal contractions or expansions was observed.

The stresses and strains reported in the present paper are all resolved shear stresses and resolved shear strains.

§ 3. Experimental Results

Figures 2 and 3 show typical stress–strain curves with temperature and strain-rate changes. No marked transients such as those reported by Conrad (1958) and Basinski (1959) for f.c.c. metals were observed following the changes in temperature and strain rate.

Fig. 2

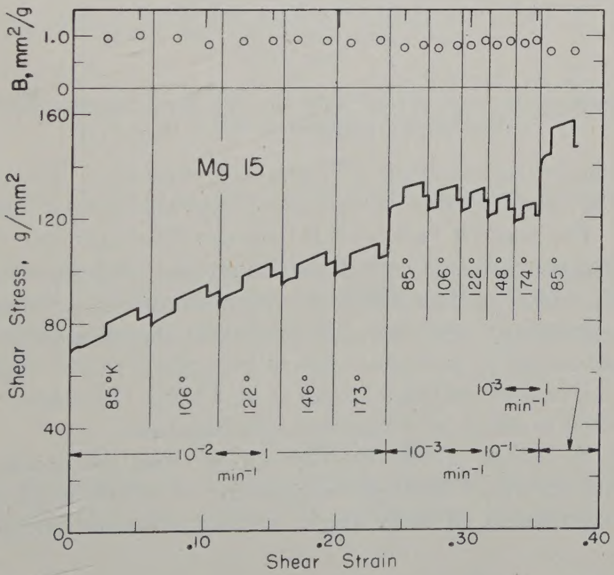

Effect of temperature and strain rate on the flow stress. Also shown are values of the parameter $B=(\partial \ln \dot{\gamma}/\partial \tau)_T$.

Also given in figs. 2 and 3 are values of the parameter $B=(\partial \ln \dot{\gamma}/\partial \tau)_T$ determined from the changes in strain rate. For temperatures of 40°K and above, B was independent of strain and relatively independent of temperature, in agreement with earlier results (Conrad and Robertson 1957, 1958, Conrad *et al.* 1960). However, at 20°K and below, the value of B was larger than that for the higher temperatures. Also, in this temperature range B decreased with strain. Furthermore, as seen in fig. 3, straining at these lower temperatures caused a decrease in B determined subsequently at higher temperatures. Thus, at temperatures below 40°K, the effect of strain on B for Mg crystals is similar to that observed for Stages II and III in f.c.c. metals. This feature is being investigated in more detail and will be covered in another paper. In the present paper only those values of B will be considered which do not include an effect of straining.

Fig. 3

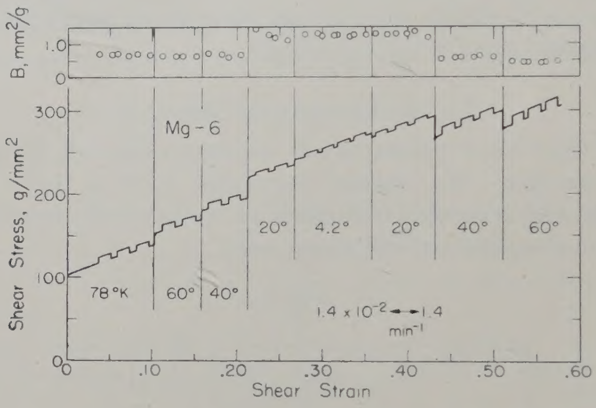

Effect of temperature and strain rate on the flow stress. Also shown are values of the parameter $B=(\partial \ln \dot{\gamma}/\partial \tau)_T$.

Figure 4 shows the variation of B with temperature. The increase in B below 40°K is clearly evident; also there appears to be a minimum in B at ~ 60°K. The present values of B between 78°K and 300°K lie between those obtained previously (Conrad and Robertson 1957, Sheeley *et al.* 1957, Conrad *et al.* 1960) for Mg crystals at approximately the same strain rate. Within the scatter of the data, B tended to decrease with increase in effective strain rate† $\dot{\gamma}_e$ over the range of 10^{-3} min^{-1} to 10^{-1} min^{-1} in agreement with the earlier results (Conrad *et al.* 1960). However, this feature was not studied in detail in the present investigation.

According to Seeger (1954), the flow stress τ can be separated into two additive components, a thermal component τ^* which is identical to the previously mentioned effective stress and an athermal component τ_μ, so that

$$\tau=\tau^*+\tau_\mu. \qquad (5)$$

τ_μ is the long-range internal stress and consequently only indirectly dependent on the temperature through the shear modulus μ; it is independent of the strain rate. τ^*, however, is a function of strain rate and temperature.

---

† $\dot{\gamma}_e=(\dot{\gamma}_1\dot{\gamma}_2)^{1/2}$ where $\dot{\gamma}_1$ is the initial strain rate and $\dot{\gamma}_2$ is the final strain rate.

To evaluate the activation energy we have to derive τ^* as a function of temperature. One procedure is to determine the critical resolved shear stress τ_0 as a function of temperature with $\dot{\gamma}=\text{const.}$ τ_{μ_0} is then obtained from τ_0 at high temperatures where $\tau^*=0$. However, this requires testing a number of crystals, each at a different temperature, and the results are always subject to specimen variations. A better way to obtain τ^* is from the change in flow stress which occurs with a change in temperature. This method seemed especially favourable in the present investigation since the previous work on Mg crystals had indicated that only τ_μ is increased by work hardening, whereas τ^* is independent of strain. Therefore the separation of the measured flow stress into τ^* and τ_μ is possible without any doubtful assumptions.

Fig. 4

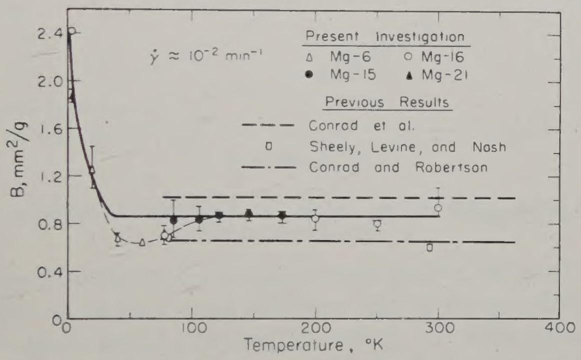

Variation of $B=(\partial \ln \dot{\gamma}/\partial\tau)_T$ with temperature for Mg crystals.

τ_μ can be calculated at any point on a stress–strain curve such as is shown in figs. 2 and 3 by adding the stress increases due to the work hardening $\Delta\tau_\mu$ (after correction for the change in shear modulus), to the initial internal stress τ_{μ_0}:

$$\tau_\mu(T_n)=\mu_{T_n}\left\{\frac{\tau_{\mu_0}}{\mu_0}+\sum_1^n\frac{\Delta\tau_{\mu_j}}{\mu_j}\right\} \quad . \; . \; . \; . \; . \; . \; . \quad (6)$$

whereby the summation is carried out over the pieces of the stress–strain curve obtained at the temperatures T_j; τ^* is then obtained from eqns. (5) and (6):

$$\tau^*(T,\dot{\gamma})=\tau(T,\dot{\gamma})-\mu(T)\left\{\frac{\tau_{\mu_0}}{\mu_0}+\sum\frac{\Delta\tau_{\mu_j}}{\mu_j}\right\}. \quad . \; . \; . \quad (7)$$

In the present investigation τ_μ was determined directly for only one crystal (Mg-2) by obtaining the critical resolved shear stress at 377°K, which is greater than the temperature at which τ^* becomes zero (~ 330°K for $\dot{\gamma}=10^{-2}$ min^{-1}). τ_{μ_0} for the other crystals was then chosen so that their

τ^* at one temperature (generally $\sim 80^\circ$K) coincided with τ^* of Mg-2. The values of τ_{μ_0} for these crystals then ranged from 37 to 47 g/mm^2, which is the order of spread one generally obtains in the critical resolved shear stress for different crystals at temperatures above 330°K.

The values of τ^* (for $\dot{\gamma} \sim 10^{-2}\,\text{min}^{-1}$) obtained by eqn. (7) are given as a function of temperature in fig. 5†. There is good agreement between the various crystals and between the values obtained in this manner and those derived from the critical resolved shear stress values designated τ_0. Of significance with regard to the curve of fig. 5 is that an inflexion occurs at approximately 30°K, i.e. at the temperature below which the parameter B increases strongly. Also one should note that $\tau^* = 0$ at $T \geqq 330^\circ$K.

Fig. 5

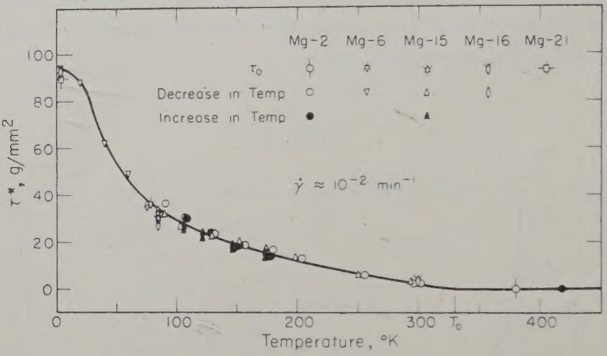

Effect of temperature on the thermal component of the flow stress τ^*.

§ 4. DISCUSSION

Employing eqn. (2) one obtains from the data given in figs. 4 and 5 the variation of H with temperature shown in fig. 6; i.e. the activation energy for plastic flow of Mg crystals is proportional to the temperature. Taking the logarithm of eqn. (1) and rearranging one obtains:

$$H = kT \ln \nu'/\dot{\gamma} \quad . \quad . \quad . \quad . \quad . \quad . \quad . \quad . \quad . \quad (8)$$

where $\nu' = \nu \exp(S/k)$. The proportionality between H and temperature in fig. 6 thus indicates that ν' is a constant over the stress and temperature range considered. Hence, either ν' is independent of temperature and stress or the combined effect of temperature and stress on ν' are such to yield a constant value of ν' at a constant strain rate. To a first approximation it was assumed in the present work that ν' is independent of stress and temperature. This approximation is reasonable if the effect of stress and temperature on the strain rate through ν' is small compared with their effect through the Boltzmann exponential. The agreement between theory and experiment to be discussed below lends support to this assumption.

---

† The shear modulus values (C_{44}) were taken from the paper by Slutksy and Garland (1957).

Since the previous work (Conrad *et al.* 1960) indicated that H for the plastic flow of Mg crystals is primarily a function of stress alone (i.e. H is relatively independent of temperature *per se*), one can obtain the effect of stress on H by substituting the stress from fig. 5 for the temperature in fig. 6.

Fig. 6

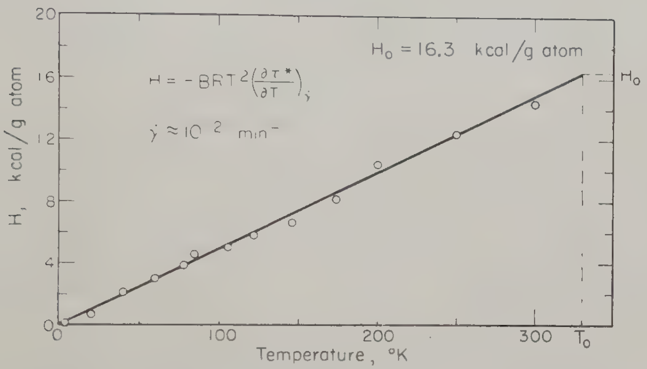

Variation of the activation energy H for plastic flow of Mg crystals with temperature.

Fig. 7

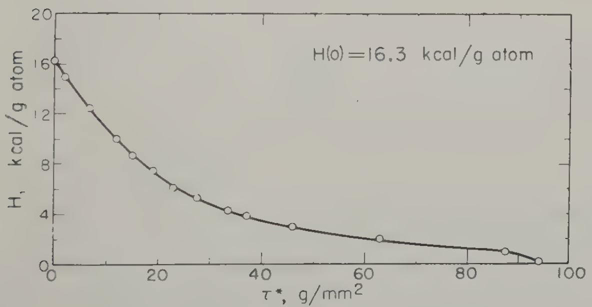

Effect of stress on the activation energy H for plastic flow of Mg crystals.

This has been done in fig. 7. The dependence of H on stress observed here supports the mutual intersection of dislocations as the rate-controlling mechanism over the Peierls mechanism. Furthermore, the value of H_0 (16·3 kcal/g atom) is in reasonable agreement with what one estimates for the energy to form a jog in Mg (14–16 kcal/g atom). For further comparison, it is desirable to determine the values of the frequency factor ν, the forest spacing l, the intersection width d and the force-distance relationship for the intersection mechanism from the experimental data.

It can be shown (Conrad *et al.* 1960) that the physically-significant activation volume v^* for the intersection of dislocations is given by†

$$v^* = l\,d\,\mathbf{b} = B\,k\,T \qquad . \quad . \quad . \quad . \quad . \quad . \quad . \quad (9)$$

where l and d may depend on the stress τ^*. An effect of stress on d will occur if the force between two intersecting dislocations varies with their relative distance of separation; see for example Basinski (1959). That l may decrease with stress due to the bowing-out of a dislocation in the slip plane has been suggested by Friedel (1960). The variation of v^* with stress obtained from eqn. (9) by using the values of B given in fig. 4 and the values of T as a function of τ^* from fig. 5 is given in fig. 8. A strong effect of τ^* on v^* is clearly evident. From $v_0 = v_0^*$ ($\tau^* = 0$) one can obtain an estimate of the average forest spacing l_0:

Fig. 8

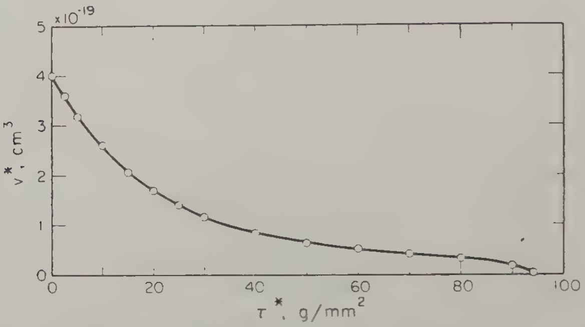

Effect of stress on the activation volume v^* for plastic flow of Mg crystals.

$$l_0 = \frac{v_0^*}{d_0\mathbf{b}} \approx \frac{v_0^*}{2\mathbf{b}^2} = 2 \times 10^{-4}\ \text{cm} \qquad . \quad . \quad . \quad . \quad . \quad . \quad . \quad (10)$$

which is in agreement with measurements of densities of dislocations in metal crystals (Cottrell 1953).

Knowing the forest spacing one can estimate the value of ν' and thus compare the estimated value with that given by the slope of fig. 6. According to Seeger (1954) ν' is given by

$$\nu' = NA\,\mathbf{b}\,\nu_0 \exp(S/k) \qquad . \quad . \quad . \quad . \quad . \quad . \quad . \quad . \quad (11)$$

where N is the number of dislocation segments per unit volume contributing to the plastic flow, A is the area swept-out per successful fluctuation, $\mathbf{b}$ is the Burgers vector and ν_0 is the frequency of vibration of a dislocation segment. Taking $N = l_0^{-3}$, $A = l_0^2$ and $\nu_0 = \nu_d\,\mathbf{b}/2l_0$, where ν_d is the Debye frequency (10^{13} sec^{-1}), and neglecting the entropy contribution one obtains $\nu' = 1 \times 10^5$ sec^{-1}. This is somewhat lower than the value obtained directly from the slope of fig. 6 (10^7 sec^{-1}); however, the agreement can be considered satisfactory in view of the assumptions made.

---

† $v^*\tau^*$ is the work done by the applied stress *during* the thermal activation. In general v^* is not equal to v_0; $v^* = v_0$ only for $\tau^* = 0$ or if the force–distance relationship is a square-type function.

Fig. 9

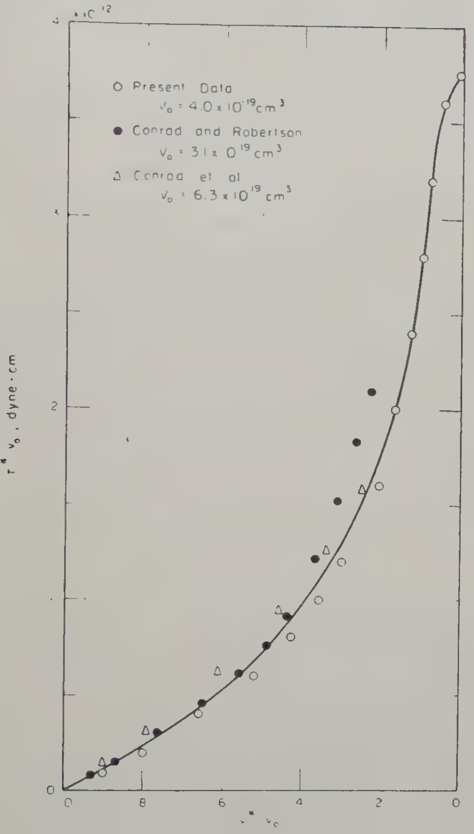

Variation of $\tau^* v_0$ with the ratio v^*/v_0.

Some indication of the form of the force-distance relationship for intersection is provided by the plot of τ^* $(=F/\mathbf{b}l)$ vs. v^* $(=\mathbf{b}ld)$ in fig. 8. However, such a plot only gives the true force-distance curve (aside from the factor bl) when two conditions are fulfilled:

(*a*) The effective forest spacing l does not vary with stress.

(*b*) The force-distance curve either decreases to zero force immediately following $F_{\max}$ or is symmetrical.

If the first condition is satisfied, the data for crystals which differ in initial forest spacing l_0 should superimpose when $\tau^* v_0$ $(=Fd_0)$ is plotted versus the ratio v^*/v_0 $(=d/d_0)$. d_0 represents the 'activation distance' at zero effective stress ($\tau^*=0$). Figure 9 gives such a plot for three separate investigations on Mg crystals. It is here seen that the curves superimpose, suggesting that l is not significantly affected by the stress.

In regard to the actual shape of the force-distance curve, one cannot make a decision based on the experimental data. Also, the theory is not developed in sufficient detail to be of help. Since there is no reason to expect the force-distance curves for intersection to have the special forms listed, one must assume that the curves of fig. 9 only represents the force-activation distance relationship. Similarly, the 'force-distance' curves derived by Basinski (1959) for the deformation of Ag, Al and Cu single crystals in Stages II and III are also actually force-activation distance curves. If one subtracts the long range stress component from Basinski's curves, their form is similar to that given in fig. 9.

§ 5. CONCLUSIONS

In conclusion the present and previous experimental data on the plastic flow of Mg crystals indicate that the rate-controlling mechanism at low temperatures is the intersection of dislocations. However, Cottrell's (1952) simple model must be modified to include an effect of stress on the activation volume. This effect of stress appears to be due primarily to the fact that the force between two intersecting dislocations varies with their distance of separation in agreement with Basinksi (1959), rather than a change in the effective forest spacing as proposed by Friedel (1956).

REFERENCES

BASINSKI, Z. S., 1959, *Phil. Mag.*, **4,** 393.

CONRAD, H., 1958, *Acta Met.*, **6,** 339.

CONRAD, H., HAYS, L., SCHOECK, G., and WIEDERSICH, H., 1960 (submitted to *Acta Met.*).

CONRAD, H., and ROBERTSON, W. D., 1957, *Trans. Amer. Inst. min.* (*metall.*) *Engrs*, **209,** 503 ; 1958, *Ibid.*, **212,** 536.

CONRAD, H., and WIEDERSICH, H., 1960, *Acta Met.*, **8,** 128.

COTTRELL, A. H., 1952, *J. mech. Phys. Solids*, **1,** 53 ; 1953, *Dislocations and Plastic Flow in Crystals* (Oxford).

FRIEDEL, J., 1956, *Les Dislocations* (Paris : Gauthier-Villars).

LYTTON, J., SHEPARD, L., and DORN, J., 1958, *Trans. Amer. Inst. min.* (*metall.*) *Engrs*, **212,** 220.

NABARRO, F. R. N., 1952, *Advanc. Phys.*, **1,** 269.

SEEGER, A., 1954, *Z. Naturf.* A, **9,** 758, 810, 856 ; 1956, *Phil. Mag.*, **1,** 651 ; 1957, *Dislocations and Mechanical Properties of Crystals* (New York : Wiley).

SHEELY, W., LEVINE, E., and NASH, R., 1957, *Trans. Amer. Inst. min.* (*metall.*) *Engrs*, **209,** 1303.

SLUTSKY, L. J., and GARLAND, C. W., 1957, *Phys. Rev.*, **107,** 972.

THORNTON, P. R., and HIRSCH, P. B., 1958, *Phil. Mag.*, **3,** 738.

WEERTMAN, J., 1958, *J. appl. Phys.*, **29,** 1685.

WESSEL, E., 1956, *Bull. Amer. Soc. Test. Mat.*, No. 211, 40.

Radiation-enhanced Helium Precipitation in Copper†

By A. N. GOLAND‡
Brookhaven National Laboratory, Upton, New York

[Received July 16, 1960]

ABSTRACT

The effect of neutron irradiation on the precipitation of helium atoms in copper has been studied at temperatures up to 425°C. At 160°C and 300°C no effect was observed. At 425°C the irradiated sample exhibited considerable precipitation around grain boundaries as compared to an unirradiated sample held at the same temperature. It is concluded that the additional vacancies introduced during the irradiation enhance the precipitation process. The resultant voids are equal in size to those obtained at higher temperatures in the absence of radiation.

ACCORDING to the theory of radiation-enhanced diffusion (Dienes and Damask 1958) neutron irradiation produces a steady-state vacancy concentration in excess of that which would have existed at a given temperature in the absence of the radiation field. Consequently, the theory implies that processes whose rates are controlled by vacancy diffusion should proceed more rapidly during irradiation than under normal conditions. This has been clearly demonstrated for the case of partially ordered alpha brass (Dienes and Damask 1958). If possible, one would like to provide some visual evidence of enhanced diffusion, and the phenomenon of helium precipitation in copper (Barnes *et al.* 1958) seemed suitable. Barnes and his co-workers have demonstrated that helium will precipitate in copper and produce visually observable voids when the copper is heated to temperatures where self-diffusion is important. These workers believe that the precipitation results from the diffusion of vacancies into the vicinity of the helium atoms, and they have performed numerous experiments which tend to confirm this hypothesis. If one accepts their supposition, then it ought to be possible to induce precipitation at a temperature below the self-diffusion range by irradiating copper with neutrons to increase the vacancy concentration, provided only that most of the vacancies live long enough to migrate to the nucleation centres. The initial results of such an experiment are described in this note.

---

† Communicated by the Author. Work performed under the auspices of the U.S. Atomic Energy Commission.

‡ Guest Scientist, Ordnance Materials Research Office, Watertown, Massachusetts.

Figure 1† shows the successive steps in the experiment. A sample of copper 0·040 in. thick with a nominal purity of 99·999% was bombarded with 40 Mev alpha-particles from the 60 in. cyclotron until a total charge of 150 μamp hrs had been injected. This is equivalent to a concentration over the bombarded volume of approximately 0·2 atm. % helium. During the α-particle bombardment, the sample temperature never exceeded 180°c, and it was probably considerably lower. After sufficient time had passed for the sample to reach a safe level of radioactivity, it was unsoldered from the target blank and cut into pieces approximately ¼ in. wide by 1 in. high. Autoradiographs of these samples were taken to determine which ones had been uniformly bombarded with α-particles. This was a necessary task because some regions of the copper target had been masked by the grid which held it in the cyclotron beam. To check

Fig. 1

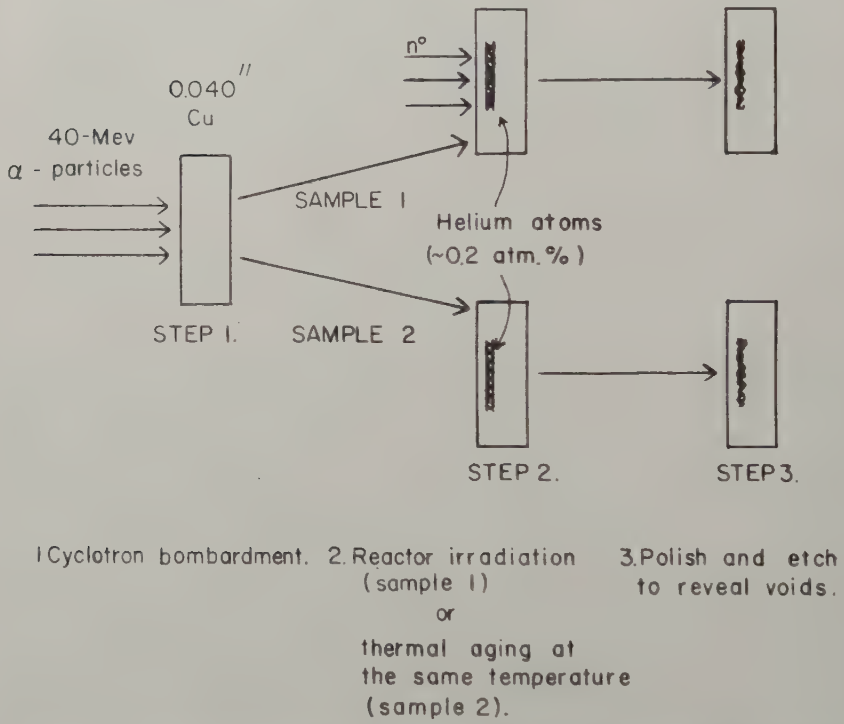
0.040″
Cu
40-Mev
α - particles
n°
SAMPLE 1
SAMPLE 2
Helium atoms
(~0.2 atm. %)
STEP 1.
STEP 2.
STEP 3.
1 Cyclotron bombardment.
2. Reactor irradiation (sample 1) or thermal aging at the same temperature (sample 2).
3. Polish and etch to reveal voids.

A schematic drawing showing the various steps involved in the experiment described in the text.

---

† Figures 2–4 are shown as plates.

the experimental technique, some of the experiments of Barnes *et al.* (1958) were repeated with excellent results.

After suitable samples had been chosen, one sample was irradiated at a selected temperature in the reactor, while another was held at the same temperature in a vacuum furnace. Each sample was maintained at temperature in its environment for the same period of time, approximately 10 days. Most of the neutron irradiations were carried out in a furnace in hole E–11 of the Brookhaven graphite reactor. The epicadmium flux in this experimental facility was approximately 2×10^{11} nv as determined by activation of bare and cadmium-covered aluminium–manganese foils. Following this treatment, the samples were stored until the in-pile sample could be safely handled once more. Finally, standard metallographic techniques were applied to the edges of the samples in order to expose voids which might have been introduced. The samples were mechanically polished first and then either electrolytically or chemically etched. Whenever voids were exposed by such polishing, they appeared in a band approximately 20 to 30 μ wide and at a depth below the surface of about 0·22 mm.

The experiments described above were performed at 300°C and 425°C in hole E–11, and in a higher flux hole at 160°C. No evidence of void formation was found in either the irradiated or control samples maintained at 160°C or 300°C. However, the samples held at 425°C both revealed that the precipitation of helium and the formation of voids in the grain boundaries was proceeding during the experiment. Moreover, the sample which was irradiated during the ageing process showed considerably more precipitation than the sample which was merely aged *in vacuo*. The surfaces of these samples were polished and etched ten or twelve times to ensure the validity of the observations. A total of from 5 to 10 mils was removed from the surfaces during this procedure, and the original observations were confirmed each time. Figure 2, which was taken with the aid of a light microscope, shows this result clearly. The surfaces of all other samples including those which were untreated except for α-particle bombardment resembled the clear regions in the figure. Thus, the results furnish one of the first visual observations of enhanced diffusion.

While providing superficial evidence that an interesting effect exists, the light microscope does not supply the detailed image which is really desired. For this purpose, one must resort to the electron microscope. Consequently, direct carbon replicas shadowed with tungsten dioxide were made of the two samples shown in fig. 2 so that the nature of the precipitation region could be investigated more fully. Since replication techniques generally are peculiar to the laboratory in which they are performed, a few words about the techniques employed in this work are in order. To begin with, the samples were mechanically polished and then etched with a solution consisting of one part H_2O_2, one part H_2O, and two parts $NH_4(OH)_2$. This solution must be fresh when it is applied to the sample or oxidation will result. Following a successful etch, the replication is carried out under vacuum. A commercial wetting agent, Victa-wet, is heated in a tungsten basket at a moderate temperature so that any water present is driven off. Then the Victa-wet is heated to incandescence for at least one minute, and deposited by evaporation onto the surface of the sample. The sample is shadowed, and subsequently covered by an evaporated layer of carbon. Finally, the shadowed carbon replica is floated off of the copper in distilled water. Replicas made in this way resulted in the electron micrographs shown in figs. 3 and 4.

Figure 3 (*a*) is an electron micrograph of the normal grain structure of the out-of-pile sample, and fig. 3 (*b*) is a similar micrograph of the in-pile sample, In each case the area shown is immediately adjacent to the area in which the helium band is prominent. Each micrograph reveals just the normal grain structure of a polycrystalline material, the background texture being a result of the etching process. Figures 4 (*a*), (*b*) and (*c*) are electron micrographs of the helium bands in the same two samples. By comparison with fig. 3 (*a*), fig. 4 (*a*) exhibits grain boundaries which are more sharply defined due to the precipitation of helium. However, this precipitation is on a relatively fine scale. In marked contrast to fig. 3 (*b*), figs. 4 (*b*) and (*c*) reveal the presence of much larger voids in the grain boundaries of the reactor-irradiated sample as a consequence of helium precipitation during reactor irradiation. Figure 4 (*b*) is an example of the phenomenon, already well established by Barnes, that certain grain boundaries are either sources or conductors of vacancies while others are neither. Following Barnes' explanation (Barnes 1959) of the void formation, we can consider several explanations for the fact that the voids are in the grain boundaries rather than separated from them by a bubble-free zone of copper. One possibility is that irradiation has permitted enhanced localized diffusion of the helium to the grain boundaries. However, this seems unlikely because all grain boundaries should then be similarly affected. Figure 4 (*b*) contradicts this. A second, more plausible, explanation is that the irradiation somehow causes some grain boundaries to become good conductors of vacancies by increasing their energy. In addition, the vacancy supply does not become exhausted readily because it is supplemented by the vacancies produced during the neutron bombardment. It is interesting to note that the sizes of the voids in figs. 4 (*b*) and (*c*) are in the range of $1{\cdot}5–3 \times 10^{-5}$ cm. This is the same range as Barnes obtained in copper after two hours of heating a sample at 800°c.

This work will be continued for different fluxes and temperatures in order to place the results on a quantitative basis. The theory of diffusion-limited precipitation (Ham 1958) predicts the rate of growth of voids in terms of the diffusion constant of the material. It is hoped that a measure of the enhanced diffusion may be obtained by applying this theory to the present technique.

ACKNOWLEDGMENTS

Thanks are due to C. P. Baker, D. Sondericker and G. Hummer for help in performing the irradiations. The author is grateful to the metallography group at Brookhaven, in particular J. Kelsch and P. Buhl, for their essential aid during the course of this study.

REFERENCES

BARNES, R. S., 1959, AERE–R 3162, Metallurgy Division, Atomic Energy Research Establishment, Harwell, Berkshire.
BARNES, R. S., REDDING, G. B., and COTTRELL, A. H., 1958, *Phil. Mag.*, **3**, 97.
DIENES, G. J., and DAMASK, A. C., 1958, *J. appl. Phys.*, **29**, 1713.
HAM, F. S., 1958, *J. Phys. Chem. Solids*, **6**, 335.

On the Fracture Behaviour of Magnesium Oxide Bi-crystals†

By A. R. C. Westwood
Research Institute for Advanced Studies, Baltimore 12, Maryland, U.S.A.

[Received July 6, 1960]

Abstract

Metallographic studies on compressed bi-crystals of magnesium oxide have revealed cracks formed at the grain boundary by piled-up groups of edge dislocations. However, these were produced only when two slip bands, one from each grain, met at the boundary ; cracks associated with a single pile-up were not observed. Crack propagation was transgranular, and by crystallographic cleavage.

A mechanism for crack formation at low strains is proposed in which a source, situated on the opposite side of the grain boundary and some two to eleven microns away from a piled-up group of edge dislocations, can be activated by the stress field of this pile-up and produce dislocations which, under certain conditions, may cooperate with the activating group to form a crack.

§ 1. Introduction

Recently it has been demonstrated that single crystals of magnesium oxide can exhibit a potentially useful measure of ductility ($\sim 5\%$) providing that such factors as environment and surface condition are carefully controlled (Gorum *et al.* 1958, Stokes *et al.* 1959 a). However, in the polycrystalline form, this and other ceramic materials are commonly noted for their lack of ductility. This suggests that the presence of grain boundaries may be responsible in some way for the brittle nature of polycrystalline magnesium oxide. A possible explanation was provided by Zener (1948) several years ago : grain boundaries may act as stable barriers against which edge dislocations can pile up and coalesce, producing a crack nucleus. The theory of this type of crack formation has been developed by Stroh (1954, 1955, 1957) and others, and cracks caused by dislocation coalescence have been observed at the intersections of bands of edge dislocations in single crystals of magnesium oxide (Stokes *et al.* 1959 b) and lithium fluoride (Westwood 1960). Such cracks were responsible for the eventual failure of the single crystals. However, in polycrystalline samples there are several ways in which failure could occur: by cracks initiating inside individual grains and then propagating transgranularly ; by Zener-type cracks initiating at a grain boundary and propagating either intergranularly or transgranularly ; or by failure of the grain boundary itself due to impurity embrittlement or the presence of voids.

---

† Communicated by the Author.

In this work the fracture behaviour of bi-crystals of magnesium oxide in compression has been studied. The specific objectives were to elucidate the role of the grain boundary in fracture and to determine whether a Zener-type fracture mechanism is operative in this material.

§ 2. EXPERIMENTAL TECHNIQUES

Polycrystalline magnesium oxide blocks were obtained from the Norton Company and bi-crystals, approximately 25 mm × 5 mm × 4 mm in size, were cleaved from these blocks so that the boundary was close to the centre of the specimen. The change in lattice orientation across boundaries was typically about ten to twenty degrees and the rotation component was small ($\ngtr 5°$).

Specimens were mounted in lucite and parallel compression faces, one of which was a {100} cleavage plane, produced by grinding and mechanical polishing. After the lucite had been removed the bi-crystals were chemically polished for two to four minutes in 85% orthophosphoric acid at 100°C, washed in distilled water and carefully dried using ethyl alcohol and ether rinses.

Specimens were then compressed in an Instron testing machine at strain rates of order 10^{-4} per sec, and a birefringence technique was utilized to study the strain pattern of the bi-crystal during testing. After an appropriate strain, the distribution of dislocations and cracks was revealed by the etching technique of Stokes *et al.* (1958).

§ 3. EXPERIMENTAL OBSERVATIONS

Bi-crystal boundaries were found to be extremely effective barriers to the movement of dislocations. In particular, the piling-up of groups of edge dislocations at the boundary was regularly observed. Often cracks were associated with such piled-up groups and these formed in a variety of ways, some of which are illustrated in figs. 1–4†. These typical micrographs suggest that a crack is formed in the grain boundary only when two slip bands, one from each grain, 'meet' at the boundary. Although a crack is not necessarily formed under such circumstances, no cracks associated with a single piled-up group of dislocations were observed. In fig. 1 for example, cracks have formed at A and B but not at C, D, E or F. Similarly, in fig. 2 cracks have not formed at G or H where relatively broad bands of edge dislocations are arrested, nor at J where two slip bands meet. However, the concept of slip bands meeting at the boundary must be more closely defined ; examination of the cracks formed at B in fig. 1 and K_1, K_2 and K_3 in fig. 2 will show that the slip bands responsible for these cracks were actually displaced some one to two microns from one another at the boundary. This displacement is thought to be a significant factor in the fracture mechanism for sometimes cracks are not formed when slip bands meet, apparently, head-on as in fig. 3 at R_2 and R_3.

---

† Figures 1–6 are shown as plates.

Although cracks were initiated frequently at the boundary and only rarely in the interior of the invididual grains, these cracks did not propagate along the boundary but always into the grains, usually on a {100} cleavage plane, fig. 2, L, or a {110} slip plane, fig. 3, R_1. Metallographic observations indicate that cracks propagate away from the boundary as soon as they reach the edge of the promoting slip band as, for example, in fig. 4 at N.

Slip bands sometimes originate from sources in the boundary as at Q in fig. 4. Figure 5 shows that a boundary can be a prolific source of dislocations, but this phenomenon was not commonly observed in these experiments—dislocations usually originated near the compression faces. However, the former may be typical of the mode of deformation of polycrystalline specimens.

The cleavage crack at P in fig. 4 may have resulted from the interaction of dislocations in slip bands Q and T. Cracks believed to have been formed in this way have been observed previously by Washburn *et al.* (1959).

§ 4. Discussion

It has been demonstrated that cracks can be formed at grain boundaries by the action of piled-up groups of edge dislocations but that two groups, and not one as predicted by Zener (1948) for metals, are necessary for this to occur. The meeting of bands of edge dislocations at a boundary is inevitable at ' high ' strains but there are two ways in which this can arise so that cracks may be formed at low strains. First, two sources, both far away from the boundary, can emit dislocations which meet fortuitously at the boundary. Second, a source close to the boundary can be activated by the stress associated with a primary piled-up group of dislocations in the neighbouring grain. Stroh (1957) has shown that sources most likely to be activated will lie at a distance $r = \alpha G\mathbf{b}/\sigma_u$ away from the primary pile-up, where α is a term of order, but greater than unity; G is the rigidity modulus; $\mathbf{b}$ the Burgers vector and σ_u the ' upper ' yield stress. For a single crystal of magnesium oxide

$$G_{[110]} = S_{11} - S_{12} + \tfrac{1}{2}S_{22} \text{ (Voigt 1928)}$$

and using values of the principal moduli determined by Durand (1936) a value of $G_{[110]} = 1{\cdot}22 \times 10^{12}$ dynes/cm² is obtained. Putting $1 < \alpha < 9$; $\mathbf{b} = 3 \times 10^{-8}$ cm and $\sigma_u = 3\text{–}3{\cdot}5 \times 10^8$ dynes/cm², we find that r lies between 2 and 11 microns. Figure 6 is a possible example of this phenomenon. A half loop source at S, lying some 8 microns from U, was activated by the stress from piled-up dislocations in slip band V and the dislocations thus produced then cooperated with the primary dislocations to produce a crack at U. In this example the shear stress at S, given by

$$\sigma_S = \beta\sigma_s(L/r)^{1/2} \text{ (Stroh 1957)}$$

where β is a numerical factor approximately unity, σ_s the resolved shear stress on the primary slip plane and L is the length of the primary slip line, was some $20\sigma_s$ and thus was more than sufficient to activate the source.

Figure 7 illustrates schematically a situation similar to that in fig. 6 and suggests one way in which grain boundary cracks may be formed at low strains. In the diagram, specimen ABCD is compressed on faces AD and BC. A suitably oriented source S_I in grain I is activated by the resolved shear stress and emits negative edge-dislocations in the direction of the boundary which become piled-up at G. The stress-field associated with this primary pile-up then activates a second source, S_{II}, situated an appropriate distance away from the boundary in grain II (Stroh 1957), and oriented so that it emits dislocations of opposite sign (positive) to those in the primary pile-up in the direction of the boundary[†].

Fig. 7

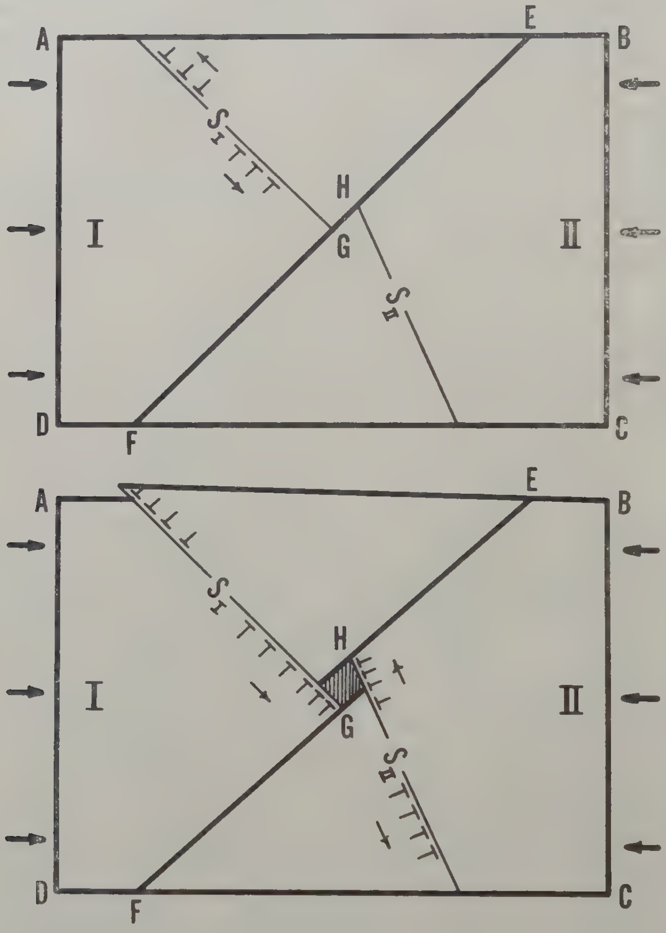

[†] It is considered unlikely that a source would be activated which would emit dislocations in the direction of the boundary of the same sign as those in the primary pile-up.

Because the activation stress on S_{II} is expected to be large, possibly $20\sigma_s$, this source is likely to produce an avalanche of dislocations (Johnston and Gilman 1960). These will also pile up at the boundary forming a secondary pile-up displaced some distance away from the primary pile-up, for example at H.

Now if H lies between G and E, fig. 7 and, from the present metallographic observations, if GH is not more than one or two microns in length, then a crack is likely to be formed in the boundary between the two promoting slip bands. This will be a consequence of the cooperation of the two piled-up groups of dislocations in producing a high tensile stress over that small area of boundary, GH, between them. Furthermore, coalescence of leading dislocations in the two pile-ups also favours crack formation in this area.

However, if H lies between G and F, then it is less likely that a crack will be formed for the pile-ups now cooperate to put the boundary between them into compression. Moreover, any cracks formed by coalescence of piled-up dislocations will be separated by the distance GH instead of being located within GH.

Stroh (1957) has suggested that if a crack is to form near a group of piled-up dislocations, then it is necessary for the material round the group to remain unyielding ; for plastic flow will tend to relieve the stresses associated with the pile-up and in this way prevent the initiation of a crack. The present observations suggest that the converse is sometimes true in magnesium oxide for, under certain conditions, edge dislocations on each side of the boundary may ‘ cooperate ’ to produce a crack.

In fig. 1 at A and in fig. 2 at K_1, K_2 and K_3, cracks have formed between slip bands believed to contain edge dislocations of opposite sign and which were suitably displaced from each other at the boundary. Taking into account the direction of the applied compressive stress, the nature and position of these cracks appears consistent with this view. However, other experiments are planned in which an x-ray technique will be used to examine the veracity of this opinion.

The investigation has demonstrated that grain boundaries in magnesium oxide are not inherently weak in compression but that cracks can be formed at the boundary by the action of piled-up groups of edge dislocations.

ACKNOWLEDGMENTS

It is a pleasure to acknowledge the encouragement of Mr. W. W. Bender, the helpful discussions with Dr. H. M. Otte and the capable assistance of H. Opperhauser, Jr., D. Goldheim and C. Feltes in this work. We are also grateful for the financial support received from Watertown Arsenal Laboratories and in particular the continued interest of Mr. Murray Jacobson.

REFERENCES

DURAND, M. A., 1936, *Phys. Rev.*, **50,** 449.

GORUM, A. E., PASK, J. A., and PARKER, E. R., 1958, *J. Amer. ceram. Soc.*, **41,** 161.

JOHNSTON, W. G., and GILMAN, J. J., 1960, *J. appl. Phys.*, **31,** 632.

STOKES, R. J., JOHNSTON, T. L., and LI, C. H., 1958, *Phil. Mag.*, **3,** 718 ; 1959 a, *Ibid.*, **4,** 920 ; 1959 b, *Trans. Amer. Inst. min. (metall.) Engrs*, **215,** 437.

STROH, A. N., 1954, *Proc. roy. Soc.* A, **223,** 404 ; 1955, *Ibid.*, A, **232,** 548 ; 1957, *Advanc. Phys.*, **6,** 418.

VOIGHT, W., 1928, *Lehrbuch der Krystallphysik* (Leipzig u. Berlin : Teubner), p. 739.

WASHBURN, J., GORUM, A. E., and PARKER, E. R., 1959, *Trans. Amer. Inst. min. (metall.) Engrs*, **215,** 230.

WESTWOOD, A. R. C., 1960, *Phil. Mag.*, **5,** 981.

ZENER, C., 1948, *Fracturing of Metals* (Amer. Soc. Metals), p. 3.

On the Edwards–Matthews Approach to π–N Scattering†

By CHAN HONG-MO‡
Department of Mathematical Physics, University of Birmingham

[Received August 2, 1960]

ABSTRACT

In an attempt to extend the Edwards–Matthews (1957 a) theory of π–N scattering to higher relativistic energy it was discovered that their evaluation of the fourth-order Feynman graphs required was incorrect, involving an expansion which fails to converge at the threshold of physical scattering energy. A new evaluation of these graphs is then carried through and the result substituted into their scattering formula. The new values do not show the agreement with experiment found in Edwards and Matthews' original results. A study of the Feynman graphs and the method of their evaluation are briefly described in § 2.

§ 1. BACKGROUND, DISCUSSION AND SUMMARY OF RESULTS

THE most prominent feature of π–N scattering at energies of a few hundred MEV is the sharp resonance-like behaviour at around 190 MEV. The resonance has been assigned with great certainty to the $T=\frac{3}{2}$, $J=\frac{3}{2}+$ state. Another surprising feature is the smallness of the s-wave scattering at low energy. A straightforward weak coupling perturbative approach failed completely to reproduce either of these features and recently several theories have been proposed to try to predict them from accepted field theoretical principles. The Edwards–Matthews (1957 a) approach is one of these.

In an earlier paper, Edwards and Matthews (1957 b) had proposed a very simple model to the problem and they obtained the Chew–Low (1956) plot. The work under discussion was an attempt to extend the same sort of treatment to a relativistic system. Starting from the Schwinger (1951) Functional Differential Equation for the single-nucleon propagator, they found an approximate solution for the scattering amplitude in terms of the first and second Born approximations of the type that Cini and Fubini (1954) had proposed for a non-relativistic system, namely

$$t_\alpha = \frac{S_\alpha^{(2)}}{1 - S_\alpha^{(4)}/S_\alpha^{(2)}} \quad . \quad . \quad . \quad . \quad . \quad . \quad . \quad . \quad (1.1)$$

where $S_\alpha^{(4)}$, $S_\alpha^{(2)}$ are the first and second Born approximations to the S-matrix projected into the various partial-wave states α. Readers are referred to the paper of Edwards and Matthews (1957 a) for details of their derivation of this formula.

---

† Communicated by Professor R. E. Peierls.

‡ After September 1960 at the Department of Mathematics, The University of Hong Kong.

Edwards and Matthews did not mean the derivation to be rigorous but merely as a guide, and several rough approximations had been made which were not really justified. But the agreement of their final formula with experiment was extremely good. Not only did they predict the 33-resonance at the right energy and of the right shape but they also gave the correct order of magnitude of the s-wave and other p-wave phases. This is remarkable since they started with the fully relativistic and renormalizable γ_5-coupling. There being no cut-off parameter, they had only one free parameter to fit the experimental results and this came out with the value $g^2/4\pi \approx 16$ in agreement with the photo-meson production data (Kroll and Rudermann (1954)) and dispersion theory (Cziffra *et al.* (1959)). This compares favourably with the Chew–Low (1956) theory, which requires two parameters, g and a cut-off parameter. Also Chew and Low started with a $\boldsymbol{\sigma} . \boldsymbol{\nabla}$ interaction and their theory thus gives no s-wave scattering whatever, whereas experiments show some, though small, s-wave scattering.

The application of the Edwards–Matthews scattering formula involves the calculation of the renormalized Feynman graphs of fourth-order in the coupling constant. These Edwards and Matthews calculated by an expansion method which will be briefly described and discussed in § 2.

Fig. 1

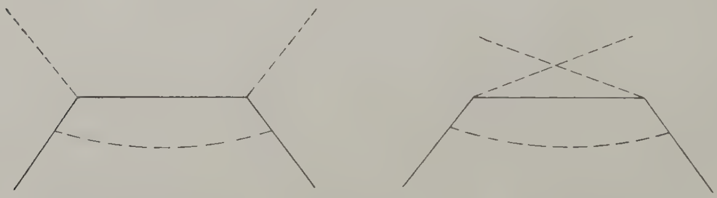

The present investigation was started with the intention of extending the Edwards–Matthews calculation to higher relativistic energy. The interest was mainly in the application rather than the justification of the formula. In the course of the investigation, it was found that the Edwards and Matthews evaluation of the fourth-order Feynman graphs was incorrect and involved an expansion which would fail to converge at the threshold of physical scattering energy. It might also be recorded here that there exists another calculation of these same graphs by Wyld (1954) which is also incorrect, for the result does not have the crossing symmetry.

We are thus led to a detailed study of the properties of these graphs and a method of their evaluation. Apart from the object of testing the Edwards–Matthews theory, it seems that a correct evaluation of these graphs is valuable though they have no direct physical significance. The investigation is unfortunately rather lengthy, but methods were found whereby Self-Energy and Vertex-Diagrams can be evaluated exactly except for an almost trivial approximation in the vertex part. The remaining diagrams (fig. 1) are more difficult but an expansion method is found which is expected to converge for energies for which $k^2/m^2 \ll 1$. The calculation was carried through and the result substituted into Edwards and Matthews' formula. The result, unfortunately, differs widely from their original values. We still have a resonance in the 33-state the position of which may be fitted to the experimental value by taking $g^2/4\pi \approx 10$. But for this value of the coupling constant g, the 11 and 13 states both show resonances at laboratory scattering energies of 270 MeV and $\approx$ 700 MeV respectively. The 11 resonance at 270 MeV is clearly inadmissible, and though the π–N scattering curve does show a $T=\frac{1}{2}$ resonance at $\approx$ 615 MeV this has been assigned to $J=\frac{3}{2}-$ from angular distribution data. We claim therefore, that Edwards and Matthews' agreement with experiment was accidental.

It is believed that the method of evaluation of the Feynman diagrams developed in this work and their properties may be useful to some readers and the main steps are briefly described in the following section.

§ 2. RENORMALIZED FEYNMAN GRAPHS OF THE FOURTH ORDER IN THE COUPLING CONSTANT

The Lagrangian on which the Edwards–Matthews theory was based was the pseudo-scalar Lagrangian

$$\mathscr{L}=\mathscr{L}_0-g\bar{\psi}_N\gamma_5\boldsymbol{\tau}\psi_N\cdot\boldsymbol{\varphi}_\pi \quad . \quad . \quad . \quad . \quad . \quad (2.1)$$

where vector-notation was used for isotopic-spin space. The diagrams under discussion are those given in fig. 2 (a), (b), (c), and the corresponding crossed ones (a'), (b'), (c'). It is often convenient in what follows to distinguish between the masses of external particles (m for nucleons, μ for mesons) and internal particles (m' for nucleons and μ' for mesons). The actual graphs are obtained by putting $m'=m$, $\mu'=\mu$.

Fig. 2

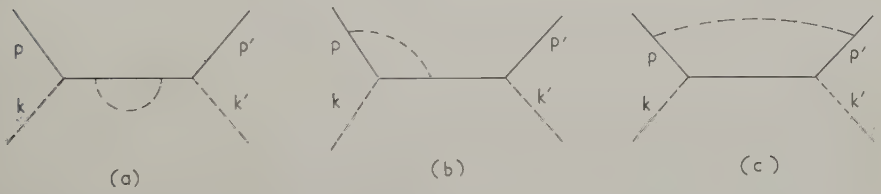

First we note that the diagrams (a) and (b) are functions of one scalar variable only which may be taken to be $s=-(p+k)^2$ for the uncrossed diagrams and $\bar{s}=-(p-k')^2$ for the crossed ones. The diagram (c) is a function of two variables, both s and $\bar{s}$. Because of the crossing symmetry, the crossed and uncrossed diagrams are actually the same functions of the scalar variables s and $\bar{s}$ but with their roles interchanged. Thus, e.g. (a'), the crossed Self-Energy diagram is, apart from isotopic spin dependence, the same function of $\bar{s}$ as (a) the uncrossed diagram is of s. The physical values are to be taken for the appropriate values of the variables. s being the total energy, has physical values $>(m+\mu)^2$ and $\bar{s}$, the four-momentum-transfer, has physical values $<(m-\mu)^2$.

Next we note that the uncrossed diagrams (*a*) and (*b*) contribute only to the partial wave $T=\frac{1}{2}$ and $J=\frac{1}{2}$. This is because we have as an intermediate state a single nucleon. The diagram (*c*) and all the cross diagrams contribute to all partial wave states.

The matrix elements represented by the diagrams are given as integrals over momentum space. These integrals can be converted into integrals over auxiliary variables by the Feynman method. Also the diagrams (*a*) and (*b*) are divergent and these have to be renormalized following the prescriptions of Dyson. The method used in this part of the calculation is familiar and will not be presented.

The resulting integrals are of the kind typical of perturbation theory, and are of the form

$$\int dx \ldots \frac{\phi(x, \ldots)}{[a(x, \ldots)]^r} \qquad \ldots \ldots \quad (2.2)$$

where $\phi(x, \ldots.)$ is some polynomial while $a(x, \ldots.)$ is a quadratic of the variables $x, \ldots.$ The number of auxiliary variables necessary is 1, 2, and 3 respectively for the graphs (*a*), (*b*), (*c*). The analytic properties of these graphs are readily studied by studying the zeros of the quadratic denominators $a(x, \ldots)$. Techniques for this are mainly algebraic-geometrical and are now highly developed by several authors (e.g. Landau (1959)). Only the most primitive techniques are necessary in our very simple cases here. The zeros of $a(x, \ldots.)$ lie on a quadric surface in general, the position and shape of which depend on the variables s and $\bar{s}$. The values of s (or $\bar{s}$) at which the quadric surface $a=0$ enters the region of integration of the auxiliary variables $x, \ldots$ usually correspond to branch-points. In the graphs under consideration these branch-points are square-root branch-points. We shall not give details of this investigation but shall only give the result.

(*a*) and (*b*) are analytic functions in s on the cut s-plane, cut from $s=(m+\mu)^2$ to ∞, with the square-root branch-point at $s=(m+\mu)^2$. The crossed diagrams (*a'*) and (*b'*) have the same analytic properties in the variable $\bar{s}$. Note that there is no pole term in spite of the single-nucleon intermediate state. This has been absorbed into the coupling constant in the subtraction procedure of renormalization.

The analytic properties of (*c*) are best stated in the two variables s, and $t=-(k-k')^2=2m^2+2\mu^2-(s+\bar{s})$. For fixed t, (*c*) is analytic in s on the cut s-plane cut from $(m+\mu)^2$ to ∞. For fixed s, (*c*) is analytic on the cut t-plane cut from $t=4m^2$ to ∞. The crossed diagram (*c'*) has the same analytic properties in the variables $\bar{s}$ and t.

These analytic properties are well known now since the intense work on dispersion relations and the subsequent work of Mandelstam (1958) and others. They are just the usual threshold branch-points. It is however exactly because of these branch-points that the Edwards–Matthews expansion method breaks down. They have expanded the diagrams about $\omega = 0$ in the unphysical region, $(\omega^2 = k^2 + \mu^2)$. Because of the branch-point at $\omega = \mu$, the expansion fails to converge at just the physical energy of scattering. We shall give a more specific example. In the Self-Energy diagram, we have a typical integral of the form

$$I = \int_0^1 dx \log \frac{a_s^2 - i\epsilon}{a_m^2} \qquad . \; . \; . \; . \; . \; . \; . \quad (2.3)$$

where

$$a_s^2 = sx^2 + (m^2 - \mu^2 - s)x + \mu^2,$$
$$a_m^2 = m^2x^2 - \mu^2 x + \mu^2.$$

Edwards and Matthews expanded the integrand into a power series in ω and integrated term by term, keeping the first non-vanishing term in a sum of such integrals. Such an expansion is justified only if the series is uniformly convergent in the region of integration. It can be seen, however, that uniform convergence fails just at threshold. The expansion method is thus invalid. In fact it gives a real value for the diagram whereas above physical threshold it should necessarily be complex.

Fig. 3

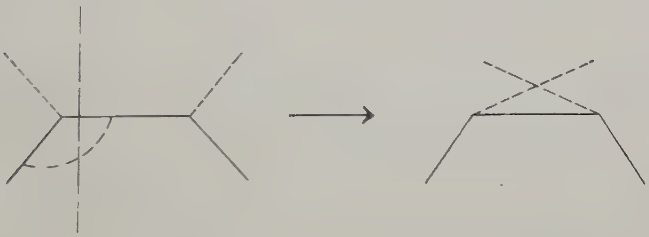

Fig. 4

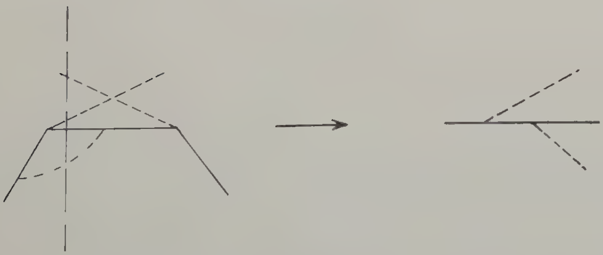

Finally it might be pointed out that from the considerations above, it can readily be seen that the physical values of the crossed diagrams (a'), (b') are real, while the uncrossed ones are complex. A convenient way to illustrate this is the following.

Cutting the uncrossed vertex diagram gives a diagram which can occur for physical energies, hence the existence of a threshold branch-point and complex values. Cutting the crossed vertex diagram gives a diagram which requires a free nucleon to decay into a nucleon and two pions which is kinematically impossible in physical region. Hence we have real physical values for (b'). These considerations may be applied to more complicated diagrams.

We next come to the task of actually evaluating these diagrams. We shall not give any details of the lengthy calculation but shall only briefly describe the techniques evolved. Two general points to note are the crossing symmetry and the infra-red divergence. Because of the crossing symmetry, the crossed and uncrossed diagrams are the same analytic functions of s and $\bar{s}$ as pointed out above. Hence any analytic evaluation of one also holds for the other. It was found convenient always to keep to these variables so as to make the crossing relations explicit. Such seemingly simplifying procedures as choosing on the onset a special co-ordinate system tend to make the evaluation more complicated. For the same reason, it is more convenient to leave partial wave projection, if required, until the end of the evaluation. Secondly, we shall in what follows neglect the external meson mass μ. This gives errors of order μ^2/m^2 which for the pion–nucleon system is only about 2%. We must, however, not neglect the terms involving μ', the internal meson mass, for this will give the well-known infra-red divergence for zero-mass mesons. Even when the infra-red divergence is not apparent, the neglect of μ' often leads to errors of order $\log \mu^2/m^2$ or higher.

The Self-Energy diagrams can be reduced to integrals of the typical form given in eqn. (2.3). All these integrals can be integrated exactly. We shall give the integrals I as example:

$$\begin{aligned} I &= Q(s) - Q(m^2), \\ Q(s) &= \frac{m^2-\mu^2-s}{2s}\log\frac{m^2}{\mu^2} + R(s), \\ R(s) &= \frac{1}{2s}\,\Delta\log\frac{m^2-\mu^2-s+\Delta}{m^2-\mu^2-s-\Delta}\cdot\frac{m^2-\mu^2+s-\Delta}{m^2-\mu^2+s+\Delta}, \\ \Delta &= [(m^2-\mu^2-s)^2-4s\mu^2]^{1/2} \qquad \ldots\ldots\ldots \quad (2.4) \end{aligned}$$

where the value of the logarithm is to be taken on the principal sheet for real values of $s<(m+\mu)^2$. This is readily seen if we follow carefully the Feynman prescription (given by $i\epsilon$). The integral has a square-root branch-point at $s=(m+\mu)^2$. The seeming branch-point at $s=(m-\mu)^2$ cancels off on the 'physical' sheet. Related integrals have similar properties and will not be separately discussed.

A typical integral in the vertex diagrams is of the form

$$J=\int_0^1 dx\int_0^x dy\,\frac{1}{a_V{}^2-i\epsilon}$$

where

$$\left.\begin{aligned} a_V{}^2 &= a_m{}^2+K(1-x)y, \\ K &= m^2-s. \end{aligned}\right\} \qquad \ldots\ldots \quad (2.5)$$

Terms of order of the external meson mass have been neglected. After integrating over y, we have

$$J=\frac{1}{K}\int_0^1 dx\frac{1}{1-x}\log\frac{a_s^2-i\epsilon}{a_m^2}. \qquad (2.6)$$

This integral cannot be done in terms of elementary functions but can be reduced to the Spence Function defined by

$$f(x)=\int_0^x dy\frac{\log(1-y)}{y}. \qquad (2.7)$$

This function has been studied and tabulated by Mitchell (1949), to whose work we refer the reader for more information. With the knowledge of the Spence Function, the whole vertex diagram can be evaluated.

The diagrams (c) are by far the most difficult to evaluate, not only because of mere complication but also because the integrals are functions of two variables s and $\bar{s}$. A typical integral is of form

$$L=\int_0^1 dx\int_0^x dy\int_0^y dz\frac{1}{a_L^2-i\epsilon} \qquad (2.8)$$

where

$$a_L^2=m^2x^2+\mu^2(1-x)+K(1-x)y+\{(K+K')y-K'x-K\}z,$$
$$K=m^2-s,\quad K'=m^2-\bar{s}.$$

Terms of order of the external meson mass have again been neglected. Integrals of this type were calculated in this work by an expansion method. For $K'+K=0$, the integral L and related integrals can all be reduced algebraically to integrals already encountered in evaluating (a) and (b). Now L is analytic in K' at $K'+K=0$. We may thus expand in K' about this point. The nearest singularity on the K'-plane is at $t=-(K+K')=4m^2$. Since $t=2k^2(1-\cos\theta)$, where k is the centre-of-mass momentum, we expect the expansion to converge uniformly for all physical values of $\cos\theta$ for $k^2<m^2$. This criterion for convergence is readily satisfied for laboratory energies of up to several Bev. Thus

$$L(K,\ K')=L(K,\ -K)+2k^2(\cos\theta-1)\left.\frac{\partial L}{\partial K'}\right|_{K+K'=0}+\ldots \qquad (2.9)$$

Similarly we may expand the crossed diagram in K about $K+K'=0$. The expansion coefficients can then be reduced after a rather tedious calculation to known integrals. In the actual calculation the expansion has been carried to the second term so that p-wave contributions are taken consistently to the leading order.

It may be remarked here that in all the calculation above only terms of order μ^2/m^2 have been neglected, the internal meson mass has been retained throughout. The same method of evaluation can thus be applied without alteration to diagrams where the virtual particles are different from the incoming ones; e.g. strange particles, whose masses are too large to be neglected.

The projection into partial-wave states follows standard procedure (see, e.g. Jacob–Wick (1959)). Uncrossed diagrams are readily handled since the integrals depend only on the energy and not the momentum-transfer. For the crossed diagrams since the integrals are functions of $\cos\theta$, the projection into angular momentum states had to be done numerically. This is, however, not difficult since the functions are regular everywhere for physical $\cos\theta$.

The implications of the result of the calculation on the Edwards–Matthews method have already been discussed in § 1. A note containing the complete result of the evaluation and some intermediate steps is deposited in the Department of Mathematical Physics, University of Birmingham. Duplicates of this are available on application to the department.

ACKNOWLEDGMENTS

The author would like to thank Dr. S. F. Edwards for suggesting this investigation and for his constant help, to Professor R. E. Peierls, Dr. P. T. Matthews, Dr. J. Uretsky for interesting discussions and encouragement, and Dr. N. Cottingham for kindly checking part of the calculation. Thanks are also due to the Inter-University Council of London for a grant in the period during which the work was carried out.

REFERENCES

CHEW, G., and LOW, F., 1956, *Phys. Rev.*, **101,** 1570.
CZIFFRA, P., MACGREGOR, M. H., MORAVCSIK, M. J., and STAPP, H. P., 1959, *Phys. Rev.*, **114,** 3.
CINI, M., and FUBINI, S., 1954, *Nuovo Cim.*, **11,** 142.
EDWARDS, S. F., and MATTHEWS, P. T., 1957 a, *Phil. Mag.*, **2,** 467; 1957 b, *Ibid.*, **2,** 176.
JACOB, M., and WICK, G. C., 1959, *Ann. Phys.*, **7,** 4.
KROLL, N. M., and RUDERMAN, M. A., 1954, *Phys. Rev.*, **93,** 233.
LANDAU, L. D., 1959, *J. exp. theor. Phys.*, **37,** 1.
MANDELSTAM, S., 1958, *Phys. Rev.*, **112,** 1344.
MITCHELL, K., 1949, *Phil. Mag.*, **40,** 351.
SCHWINGER, J., 1951, *Proc. nat. Acad. Sci., Wash.*, **37,** 452.
WYLD, H. W., 1954, *Phys. Rev.*, **96,** 1661.

The Flow Stress of Metals at Low Temperatures†

By P. Feltham
Department of Metallurgy, The University, Leeds

[Received July 18, 1960]

Abstract

The collapse of narrow V-shaped notches formed in glide dislocations at points of close approach to dislocations threading the glide plane is shown to facilitate intersection without thermal activation. The force effecting intersection, which is a component of the line tension of the notches, subsequently assists the glide dislocation to overcome the drag of jogs formed in the process. A consequence of this dual function of the force is the Cottrell–Stokes law, i.e. the strain invariance, at any given temperature and strain rate, of the ratio τ_T/τ_G, where τ_T and τ_G are the temperature dependent and independent parts of the flow stress respectively. Linear and parabolic work-hardening laws are deduced from the model. On equating the slip distance to grain size in the parabolic relation the flow stress is found to be linear in (grain size)$^{-1/2}$, which is known to apply for example to zinc. The activation energy of the jog migration associated with τ_T, estimated from low temperature flow stress data, is equal to about $\frac{1}{3}$ ev in copper.

§ 1. Introduction

In his theoretical treatment of work-hardening Seeger (1954) suggests that the flow stress of a pure metal, $\tau(T)$, should be resolvable into two independent parts at low temperatures:

$$\tau(T)=\tau_G+\tau_T, \quad . \quad . \quad . \quad . \quad . \quad . \quad . \quad . \quad (1)$$

where τ_G depends upon temperature only as the shear modulus G, while τ_T increases approximately linearly with decreasing temperature, and depends logarithmically on the strain rate. Cottrell and Stokes (1955), and Cottrell and Adams (1955), who investigated the flow stress of aluminium and copper crystals, found that the ratio of the flow stresses at two temperatures $\tau(T_1)/\tau(T_2)$ was the same at any given strain, implying a proportionality between τ_G and τ_T. The relation was subsequently confirmed to hold also in polycrystaline metals (Basinski 1959), as well as in precipitation hardened alloys (Kelly *et al.* 1959). The object of the present work was to study this proportionality, and to attempt to elucidate its significance.

§ 2. The Dislocation Model

We shall relate our discussion to the dislocation configuration shown in the figure (a). The dislocation, in the form of circular arcs, is held up at lattice defects such as I; the precise nature of the defects will be considered later. For simplicity the dislocation will be assumed to be undissociated and of the edge type; the generality of the argument is not thereby affected. In order to migrate forward the dislocation must cut through the obstacle or drag it along. An activation energy, $Q(T)$, which may be a function of temperature, would therefore be required.

---

† Communicated by the Author.

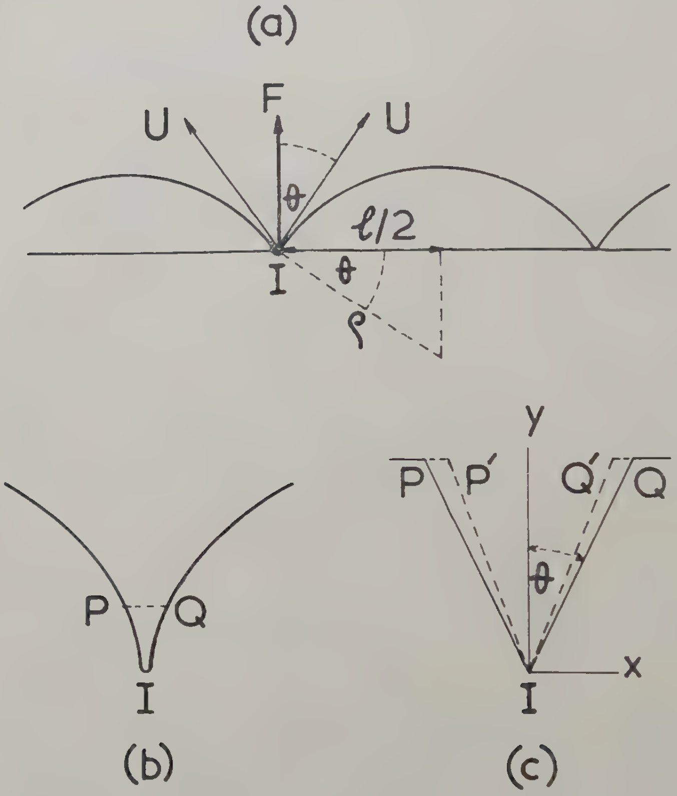

Early (*a*) and (*b*) late stages in the process leading to the intersection of the forest dislocation I; (*c*) idealized form of the cusp prior to collapse.

Now, if U is the line tension of the dislocation, and θ the angle between the tangent at I (figure (*a*)) and the direction of the Burgers vector (IF), the force on the defect is

$$F = 2U\cos\theta.$$

Expressed in terms of the curvature of the arc

$$U = \rho b(\tau - \tau_G), \qquad \ldots \ldots \ldots \qquad (2)$$

where, as in Seeger's model, τ_G is the temperature independent elastic stress opposing the applied stress, and b is the Burgers vector. As $\cos\theta = l/2\rho$, with l equal to the mean spacing between pinning points, we have

$$F = (\tau - \tau_G)bl \qquad \ldots \ldots \ldots \qquad (3)$$

and hence

$$Q(0)=(\tau-\tau_G)b^2l.$$

If flow is to take place at an observable rate then

$$Q(T)-(\tau-\tau_G)b^2l=mkT, \quad \ldots\ldots\ldots \quad (4)$$

where m is a constant approximately equal to 30; the actual value chosen will determine the flow rate at which the deformation takes place.

On writing

$$W(T)=Q(T)-mkT, \quad \ldots\ldots\ldots \quad (5)$$

the flow criterion becomes

$$b^2l(\tau-\tau_G)=W(T), \quad \ldots\ldots\ldots \quad (6)$$

which, on putting

$$\tau_G=\alpha Gb/l, \quad \ldots\ldots\ldots \quad (7)$$

yields

$$\tau=W(T)/b^2l+\alpha Gb/l. \quad \ldots\ldots\ldots \quad (8)$$

For the present we take α to be a constant of order 0·1–1; a more precise estimate will be obtained below. Fluctuations of internal stresses will be small in a work-hardened crystal, for at spots where α differed appreciably from the most probable value, e.g. where it is smaller, work-hardening would tend to occur preferentially, largely removing the discrepancy†.

On comparing eqns. (1) and (8) one finds

$$\tau_T=W(T)/b^2l, \quad \ldots\ldots\ldots \quad (9)$$

so that the ratio

$$\tau_G/\tau_T=\alpha Gb^3/W(T) \quad \ldots\ldots\ldots \quad (10)$$

is independent of l, and hence of the state of work-hardening of the crystal. The ratio of the flow stresses at two temperatures, obtained with the same specimen without intermediate recovery or deformation, i.e. with l constant, is also independent of the strain, as is clear from eqn. (8). The Cottrell–Stokes law is therefore obeyed by the model‡.

§ 3. WORK-HARDENING LAWS

Specific relations between l and the strain γ have to be assumed in deducing the work-hardening law of the metal. To do this we shall take as model a crystal cube of side L, with one set of parallel active slip planes

---

† This argument would not necessarily apply under conditions of 'easy-glide', when only a few widely spaced slip planes are active. In fact Seeger *et al.* (1957) and Basinski (1959) find deviations from the Cottrell–Stokes relation at low strains.

‡ The Cottrell–Stokes law is in fact implicit in power laws of the type $\tau=K(T,\dot{\gamma})(\gamma-\gamma_0)^m$ irrespective of the magnitude of the exponent m, for the ratio $\tau(T_1)/\tau(T_2)\neq f(\gamma)$ at $\gamma=$const.

d apart, each plane containing a group of equidistant dislocations of equal sign, with a mean spacing l. The total shear strain due to the dislocations is then

$$\gamma=(L^2/ld)(\tfrac{1}{2}b/L)=bL/2ld, \quad . \quad . \quad . \quad . \quad . \quad . \quad . \quad (11)$$

so that

$$l=bL/2\gamma d, \quad . \quad . \quad . \quad . \quad . \quad . \quad . \quad . \quad . \quad (12)$$

or, if $l=d$:

$$l=(bL/2\gamma)^{1/2}. \quad . \quad . \quad . \quad . \quad . \quad . \quad . \quad . \quad . \quad (13)$$

Equation (12), with $d>l$, should be applicable to single crystals or well-annealed polycrystals in the early stages of deformation, while eqn. (13) would be expected to represent the relation between the strain and the dimensions of the sub-structure more correctly at strains at which more than one slip system have become fully operative. On eliminating l between eqns. (8) and (12), and between (8) and (13) respectively. one obtains the linear and parabolic work-hardening laws

$$\tau=\lambda(T)\,\gamma, \quad . \quad . \quad . \quad . \quad . \quad . \quad . \quad . \quad . \quad . \quad . \quad . \quad (14)$$

with

$$\lambda=[W(T)+\alpha Gb^3](2d/Lb^3), \quad . \quad . \quad . \quad . \quad . \quad . \quad . \quad (15)$$

and

$$\tau=\zeta(T)\,\gamma^{1/2}, \quad . \quad . \quad . \quad . \quad . \quad . \quad . \quad . \quad . \quad . \quad . \quad . \quad (16)$$

where

$$\zeta=[W(T)+\alpha Gb^3](\tfrac{1}{2}b^5)^{-1/2}L^{-1/2}. \quad . \quad . \quad . \quad . \quad . \quad (17)$$

If the slip distance is equated to the grain size, then the flow stress given by eqn. (16) is linear in (grain size)$^{-1/2}$, which is known to be the case in zinc (Zein 1955) and molybdenum (Johnson 1959). Subgrain dimensions (Ball 1957), or even smaller elements of substructure (Feltham and Meakin 1957) may determine L in face-centred cubic metals. In eqn. (15) L and d, but not L/d may vary with the strain.

§ 4. THE ACTIVATION ENERGY Q

At 4·2°K the ratio τ_G/τ_T in copper crystals is about 10, (Basinski 1959), so that eqns. (5) and (10) yield, on taking $T=0$,

$$Q=0{\cdot}1\alpha Gb^3 \quad (\text{at } 4{\cdot}2^\circ\text{K}). \quad . \quad . \quad . \quad . \quad . \quad . \quad . \quad (18)$$

As $Gb^3\simeq 5$ ev in copper we have

$$Q=0{\cdot}5\alpha\,\text{ev}. \quad . \quad . \quad . \quad . \quad . \quad . \quad . \quad . \quad . \quad . \quad (19)$$

Now, a further estimate of Q can be made by considering that the pronounced temperature dependence of the flow stress in copper on lowering the temperature begins to be observed at about 150°K; at still lower temperatures $W(T)$ in eqn. (16) must therefore be positive, i.e. non-zero. Thus, taking $W(T)=0$ at 150°K, and $m=30$, eqn. (5) yields

$$Q=0{\cdot}37\,\text{ev} \quad (\text{at } 150^\circ\text{K}). \quad . \quad . \quad . \quad . \quad . \quad . \quad . \quad (20)$$

If the temperature dependence of Q is assumed inappreciable between 4 and 150°K, comparison of eqns. (19) and (20) shows that

$$\alpha = 0{\cdot}75. \qquad (21)$$

suggesting that the applied stress at low temperatures is close to the 'Frank–Read stress' Gb/l. This result indicates that the obstacle (I in figure 1 (a)) is not intersected by a cutting mechanism of the type considered, for example, by Thornton and Hirsch (1958), which would require an activation energy considerably higher than the value of Q indicated above (Friedel 1956, Seeger 1955 a, Seeger *et al.* 1959). We believe that the mechanism by which the glide dislocation passes through the obstacle I, which we shall now take to be a dislocation on an intersecting glide plane, probably occurs as follows.

Considering the edge dislocation in the figure (a), we see that on increasing the stress the arms of the dislocation cusp with node at I will reach a critical configuration (figure (b)) at which the segments IP and IQ, which are virtually pure screw dislocations of opposite signs, will cancel, leaving a small jogged loop around I. If I is a screw dislocation a jog will also remain on the glide dislocation. As IP and IQ lie on adjacent slip planes, a line of vacancies or interstitial atoms will remain over the length over which the screw dislocation segments annihilated. The jogged loop around I would shrink under its own line tension, and disappear, leaving a jog in the forest dislocation I. This process of dislocation intersection would not be significantly temperature dependent, but it would not lead to flow unless the glide dislocation can migrate from points such as I after intersection. If a jog is left in the glide dislocation after intersection then the subsequent migration will be assisted by thermal activation of the movement of the jog, the latter being subject initially to the *same* force as the forest dislocation I at the instant of 'intersection'. The rate determining process of the flow can therefore be regarded as consisting of two stages; the first, which is not thermally activated, results in the formation of jogs in (glide) dislocations, while the second involves slip of the glide dislocation. The second should be temperature dependent, with an activation energy equal to that of jog migration, i.e. numerically equal to that of vacancy formation for screw/screw jogs (Seeger 1955 b) or somewhat less for jogs in edge dislocations (Maddin and Cottrell 1955). Activation energies determined from flow stress and logarithmic creep data by Thornton and Hirsch (1958) are $0{\cdot}7 \pm 0{\cdot}35$ ev for copper at 80°K; Feltham (1961) associates about $\frac{1}{3}$ ev with the migration of jogs in edge dislocations in copper, with somewhat higher values for alpha-brasses. These experimentally determined activation energies are therefore comparable with the Q's deduced above (eqn. (20))

A further inference of the anlysis relates to the dislocation configuration near I (figure (b)) just prior to collapse of the cusp; eqn. (21) indicates that a narrow cusp is to be expected, with PIQ only a few degrees. Now, the approximate shape of the cusp as the flow stress is being attained can be established from the following considerations.

We assume *PI* and *QI* to be coplanar screw dislocations of opposite signs, and take for the stress between them

$$\tau_i(s)=Gb/2\pi(2s\theta+w), \qquad (22)$$

where s is the distance of a point along *IQ* (or *IP*) measured from *I* along the curve, θ is now taken to be the angle of a notch with straight sides obtained by joining *IP* and *IQ* as shown in the figure (*c*), and w is a length of the order of the diameter of the cusp at the node. Taking the applied stress to be $\alpha Gb/l$, the radius of curvature is

$$\rho(s)=(U/b)/[\alpha Gb/l + Gb/2\pi(2s\theta+w)], \qquad (23)$$

or, with $U=\frac{1}{2}Gb^2$,

$$1/\rho=2\alpha/l + 1/\pi(2s\theta+w). \qquad (24)$$

The curvature ρ^{-1} is thus high for small s†. The interaction will therefore be negligible beyond a small region of the cusp close to *I*, and we shall confine our attention to a small zone *PIQ*, approximating to the arms of the cusps by straight segments bent sharply at *P* and *Q* figure (*c*). Again measuring s along *IQ*, the work done on the field between the dislocation, in moving them from *PIQ*, to *P'IQ'* as shown in the figure (*c*), is

$$dE(\theta)=-2\int_I^Q \frac{(Gb^2d\theta)}{2\pi}\cdot\frac{s\,ds}{2s\theta+w}, \qquad (25)$$

which, omitting w in the denominator of the integrand, gives

$$dE(\theta)=-(s_{IQ}Gb^2/2\pi\theta)d\theta. \qquad (26)$$

The associated increase in the line energy of the cusp is

$$dE(U)=2Us_{IQ}\,d\theta=Gb^2s_{IQ}\,d\theta. \qquad (27)$$

The criterion of instability

$$d[E(\theta)+E(U)]/d\theta=0 \qquad (28)$$

then yields

$$\theta_{\text{crit}}=1/2\pi. \qquad (29)$$

The 'clipping-off' process of intersection will therefore occur when the angle *PIQ* has diminished to about 18°. This estimate agrees with the implications of eqn. (21).

---

† On using the intrinsic equation $d\psi/ds=1/\rho$, eqn. (24) is easily shown to represent the spiral

$$\psi=2\alpha s/l+(1/\pi\theta)\ln(1+2s\theta w^{-1}).$$

REFERENCES

BALL, C. J., 1957, *Phil. Mag.*, **2,** 1011.
BASINSKI, Z. S., 1959, *Phil. Mag.*, **4,** 393.
COTTRELL, A. H., and ADAMS, M. A., 1955, *Phil. Mag.*, **46,** 1187.
COTTRELL, A. H., and STOKES, R. J., 1955, *Proc. roy. Soc.* A, **233,** 17.
FELTHAM, P., and MEAKIN, J. D., 1957, *Phil. Mag.*, **2,** 1237.
FELTHAM, P., 1961, *Phil. Mag.*, **6,** 259.
FRIEDEL, J., 1956, *Les Dislocations* (Paris: Gauthier-Villars).
JOHNSON, A. A., 1959, *Phil. Mag.*, **4,** 194.
KELLY, A., LASSILA, A., and SATO, S., 1959, *Phil. Mag.*, **4,** 1260.
MADDIN, R., and COTTRELL, A. H., 1955, *Phil. Mag.*, **46,** 735.
SEEGER, A., 1954, *Z. Naturf.* A, **9,** 870; 1955 a, *Phil. Mag.*, **46,** 1194; 1955 b, *Defects in Crystalline Solids* (London : The Physical Society).
SEEGER, A., DIEHL, J., MADER, S., and REBSTOCK, H., 1957, *Phil. Mag.*, **2,** 323.
SEEGER, A., BERNER, R., and WOLF, H., 1959, *Z. Phys.*, **155,** 247.
THORNTON, P. R., and HIRSCH, P. B., 1958, *Phil. Mag.*, **3,** 738.
ZEIN, F. N., 1955, Ph.D. Thesis, The University, Leeds.

Evidence for the Production of Debris by Moving Dislocations in Sodium Chloride†

By R. W. DAVIDGE and R. W. WHITWORTH‡
Department of Metallurgy, Imperial College, London, S.W.7

[Received June 16, 1960]

ABSTRACT

Several kinds of etch pit are formed when NaCl is etched with a mixture of acetic acid and methyl alcohol. In particular, slip bands contain shallow pointed pits in addition to the normal pits formed at dislocations. The density of these shallow pits is reduced by an anneal at around 300°c before etching, and it is believed that they originate at ' debris ' left behind moving dislocations. Debris is also produced by the to-and-fro motion of edge and screw dislocations in crystals vibrated at high amplitudes at 90 kc/s, and this effect is related to a decrease in the internal friction. Experiments on LiF show that three etches which reveal dislocations differ in the extent to which they also reveal debris.

§ 1. INTRODUCTION

THE technique of etching ionic crystals to reveal dislocations is now well established (see for example Gilman and Johnston 1957), and the present paper describes the results of a series of etch-pit observations on crystals of NaCl. The main feature of these experiments is that the etch produces pits of various types, only some of which can be attributed to the presence of normal dislocation lines. Slip bands in crystals etched after static deformation or vibration at 90 kc/s have often been observed to contain pits which do not appear to be formed at dislocations ; the presence of these additional pits suggests that under certain conditions ' debris ' is left behind moving edge or screw dislocations.

In the case of LiF somewhat similar results have been reported by Johnston and Gilman (1960), who observed indistinct pits on the slip planes of expanded dislocation loops. They attribute these pits to debris produced by moving dislocations, and Keith and Gilman (1959) suggest that this debris consists of point-defect clusters. The extent to which pits are formed at debris depends on the etch used, and in this respect the etches of Gilman and Johnston are not very effective.

§ 2. EXPERIMENTAL TECHNIQUES

The experiments were performed on specimens cleaved in $\{100\}$ orientation from single crystals grown from Analar grade NaCl by a modified Kyropoulos method. These specimens were annealed at 650°c to remove the internal stresses produced by cleavage, and then cooled to room temperature over a period of several hours.

---

† Communicated by Dr. P. L. Pratt.
‡ Now at Department of Physics, University of Birmingham.

The specimens were etched in a mixture of 1 part of methyl alcohol with 2 to 4 parts of glacial acetic acid for 10 to 30 sec, washed in anhydrous ether and dried in a stream of cold air. This method was found to be more satisfactory than those described by Amelinckx (1954) and Moran (1958), which required very short etching times.

A chemical polish was used to remove the surfaces of specimens so that internal surfaces could be etched. It consisted of a mixture of 1 part of methyl alcohol with 2 parts of ethyl alcohol, and removed about 0·7 μ per min leaving the surface covered with extremely shallow overlapping pits.

The etch pits were photographed in oblique incident light, except in a few cases where incident phase-contrast microscopy was used.

§ 3. OBSERVATIONS

3.1. *Etch Pits in Undeformed Crystals*

Figure 1† shows part of the etched as-cleaved surface of an undeformed crystal. The pyramidal pits have their edges in $\langle 100\rangle$ directions, and the faces of most of these pits make an angle of about 10° to the crystal surface. However, some of them are shallower than this, and a similar effect has been reported by Amelinckx (1954). It is believed that all these pyramidal pits are formed at dislocations, and this is supported by the observation that there is a one-to-one correspondence between such pits on the matched cleaved faces of undeformed crystals. The etch often produces flat-bottomed pits along cleavage steps, as shown in fig. 1, and these pits may originate at very small dislocation loops formed at the step. Similar flat-bottomed pits also form at random sites, particularly on annealed surfaces.

In addition to pyramidal and flat-bottomed pits, a high density of very shallow poorly resolved pits was observed in a specimen that was x-irradiated to produce some permanent coloration and then polished and etched. Pits of this type have been observed by Aerts *et al.* (1959), who attributed them to point defect clusters produced during the irradiation. Similar unresolved pits are formed in crystals containing 0·02% $CdCl_2$.

3.2. *Statically Deformed Crystals*

3.2.1. *Dislocations produced at indentations*

A convenient way of introducing a controlled number of dislocations into a specimen is to deform it with a microhardness indenter; subsequent etching produces a ' rosette ' of pits, and fig. 2 shows part of such a rosette. Practically all the pits formed in rosettes are identical, both on external surfaces and on surfaces polished after indentation; these pits are similar to the majority of those attributed to dislocations in undeformed crystals. When indented and etched specimens were strained slightly to move the dislocations and re-etched, many flat-bottomed pits were observed together with similar numbers of smaller pointed pits. These observations indicate that the pointed pits originate at dislocations, and they will hereafter be called normal pits; it seems reasonable to assume that all fresh dislocations should produce this type of pit.

---

† All figures are shown as plates.

3.2.2. *Edge slip bands*

Many experiments have been performed to study the pits formed by etching crystals which had been deformed until a few slip bands were produced. The surface of the crystal present at the time of deformation will be called an external surface, and one subsequently exposed by cleavage or polishing an internal surface. A slip band in a $\langle 110\rangle$ direction where pits are formed at edge dislocations will be called an edge slip band, while one in a $\langle 100\rangle$ direction with pits at screw dislocations will be called a screw slip band.

Figure 3 shows etch pits along part of an edge slip band on an internal surface, which was exposed by cleavage and then etched. It is clear that there are at least two types of pit in this band: normal pits, and others which are shallower and somewhat smaller. The proportion of normal to shallow pits varies considerably, there being rather more shallow pits than average in fig. 3. There are, however, almost always some shallow pits in slip bands on internal surfaces, unless the density of normal pits is so large that the others are masked. The density of shallow pits on external surfaces is usually much smaller than that on internal surfaces. Both normal and shallow pits sometimes become flat-bottomed during a single etch, and in some cases they start to grow again at a point slightly displaced from the centre of the original pit. This intermittent etching is similar to that described by Johnston and Gilman (1960), and some examples are shown in fig. 4.

Relatively few shallow pits form on slip bands in crystals that have been annealed at 200–300°C subsequent to deformation. To demonstrate this effect a specimen was lightly deformed, cleaved in half to expose an internal surface, polished for 1 min and etched. It was then annealed for 1 hr at 250°C, furnace cooled, polished for 1 min to remove all the etch pits, and re-etched. Figure 5 (*a*) shows a region of the cleaved surface after the first etch, in which several edge slip bands are visible with normal and shallow pits along them. The same region photographed after the second etch is shown in fig. 5 (*b*), where the shallow pits are considerably fewer in number and less distinct than in fig. 5 (*a*).

Similar investigations have shown that the number of shallow pits of this type formed on a given surface can also be reduced by irradiating the surface with unfiltered 50 kv X-rays until some permanent coloration is produced.

The different appearance of normal and shallow pits and their different behaviour in the annealing and irradiation experiments indicate that they do not originate at the same type of defect. The normal pits can fairly reliably be attributed to ordinary dislocation lines or to pairs of edge dislocations of opposite sign as proposed by Johnston and Gilman (1960). The origin of the shallow pits, however, must differ from that of the normal pits, and they are probably formed at some kind of ‘debris’ left on the slip planes by moving dislocations. The effect of annealing or irradiation must be to disperse this debris, or to modify it so that it is no longer attacked by the etch.

3.2.3. *Screw slip bands*

Pits other than normal etch pits are formed on screw as well as edge slip bands, but in this case the situation is more complicated. When the external surface of a lightly deformed crystal is etched, screw slip bands are found to contain pits of many depths and sizes ranging from normal pits down to ‘streaks’ comprised of very shallow pits lying in ⟨100⟩ directions. Part of such a slip band photographed in oblique incident light is shown in fig. 6 (*a*), and fig. 6 (*b*) shows the same area under phase-contrast illumination, which reveals the streaks more clearly. After polishing or cleaving through an existing slip band, the streaks formed on etching are fewer and much less distinct, although both normal and shallow pointed pits are still formed; figs. 6 (*c* and *d*) show the same areas as figs. 6 (*a* and *b*) after polishing for 1 min and re-etching. The dislocations revealed as normal pits have moved during handling between the two etches, and there are indications that some dislocations have also moved during etching.

In contrast to the streaks, the shallow pits observed on screw slip bands occur both on external and internal surfaces; they will be attributed to debris, and this may be related to that giving rise to shallow pits on edge slip bands. The density of shallow pits is considerably reduced in specimens etched after annealing at 250–350°c subsequent to deformation, this temperature range being slightly higher than that quoted for edge slip bands.

The streaks of very small pits on screw slip bands are observed on surfaces across which screw dislocations have moved, whether the surfaces be annealed, as cleaved or polished, and it is interesting to note that slip steps should occur under these conditions. Streaks have not been seen, however, in the vicinity of screw dislocations in rosettes. It is not clear whether streaks on internal surfaces, like those in fig. 6 (*d*), arise from defects present in the crystal, or whether they are associated with movement of dislocations across the newly formed surface during handling. On several occasions similar streaks have been seen on freshly cleaved and etched surfaces in regions where there are no dislocations other than those in sub-grain boundaries. An example is shown in fig. 7, where the streaks are seen to consist of small pits in ⟨100⟩ rows which terminate at a sub-grain boundary and a cleavage step.

3.3. *Crystals Vibrated at High Amplitudes*

In a previous paper Whitworth (1960) described some changes in the internal friction of NaCl crystals vibrated at high amplitudes at a frequency of 90 kc/s. In particular, these experiments showed that the amplitude-dependent damping of lightly deformed specimens is reduced by vibration at strain amplitudes above about 3×10^{-5}. Specimens given this vibration treatment have now been studied by etching, and the observations suggest that debris is produced by oscillating edge and screw dislocations; this result probably accounts for the reduction in damping by a mechanism involving the pinning of dislocations. Somewhat similar observations of the production of debris by dislocations moving in LiF under a cyclic stress have been made by Keith and Gilman (1959).

The results of § 3.2.1 indicate that very little debris is formed around indentations, and the specimens used in the present work were therefore deformed in this manner. In a typial experiment a specimen was polished, indented, and vibrated at a maximum strain amplitude of $2{\cdot}6 \times 10^{-4}$, where the maximum reduction in damping was obtained. This crystal was then etched, and a portion of one of the rosettes so formed is shown in fig. 8 (*a*). Figure 8 (*b*) shows the same area after polishing for 3 min and re-etching. These figures show that shallow pits are produced on the slip planes of edge and screw dislocations, both on external and internal surfaces. Streaks are also produced by individual screw dislocations, but only on the external surface. Vibration of crystals at the amplitude reached in this case creates new dislocations, as was shown by Whitworth (1960), and it is possible that this effect has caused some multiplication of the dislocations in the rosette, giving rise to more normal pits than are usually observed.

Figure 9 shows the shallow pits associated with some edge dislocations in a rosette in another crystal vibrated at a smaller strain amplitude ($2{\cdot}0 \times 10^{-4}$), where nucleation of new dislocations does not occur; the pits shown are on an internal surface, the crystal having been polished for 3 min between vibration and etching. Shallow pits of this type have never been observed at rosettes in any crystal which had not been given a high amplitude vibration. When the specimen of fig. 9 was annealed for 1 hr at 300°C, polished and re-etched, very few shallow pits were formed.

From these observations it appears that a single dislocation, moving backwards and forwards on its slip plane under the oscillating stress, produces some form of debris in its vicinity. The length of each group of pits is of the order of 10^{-3} cm, which is quite comparable with estimates from internal friction measurements of the distances through which the dislocations should move.

3.4. *Experiments on Lithium Fluoride*

A few experiments on LiF have been performed, to look for evidence of debris which could be revealed by etching. The LiF used was supplied by Taylor, Taylor and Hobson Ltd. and was harder and probably more impure than the crystals from the Harshaw Chemical Co. used by Gilman and Johnston. Before use, the material was annealed for 12 hr at 800°c and cooled over 12 hr.

Three reagents were used to etch the crystals: the etches A and W of Gilman and Johnston (1957), and another etch, ' H ', consisting of a 6% aqueous solution of hydrogen peroxide, similar to that used by Urusovskaya (1958). It was found that only etch H formed an appreciable number of shallow pits on slip planes in lightly deformed crystals. To illustrate this observation, fig. 10 shows the matched faces of a crystal which was cleaved in half after deformation; one half (*a*) was etched with W, and the other (*b*) with H. It is seen that on edge slip bands H forms poorly defined pits which are additional to the normal pits formed by both H and W. Experiments to study the effect of annealing on the debris are unsatisfactory, because etch H, like etch W, produces poorly defined pits at dislocations in crystals annealed at temperatures above 200°c.

Although etch H is more successful than A or W in revealing debris on active slip planes in LiF, it compares unfavourably with the present etch for NaCl. Nevertheless, the results provide evidence that debris is formed by the deformation of both LiF and NaCl.

§ 4. Discussion

The preceding paragraphs describe the production of etch pits in variously treated crystals of NaCl. Three main types of etch pit are formed as a consequence of plastic deformation: normal pits due to dislocations, shallow pits, and streaks. The streaks appear to be mainly a surface phenomenon, and as their origin is obscure, they will not be discussed further. Shallow pits, however, occur on internal as well as external surfaces, and thus show that some defects other than normal dislocation lines are left on slip planes during deformation; these defects are referred to as debris. It should be noted that very few shallow pits occur in rosettes, and the nature of the deformation must therefore be important in determining the amount and distribution of the debris produced.

Some indication as to the nature of the debris can be obtained from the shape of the shallow pits, which are pointed and fairly well defined. In this respect they differ from the very shallow poorly resolved pits, which are formed in irradiated and impure crystals, and believed to be due to clusters of point defects. A piece of debris therefore differs from a simple cluster of defects, probably because it extends into the crystal for a distance at least equal to the depth of its etch pit ($\sim 0{\cdot}1\,\mu$ in fig. 3).

One possible mechanism for the production of these linear defects is the process of dislocation multiplication by the cross-glide of screw dislocations discussed by Johnston and Gilman (1960). When the distance of cross-glide is large, {100} dislocation loops are produced, and these should etch-up on screw slip bands. However, small amounts of cross-glide lead to the formation of pairs of edge dislocations of opposite sign lying on nearby slip planes, and these pairs, or dipoles, probably give rise to many of the normal etch pits in edge slip bands in LiF and NaCl. This belief is supported by observations of intermittent etching, although in NaCl it is hard to distinguish this effect from the movement of dislocations during the etch. When the dislocations forming a dipole are only a few atomic spacings apart, their elastic fields largely cancel out, and in the limiting case the dipole becomes a column of vacancies or interstitial ions. Such close dipoles may etch up differently from dislocations or wider dipoles, and could be the origin of the shallow pits in edge slip bands; the depth of the pit might then depend on the precise nature of the dipole.

The motion of jogged dislocations can produce similar trails of defects lying in any direction on the slip plane other than that parallel to their Burgers vector. These trails should, however, be most stable when the density of defects along them is high, and this would favour the $\langle 100 \rangle$ orientation. Shallow pits may form at such trails, and could thus occur in both edge and screw slip bands, although the former will be favoured if the stability criterion is important.

The above suggestions about the nature of the debris are only a few of the many which could, no doubt, be proposed. They do suggest, however, that the pits in edge and in screw bands may be formed at different kinds of debris. Almost any type of debris, such as close dipoles, columns of defects or very small dislocation loops, would be expected to disperse on annealing at some temperature lower than that required for large scale dislocation climb, and this is consistent with the observed annealing characteristics of the shallow pits. The results indicate that x-irradiation also breaks up debris, either directly or by the motion of the point defects which it produces. There does not seem to be sufficient information available to make deductions about the precise nature of the debris from the annealing and irradiation experiments.

No process has yet been proposed which would give rise to debris by the backward and forward motion of a pure edge dislocation, and yet debris is observed around edge dislocations in vibrated crystals. A possible explanation is that the motion of edge dislocations may be rather complex in this case, involving the production of kinks in screw orientation which can then cross-glide. The formation of large amounts of debris around dislocations should interfere with their motion, and the production of debris may therefore account for the decrease in damping of vibrated crystals that was observed by Whitworth (1960).

ACKNOWLEDGMENTS

This work was supported by a D.S.I.R. Grant for Special Research, one of us (R.W.W.) holding a research fellowship on this grant, and the other (R.W.D.) a D.S.I.R. research studentship. We wish to thank Professor J. G. Ball for the provision of research facilities in the Department of Metallurgy at Imperial College, and the leader of the Research Group, Dr. P. L. Pratt, for his encouragement and his criticism of the manuscript.

REFERENCES

AERTS, E., AMELINCKX, S., and DEKEYSER, W., 1959, *Acta Met.*, **7,** 29.
AMELINCKX, S., 1954, *Acta Met.*, **2,** 848.
GILMAN, J. J., and JOHNSTON, W. G., 1957, *Dislocations and Mechanical Properties of Crystals*, ed. Fisher *et al.* (New York : Wiley), p. 116.
JOHNSTON, W. G., and GILMAN, J. J., 1960, *J. appl. Phys.*, **31,** 632.
KEITH, R. E., and GILMAN, J. J., 1959, *A.S.T.M. Symposium on Basic Mechanisms of Fatigue.* Special Technical Publication No. 237, p. 3.
MORAN, P. R., 1958, *J. appl. Phys.*, **29,** 1768.
URUSOVSKAYA, A. A., 1958, *Kristallografia*, **3,** 726.
WHITWORTH, R. W., 1960, *Phil. Mag.*, **5,** 425.

Demagnetization of Igneous Rocks by Alternating Magnetic Fields†

By E. Irving, P. M. Stott and M. A. Ward
Department of Geophysics, Australian National University,
Canberra, A.C.T.

[Received May 31, 1960]

Abstract

The presence of secondary components of magnetization in basalts often limits the usefulness of their directions of natural remanent magnetization for palaeomagnetic work. These secondary components may be removed by alternating magnetic fields. The procedures for doing this are described and tests based on the internal consistency of the results are devised to judge their reliability. These are applied successfully to a series of results from specimens collected from the Tertiary basalts of New South Wales, Australia, and a determination of the geomagnetic field in S.E. Australia during the Lower Tertiary is obtained. A study of the behaviour of these basalts in high alternating fields suggests that most of the iron mineral grains have a multi-domain character, and contain a hard and soft component in the ratio of about 1 : 10.

§ 1. Introduction

In order to obtain the direction of the ancient geomagnetic field from a study of rock magnetism it is necessary to measure the direction of the primary component of magnetization acquired at the time the rock is formed. This primary magnetization is often seriously affected by secondary components, which are added later, and which render the direction of the *natural remanent magnetization* (NRM) of little use for precise palaeomagnetic work.

Lavas, on cooling through their Curie point, acquire a primary *thermo-remanent magnetization* (TRM) in the direction of the earth's field. If magnetic particles with relaxation times less than the geological age of the rock are present, a secondary component is acquired different in direction from the primary one if the direction of the geomagnetic field has changed since the latter was acquired. This is viscous magnetization and such components have the form of an *isothermal remanent magnetization* (IRM). Rock specimens containing grains with relaxation times in the earth's field of the order of 10^2 or 10^3 years will contain components of magnetization along the present dipole field. Relaxation times of 1 to 100 years will produce magnetizations close to the present field, whereas shorter relaxation times produce further viscous components dependent on the conditions of storage. This latter type of secondary components has been termed temporary components by Creer (1957). Secondary components are the most substantial source of error in palaeomagnetic studies and may be removed by alternating magnetic fields. The problem is to find the alternating field conditions necessary for their removal and yet ensure that a measurable component of primary origin remains. Because of the variation in magnetic minerals the field strength will not necessarily be the same for all lava types even within the same formation.

---

† Communicated by the Authors.

In general the removal of unwanted secondary components from specimens collected from a lava sequence will decrease the scatter in the directions of magnetization. We suggest that certain consistency conditions should be fulfilled before the secondary components may be judged to have been removed. Compared with the directions of NRM ($\mathbf{M}_n$) the directions after removal of the secondary components should have these characteristics.

(1) The scatter between specimens taken from the same lava flow (within-site dispersion) should either remain constant or should decrease.

(2) The agreement between the mean directions of different lava flows (between-site dispersion) should be much improved.

(3) Assuming the average dipole character of the earth's field the mean direction of magnetization for all flows should agree with similar results from rock formations of comparable age in the same region after correction for differences in geographical location.

These conditions apply to the great majority of lava sequences which were laid down in a period of time during which the geomagnetic field had an approximately constant direction (irrespective of sign) different from the present field. The first will in most cases be necessary, but it is possible to envisage situations in which the within-site scatter increases slightly after removal of the secondary component. The second is a necessary and the most important condition. The third is also necessary given the stated assumption. As a test of these conditions basalt specimens from several lava flows have been treated in alternating magnetic fields (§§ 2, 3, 4 and 5).

Further experiments on the same specimens were carried out in alternating magnetic fields to study the behaviour after removal of most of the primary magnetization and it was not found possible to reduce the moment beyond a certain limit, called the *minimum intensity*. This property, which may be of some interest in the theory of NRM of basalts, is discussed in § 7. In § 8 an attempt is made to relate the primary and secondary components to the ferromagnetic grains present.

2. DEMAGNETIZATION BY ALTERNATING MAGNETIC FIELDS

The procedure is to subject a rock specimen (in the absence of a steady field) to an alternating field which is reduced smoothly. The demagnetizing instrument used is similar to that recently described by Creer (1959). Specimens are placed in a holder which spins inside a set of coils which annul the earth's field. The alternating field is provided by a solenoid mounted on a trolley running on an aluminium tramway. The field at the specimen is reduced by withdrawing the trolley to a distance of 3 m at which point the field is reduced by a factor of 3×10^5.

Two pairs of square coils (Parry 1957) side length 180·2 and 165·9 cm and separations 98·2 and 90·4 cm and each with 100 turns annul the horizontal and vertical components of the earth's field respectively. Chokes are included in both circuits to reduce the effect of any mutual inductance with the solenoid, which in any case should be zero since the solenoid axis and tramway are set perpendicular to the magnetic meridian and to the axes of the Parry coils. The demagnetizing solenoid (i.d. 14·7 cm, o.d. 20·8 cm, length 12·5 cm) contains 1920 turns in 20 layers of 18 s.w.g. enamelled copper wire and is similar to that described by Parry (1957). The resistance is 15·6 Ω and inductance 0·5 H. The coil has been calibrated by a.c. and d.c. methods and both methods agree to 1% and give a calibration of 105 oersteds/amp. Power is provided by public supply mains (240 V; 50 c/s) through a bank of condensers (20 μF), which, with the coil, form a circuit tuned to 50 cycles. This reduces undesirable harmonics and as an extra precaution a series-resonant circuit tuned to 100 cycles has been connected in parallel. The required voltage is obtained from a variable transformer. The rotations about the vertical and horizontal axes are in the ratio 15 : 16. Gears provide primary rotation rates about the vertical axis of 140, 350, 525 and 700 rev/min, which do not resonate with any simple fraction of the mains frequency. It was found experimentally that the results are unaffected by changes within this range and the lowest rate has been used in these experiments.

The direction and intensity of magnetization of each specimen is first measured using an astatic magnetometer. Directions are determined to 3° and intensity to 5%. The specimen is treated in a small alternating field and then remeasured. Treatment in a higher field is then given and further measurements taken, and so on. The peak values ($H_{\mathrm{p}}\sim$) of the alternating fields used are always quoted. The field strengths generally used are 75, 150, 300, 450, 600 and 750 oersteds, although in many cases intermediate steps are included. Provided the field used is less than that required to reduce the specimen to its minimum intensity (a situation which is explained later) repeat treatments give the same results.

§ 3. Rock Specimens Studied

The rock specimens chosen for study were collected from eight sites (fig. 1) in the Tertiary Basalts of New South Wales (see general account of geology in David (1950)). The specimens were chosen because they showed different degrees of magnetic stability. The NRM consists of a primary component together with secondary components of varying magnitude directed approximately along the present geomagnetic field or along the field during storage in the laboratory.

Natural exposures in these basalts are always extensively weathered and the collections have been made in fresh exposures in quarries and

Fig. 1

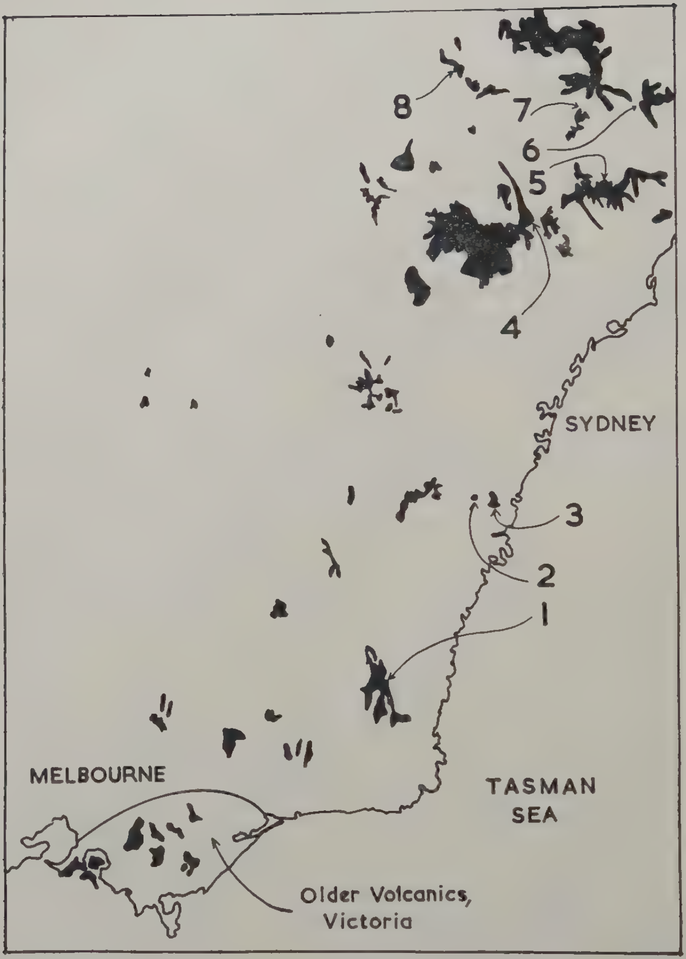

Locality sketch-map. The basalt outcrop is in solid black. The collecting localities are numbered **1** to **8** as in the text and tables. The Older Volcanics of Victoria which has been studied previously are also marked.

1. Road cutting 2 km N of Nimmitabel on Monaro Highway.

2. Road cutting on Hume Highway, 5 km NE of Berrima (Site B, Green and Irving 1958), (Map reference : Mittagong 370437).

3. Three sites, one in Robertson village (Kiama 627294), one on Robertson-Moss Vale Road, 3 km W of Robertson (Kiama 560284) and the third on Belmore Falls Road (Kiama 594275).

4. Road cutting, Nundle–Timor Road, 18 km SW of Nundle.

5. Road cutting on Oxley Highway, 53 km E of Walcha.

6. Road cutting on the Guyra Road, 5 km S of Ebor.

7. Two quarries, one on site of University of New England and the second $2\frac{1}{2}$ km NW of Armidale.

8. Road cutting 50 m W of bridge over Myall Creek on Delungra–Bingara Road, 24 km E of Bingara.

Table 1. Mean site directions and poles. The collecting sites are numbered in the text and figures. S is the number of samples and N is the number of specimens cut from these. Mean site directions of NRM and the mean directions after removal of the secondary and temporary components are given. The lavas are flat-lying and no correction for geological tilt is necessary. D is the declination east of true north, I is the inclination positive downwards, R is the resultant and k is Fisher's (1953) precision parameter. The mean pole is 63 S, 137 E ($N=8$, $R=7{\cdot}21$, $\alpha(P0{\cdot}05)=20°$)

Collecting sites	Lat. S.	Long. E.	S	N	Mean directions of NRM				Mean directions after treatment in alternating fields				Pole position (primary magnetization)	
					D	I	R	k	D	I	R	k	Lat. S	Long.
1. Nimmitabel	36° 30′	149° 16′	2	4	167	+59	3·50	6	166	+88	3·63	8	40	150E
2. Berrima	34° 28′	150° 23′	7	11	187	+76	10·78	44	164	+79	10·92	177	54	160E
3. Robertson	34° 36′	150° 34′	6	11	Random		3·43	—	240	+75	8·43	4	44	117E
4. Liverpool Ranges	31° 38′	151° 41′	2	4	57	−12	3·94	54	140	+47	3·92	41	55	126W
5. Yarrowitch	31° 15′	151° 58′	7	16	274	+46	13·32	6	219	+60	15·35	23	57	91E
6. Ebor	30° 25′	152° 20′	3	5	190	+60	4·41	7	191	+62	4·53	8	74	122E
7. Armidale	30° 31′	151° 39′	6	10	166	− 3	7·78	4	199	+45	9·46	17	73	55E
8. Myall Creek	29° 47′	150° 44′	3	5	92	+84	4·94	65	209	+82	4·88	33	44	140E

road-cuttings spread over a meridional distance of 650 km. The basalts are flat-lying and no geological correction to the directions of magnetization is necessary. In six cases, each site is a quarry or road-cutting in which the samples cover 5–10 m in a single flow. At Armidale (Site **7**) samples were obtained from two quarries about 1 km apart. At **3**, three road-cuttings 2–3 km apart west of the village of Robertson were sampled. At both these sites more than one flow may be represented, although if this is so they cannot be much separated in time. Several separately orientated samples have been taken at each site and from each sample one or more cylindrical specimens (3·5 cm diameter, 3·5 cm height) have been cut. The details are given in table 1. Altogether there are 37 samples and 66 specimens.

§ 4. Results

The demagnetization procedure has been carried out on all specimens, about 500 determinations of the direction and intensity of magnetization being necessary. The effect on the directions of magnetization in specimens from the same site is shown for two sites in figs. 2 and 3. The variation in the within-site dispersion may be illustrated by plotting k/k_{sig} against the

Fig. 2

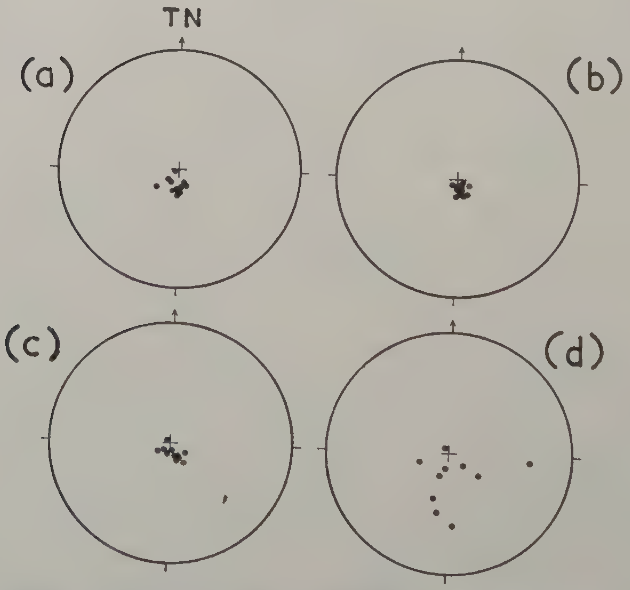

Effect of alternating fields on the directions of magnetization at site **2**. (*a*) NRM, and after treatment in (*b*) 150, (*c*) 300, and (*d*) 450 oersteds. The projections used in this and figs. 3, 7 and 8 are polar stereographic. North-seeking directions are plotted as dots on the lower hemisphere or circles on the upper hemisphere. The inclination scale is given in 7 (*a*).

Fig. 3

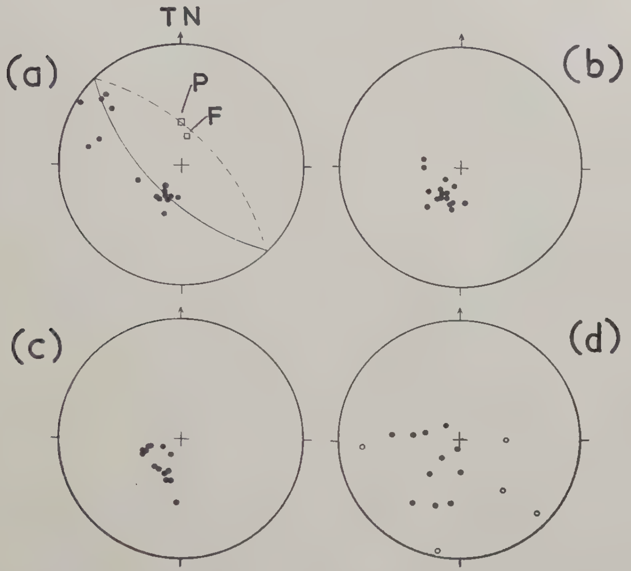

Effect of alternating fields on the directions of magnetization at site **5**. (*a*) NRM, and after treatment in (*b*) 75, (*c*) 150 and (*d*) 750 oersteds. In (*a*) **P** is the dipole field direction and **F** the present field both on the upper hemisphere. The great circle (continuous on the lower hemisphere and dotted on the upper) through **P** and the mean direction after treatment in 75 oersteds is given in (*a*) and shows the 'stringing' of $\mathbf{M}_n$.

Fig. 4

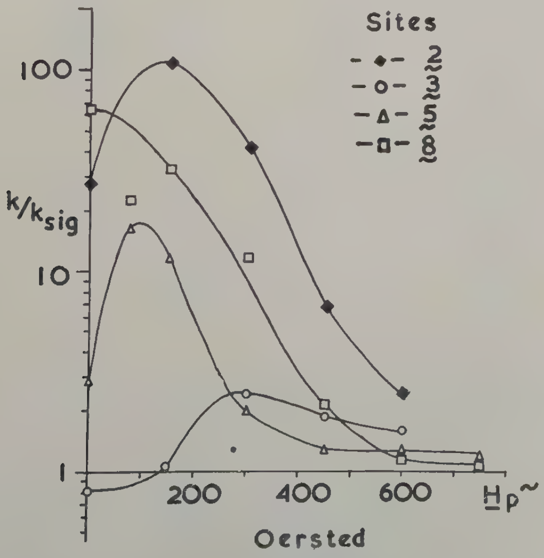

Effect of alternating magnetic fields on the within-site dispersion. This is illustrated by plotting the parameter k/k_{sig} (see text), which is proportional to the inverse of the dispersion against alternating field. The horizontal axis is drawn at $k/k_{\text{sig}} = 1$ and values below this indicate a random within-site dispersion.

Fig. 5

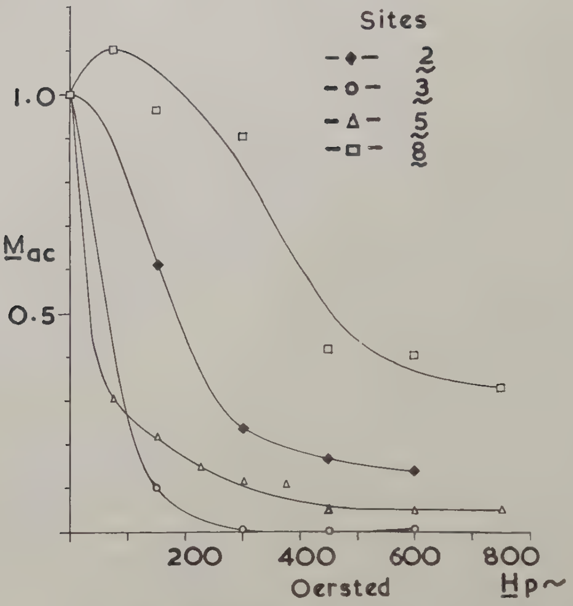

Demagnetization curves for specimens from sites **2, 3, 5** and **8.** The value M_{ac} is plotted against alternating field $H_p\sim$ and M_{ac} is the intensity after treatment, normalized to $M_{ac}=1$ at $H_p\sim=0$.

Fig. 6

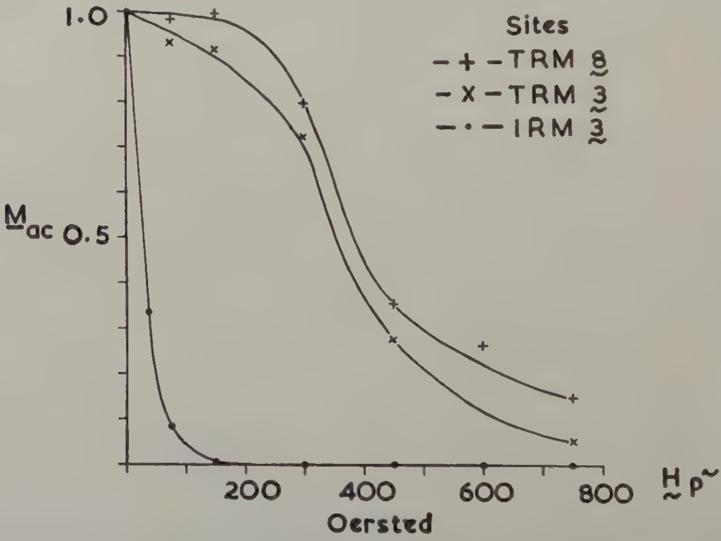

Demagnetization of IRM and TRM. The value of M_{ac} is plotted as in fig. 5. The initial intensities of TRM in 0·6 oersted ($M_{t(0\cdot6)}$) are $0{\cdot}54\times10^{-3}$ e.m.u./cm³ for a specimen from **8** and $22{\cdot}5\times10^{-3}$ for a specimen from **3.** The IRM ($M_{i(300)}$) acquired by another specimen from **2** in a field of 300 oersteds is 108×10^{-3}.

strength of applied alternating field. This has been done for all sites and representative curves for four sites are given in fig. 4. The parameter k is an estimate of κ the dispersion parameter occurring in the direction distribution $\exp(\kappa \cos \theta)$ (Fisher 1953), and $k_{\mathrm{sig}} = (N-1)/(N-R_0)$ where R_0 is the value, tabulated by Watson (1956), of the resultant of N random vectors which will be exceeded in only 5% of cases. When $k/k_{\mathrm{sig}} \leqslant 1$ the distribution may be considered random.

The associated variations in intensity are illustrated by results from specimens from the same four sites (fig. 5). For comparison the demagnetization of IRM and TRM are given in fig. 6. The specimens were first demagnetized in 900 oersteds alternating field and then magnetized in 300 oersteds steady field to give $M_{\mathrm{i}(300)}$, or heated in nitrogen to 625°C and cooled in the earth's field (0·6 oersted) to induce $M_{\mathrm{t}(0\cdot6)}$.

Table 2. Some magnetic properties. M_{n} is the intensity of the natural remanent magnetization M_{min} is the minimum intensity (see § 7), $M_{\mathrm{i(sat)}}$ is the saturation isothermal remanence, H_{sat} is the field required to saturate and H_{cr} is the coercivity of remanence of $M_{\mathrm{i(sat)}}$ obtained by the methods described by Creer *et al.* (1959). Intensities are given in units of 10^{-3} e.m.u./cm³ and field strengths in oersteds

Site number	M_{n}	M_{min}	$M_{\mathrm{i(sat)}}$	H_{sat}	H_{cr}
1	10·48	0·06	101·8	900	200
2	5·95	0·82	188·0	1700	225
3	32·25	1·34	224·5	1000	205
4	13·74	0·26	354·0	1500	190
5	2·52	0·24	354·0	900	180
6	1·25	0·11	405·0	1200	180
7	7·13	0·86	236·5	900	160
8	0·014	0·005	0·32	4000	600

Certain other magnetic properties are listed in table 2; amongst these it may be noted that the 'back field' (the coercivity of remanence, H_{cr}) required to remove the saturation isothermal remanent magnetization ($M_{\mathrm{i(sat)}}$) is usually about 200 oersteds.

These results are now discussed dealing first with the effects in low alternating fields.

§ 5. EFFECTS IN LOW ALTERNATING FIELDS ($H_p \sim < H_{cr}$)

The results within each site which are relevant to the first condition in § 1 are considered first. At site **8** the directions of NRM ($\mathbf{M}_n$) have large positive inclinations. The directions are well grouped and this is not improved by treatment in alternating fields. In fields up to 400 oersteds the demagnetization curve of M_n is convex upwards very similar to $M_{t(0\cdot6)}$ induced in the laboratory. The small initial rise is presumably due to the removal of a soft component, along the earth's field and which is approximately anti-parallel to the hard component. The coercivity of remanence (H_{cr}) is high (table 2). It may be concluded that the NRM is predominantly stable and of TRM type.

At site **3** the directions $\mathbf{M}_n$ are random (see fig. 5 (*b*), Boesen *et al.* 1961), but these become grouped together with steep positive inclinations after treatment in alternating magnetic fields of 300 oersteds (table 1). The demagnetization curve is convex downwards similar to that for IRM induced in the laboratory although the initial decrease is not so rapid. The directions in specimens after storage in the laboratory for three months can change by as much as 180°. The value of H_{cr} is low (table 2). We conclude that the NRM of this basalt consists of a highly unstable magnetization and a stable component of much smaller magnitude with steep positive inclination.

At site **2** the directions $\mathbf{M}_n$ are well grouped with steep positive inclinations (fig. 2 (*a*)). At **5** there is a group of specimens with similar directions but also there are others with low inclinations and north-westerly declinations strung out close to a great circle through the dipole field (fig. 3 (*a*)). At both sites after treatment in small alternating fields the dispersion decreases and the directions all become southerly with large positive inclinations. The minimum dispersion occurs after treatment in 100–200 oersteds. The demagnetization curves lie mainly between those for **8** and **3** and between $M_{t(0\cdot6)}$ and $M_{i(300)}$ induced in the laboratory. The values of H_{cr} are low. The conclusion is that the NRM consists of a comparatively stable component of TRM-type and an unstable IRM-type component of similar or lesser magnitude. The stable component is reversed and is appreciably affected by low demagnetization fields since the demagnetization curves do not show the initial rise as at **8**. The behaviour of specimens at the other sites (**1**, **4** and **7**) is similar to that at **2** or **5**.

Turning now to the comparison of results between-sites (condition (2) in § 1) it is immediately clear that the effect of treatment in low fields (300 oersteds for site **2** and 150 oersteds for the remaining sites) is to bring the widely scattered mean directions of NRM at each site into close agreement (table 1 and fig. 7 (*a*) and (*b*)). The divergences remaining between the site mean directions are due mainly to experimental error and any residue may be satisfactorily explained as due to the secular variation in the geomagnetic field during the time spanned by the lavas.

The third condition may now be tested by comparing the directions with those previously obtained from Victoria (see fig. 1). The directions irrespective of sign are very similar to those observed in the Older Volcanics of Victoria (compare fig. 7 (*b*) with fig. 6 of Irving and Green (1957)). The poles for each site are given in table 1 and the mean of these (63 S, 137 E)

Fig. 7

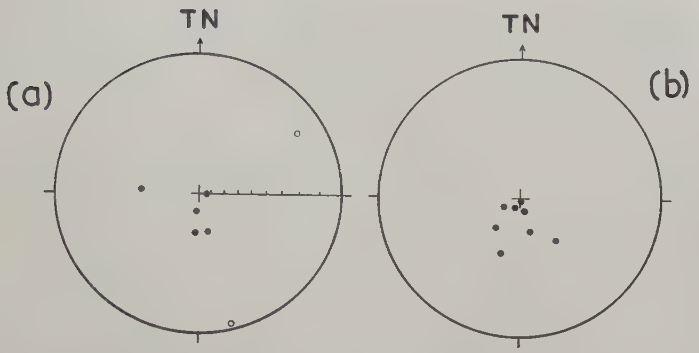

Site mean directions. (*a*) NRM, (*b*) after treatment in low alternating fields. The initial within-site directions at **3** are random and there is no significant mean, but after treatment in 300 oersteds alternating field the directions become grouped together and the mean of these is included in (*b*).

Fig. 8

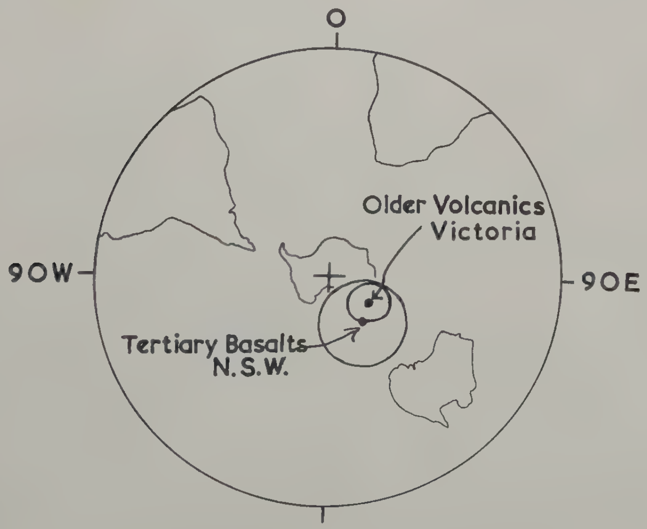

Pole position for the N.S.W. basalts. The pole for the Older Volcanics of Victoria is added for comparison. The ovals around the poles mark out the zones within which the pole lay at a probability of 95%. The south geographic pole is marked with a cross.

agrees well with the pole for the Older Volcanics of Victoria (67 S, 123 E) (see fig. 8). The spread of time of the New South Wales basalts is probably considerable, but does not necessarily overlap that of the Older Basalts of Victoria although both are Lower Tertiary. The Lower Tertiary sequence of Victoria has in some places been gently folded but the lavas have been sampled only at those places where the dip of adjacent sediments is 5° or less (Irving and Green 1957). Thus here is an example of agreement between pole positions obtained from rocks from the same land unit which have suffered no appreciable tectonic movement and which are of similar geological age.

It is evident that after treatment in low alternating fields the three conditions listed in § 1 are satisfied and that the effects of the secondary magnetizations imposed by the present earth's field have been removed. Since the stable magnetization, for instance, at site **8** where the basalt has not been appreciably affected by a secondary magnetization, is of TRM type, and in the absence of any other known geophysical force adequate to produce consistent directions of magnetization over a meridional distance of a 1000 km we may assume that the directions of magnetization remaining after this treatment are the directions of the primary TRM and thus of the geomagnetic field at the time the lavas cooled.

One further point which for the sake of completeness needs to be considered here is the effect of burial stress, which could conceivably have had a systematic effect on the inclination. Except for laterite and soil cover, no deposits overlie the basalts. The thickness of the lavas is not usually more than 100 m. The maximum is probably to be found in the Liverpool Ranges (fig. 1) where 500 m of lavas occur which may be taken to be not more than a factor of two less than the maximum burial depth. To test this point the magnetization of pairs of discs cut from two samples at each of sites **5** and **7** was further examined in the laboratory. In one of each pair, IRM in a field of 100 oersteds, $M_{i(100)}$ and TRM in the earth's field, $M_{t(0\cdot 6)}$ was induced whilst the specimens were subjected to an axial load of 500 kg/cm^2, and in the other, the same magnetizations were produced without load. The apparatus and method have been described by Stott and Stacey (1960). There was no measurable deflection of the magnetization due to the application of stress. The directions of magnetization in each pair agreed to within the measurement error. The applied stress corresponds to a depth of burial of about 1500 m and it is unlikely therefore that any systematic effect due to stress during burial is present. No self-reversal of TRM was found, with or without stress.

§ 6. Procedure for Removal of Secondary Magnetization

We suggest that the following procedure may be applied to volcanic rocks.

1. At a particular site measure H_{cr} for one specimen; there is not usually much variation between specimens from the same site.

2. Measure the directions of NRM of 5 (say) specimens preferably from different samples and the directions after treating in alternating fields ($H_p \sim$) of $\frac{1}{4}H_{cr}$, $\frac{1}{2}H_{cr}$, H_{cr} and $2H_{cr}$. Find the field at which the points are least scattered, either by plotting k against $H_p \sim$ or by plotting on a stereogram.

3. Treat all specimens in this alternating field. In those cases where the primary and secondary components are of the same magnitude (that is, when the directions $\mathbf{M}_n$ are distributed along a great circle between the present field and the directions of the primary magnetization) the strength of alternating field required is usually about $\frac{2}{3}H_{cr}$. When the primary component is small compared with the secondary ones alternating fields as high as $1\frac{1}{2}H_{cr}$ may be necessary.

§ 7. TREATMENT IN HIGH ALTERNATING FIELDS ($H_p \sim \gg H_{cr}$)

After treatment in alternating fields of 600 oersteds, which in most cases is several times greater than H_{cr}, the directions at each site approach a random distribution. The intensity does not diminish regularly with increasing alternating field, but levels off to an almost constant average value at about that field at which the dispersion begins to increase. There are however, fluctuations about this average. This value which is called the *minimum intensity* (M_{min}), is now discussed.

The effects may be due to instrumental imperfections or to inherent properties of the rocks. As and Zijderveld (1958) found that "during the experiments of demagnetization by powerful alternating fields a disturbing magnetization appears to be induced in the samples". Creer (1959), however, finds that spinning "prevents the specimens acquiring an IRM due to DC components", but even so he still finds "stray magnetizations acquired during 'cleaning'". We suggest that while the effects due to instrumental imperfections can be important if precautions are not taken, there will always be some residual, fluctuating magnetization, even when the demagnetization takes place under perfect conditions. The reason for this is that spontaneous magnetization of domains is lost only at temperatures above the Curie point, so that the effect of alternating magnetic fields is one of rearrangement of domains, and because of statistical fluctuations the resultant moment of a specimen is never likely to be zero. The observed minimum intensity, and the scattered, almost random directions in alternating fields whose strength is much greater than the coercivity of remanence may therefore be a result of such fluctuations and will depend on the number of domains in a specimen. An estimate of this number may be made as follows.

Assume firstly that there are n_1 ferromagnetic grains per cm³ of equal size and moment M_p whose directions are random in an isotropic demagnetized rock. Rayleigh (1919) has given the probability distribution of the magnitude of the resultant r_0 of n randomly oriented unit vectors for large values of n. The value of r_0 is given by $r_0 = Cn^{1/2}$

where C is a constant having the value 1·61 for $P(r>r_0)=0{\cdot}05$ and 0·89 for $P(r>r_0)=0{\cdot}50$. The latter will give an average value for the mean random magnetization so that the *random moment* (M_r) per cm³ is given by $M_r=M_p\,.\,0{\cdot}89\,.\,n_1^{1/2}$. Assume further that in each ferromagnetic grain there are n_2 domains of equal moment m so that the total number of domains per cc is $n_1\,.\,n_2$. We may say that domains have randomly arranged directions in a single demagnetized grain and the average moment of each grain will thus be $M_p=m\,.\,0{\cdot}89\,.\,n_2^{1/2}$. However it is more likely that the domains behave as an assembly of anti-parallel vectors having the values +1 and −1 with equal probability. Rayleigh (1880) has given the probability for the length of the resultant in this situation also and we obtain $r_0=An^{1/2}$ where $A=0{\cdot}83$ for $P(r>r_0)=0{\cdot}50$. The average moment per demagnetized grain in this case will be $M_p=m\,.\,0{\cdot}83\,.\,n_2^{1/2}$. The correct distribution probably lies somewhere between the random and anti-parallel situations but the difference for these purposes is negligible. Taking an average for the constant as 0·86 the random moment per cc becomes:

$$M_r=m\,.\,0{\cdot}76\,.\,(n_1\,.\,n_2)^{1/2}. \qquad (1)$$

Now the saturation moment $M_s=n_1\,.\,n_2\,.\,m$ and the ratio of this to the random moment will have the average value

$$M_s/M_r=1{\cdot}31(n_1\,.\,n_2)^{1/2}. \qquad (2)$$

Taking the observed values of $M_{i(sat)}$ and M_{min} as estimates of M_s and M_r respectively we find for a specimen from site **5** that $M_s/M_r=1{\cdot}5\times10^3$ which give $1{\cdot}3\times10^6$ domains per cm³. But $M_{i(sat)}\leqslant\frac{1}{2}M_s$ and also $M_{min}>M_r$, since the directions after the minimum intensity have been reached are not completely random due to the persistence of a very hard component even after treatment in high alternating fields. This will, therefore, be a minimum estimate. A better estimate may be obtained by putting $M_s=2M_{i(sat)}$ and $M_r=\frac{1}{2}M_{(min)}$ which gives $M_s/M_r=5{\cdot}9\times10^3$ and $20{\cdot}4\times10^6$ domains per cm³.

Examination of a thin section of this specimen shows that although there is wide range in the size of visible magnetic grains, about 80% of the magnetic material is contained in grains of size 25–150 μ and over 99% in the range 25–175 μ. A modal analysis of this section shows that the magnetic minerals occupy more than 10% by volume of the rock. Assuming that the material of grain size $>25\,\mu$ is responsible for the observed minimum intensity and that these grains are spheres of average diameter 100 μ, there will be $1{\cdot}9\times10^5$ per cm³. From the estimates of the total number of domains, this gives the order of 10 or 100 domains per particle and suggests that the minimum intensity is due to the presence of multi-domain particles. For the reasons just mentioned the estimate of ten domains per particle will be a minimum. The estimate of the order of 100 is likely to be more correct and there is no reason to regard this as a maximum estimate.

Since this paper was written 30 specimens from these basalts have been thermally 'demagnetized', by heating to 610°C (more than 50° higher than the Curie Points of the iron minerals they contain) in nitrogen in a non-magnetic oven followed by cooling in zero field. After this treatment the specimens still retained an appreciable moment. The values, which are to be compared with the minimum intensities obtained by demagnetization in alternating magnetic fields (table 2, column 3) are these: site **1**, 0·11; **2**, 0·64; **3**, 1·67; **4**, 0·22; **5**, 0·23; **6**, 0·16; **7**, 0·43; **8**, 0·01. The values are an average of about four specimens per site and are given in units of 10^{-3} e.m.u./cm^3. As with demagnetization by alternating fields these small residual moments could result from instrumental imperfections due, for instance, to incomplete cancellation of the earth's field. The de-gaussing coils have a central space of about 8000 cm^3 which is uniform to about 1 part in 10^5 and the oven, which has a working space rather less than this, holds about 20 specimens spaced sufficiently far apart to avoid mutual interference from their moments. The directions in each batch after treatment are random so that it appears that the residual field in the oven has negligible aligning force on the specimens. The important point in the present context is that the magnitudes of the moments, M_{min}, are the same whether they are obtained by thermal or alternating field demagnetization; it would be a remarkable coincidence if instrumental imperfections in two different methods produce such closely comparable effects. These results therefore provide strong evidence confirming the view that the minimum intensity is an inherent property of these basalts and results from the statistical nature of the remanent magnetization.

The accuracy of the procedure of removal of the unwanted secondary magnetizations by alternating magnetic fields will be limited by the presence of the minimum intensity, in those cases where the magnitude of the soft component is large, since the minimum intensity of this may exceed the magnitude of the hard component. However, since the minimum intensity directions are random, the average of several specimens will give an estimate of the direction of the primary component although the individual specimen directions will be widely scattered. This is probably the case at site **3** where even after removal of the secondary component the directions are widely scattered but the mean is significant and agrees with the direction of the primary component obtained at the other sites. In rocks containing multi-domain particles which have become demagnetized over long periods of time a minimum intensity will always be present and may be the cause of the random scatter in the directions of NRM observed in specimens taken from the same sample of lava and which in our experience is usually greater than the experimental error. The presence of small temporary components could also explain this.

§ 8. FERROMAGNETIC COMPONENTS

In addition to the grain sizes notes above there are a large number of very small grains of the order of a micron in diameter and a small portion of the stable NRM may be due to these. The directions of magnetization do not become completely random (figs. 2 (*d*) and 3 (*d*)) even after treatment in high alternating magnetic fields suggesting that there is an exceedingly hard component present and these grains, acting as single domains, may be responsible for this. They could not be responsible for all the stable NRM since they represent less than 0·1% (by volume) of the total ferromagnetic content. It seems therefore that both the primary and secondary magnetizations reside in grains which, because of their size and the considerations in the previous sections, are multi-domain. The evidence presented in this paper is consistent with the view that in the natural rock these grains are for the most part either demagnetized and contribute only their minimum intensity, or possess a secondary magnetization, but that they contain within themselves regions of much higher magnetic stability responsible for the primary NRM which, as was shown in § 5, is probably thermo-remanent in origin. It may be noted in fig. 6 that the IRM induced in a steady field of 300 oersteds ($M_{\mathrm{i}(300)}$) is removed by alternating magnetic fields of the same strength. Moreover, if $M_{\mathrm{i}(300)}$ is induced in a specimen previously possessing a TRM ($M_{\mathrm{t}(0\cdot6)}$) which has been treated in alternating fields in excess of 300 oersteds (say 500 oersteds), the underlying TRM remains unaffected after the removal of $M_{\mathrm{i}(300)}$. The two components ($M_{\mathrm{i}(300)}$, and $M_{\mathrm{t}(0\cdot6)}$ after treatment in 500 oersteds $H_{\mathrm{p}}\sim$) are independent of one another and are probably related to two different ferromagnetic components in these basalts, the former perhaps to the multi-domain ferromagnetic grains and the latter to high stability regions within these.

An estimate of the fractional content of grains represented by high stability regions may be obtained from considering the demagnetization of $M_{\mathrm{t}(0\cdot6)}$ (fig. 6). The softer component which makes up about 90% of the intensity is largely removed in 500 oersteds, and it is this component which is likely to become demagnetized in the natural rock over a long period of time, or which has acquired a secondary magnetization. In fields above this value a hard component, which is 6% of $M_{\mathrm{t}(0\cdot6)}$ in the highly unstable Robertson basalt (site **3**) and 15% of $M_{\mathrm{t}(0\cdot6)}$ in the stable basalt at site **8**, still remains. It seems that these high stability regions occupy approximately 10% of the ferromagnetic grains.

Verhoogen (1959) has recently suggested in general terms that such high stability regions within ferromagnetic grains are due to structural dislocations. Another possibility is that intergrowths are responsible; the fine scale intergrowths contributing the hard magnetic component and the coarser-grained matrix providing the softer component. Dislocations are more likely to occur in rapidly cooled rocks whereas slow cooling will favour the development of suitable intergrowths. It is noteworthy that in extensive work on hypabyssal dolerite intrusives (Almond *et al.* 1956, Irving 1956, Graham and Hales 1957, Bull and Irving 1960, Creer *et al.* 1959) and plutonic intrusions of gabbro (Gough and Niekerk 1959, Khan 1960) few cases of instability have been found, whereas instability in basalts is very common (Brynjólfsson 1957

Creer 1958, Khan 1960, this paper). In dolerite and gabbro the ferromagnetic grains are larger than those in basalt and it is clear that there is no simple correlation between stability and the overall size of the iron mineral grains. It seems more likely that the question of their internal subdivision is of more importance. It seems not unlikely that the explanation for the hard and soft magnetic components which are found not only in these basalts discussed in this paper but also in most other igneous rocks studied is to be sought in the exsolved phases of differing grain size in ferromagnetic grains.

ACKNOWLEDGMENTS

We wish to express our thanks to Mr. R. Boesen who collected most of the specimens from sites **2** and **3**, and to Drs. K. M. Creer and J. H. Parry for much helpful discussion.

REFERENCES

ALMOND, M., CLEGG, J. A., and JAEGER, J. C., 1956, *Phil. Mag.*, **1,** 771.
AS, J. A., and ZIJDERVELD, J. D. A., 1958, *Geophys. J.*, **1,** 308.
BOESEN, R., IRVING, E., and ROBERTSON, W. A., 1961, *Proc. roy Soc. Qd,* **94** (in the press).
BRYNJÓLFSSON, A., 1957, *Advanc. Phys.*, **6,** 247.
BULL, C., and IRVING, E., 1960, *Geophys. J.*, **3,** 211,
CREER, K. M., 1957, *Phil. Trans. roy. Soc.* A, **250,** 130 ; 1958, *Ann. Geophys.*, **14,** 373 ; 1959, *Geophys. J.*, **2,** 261.
CREER, K. M., IRVING, E., and NAIRN, A. E. M., 1959, *Geophys. J.*, **2,** 306.
DAVID, T. W. E., 1950, *Geology of the Commonwealth of Australia*, **1** (Arnold).
FISHER, R. A., 1953, *Proc. roy. Soc.* A, **217,** 295.
GOUGH, D. I., and NIEKERK, C. B., 1959, *Phil. Mag.*, **4,** 126.
GRAHAM, K. W. T., and HALES, A. L., 1957, *Advanc. Phys.*, **6,** 149.
IRVING, E., 1956, *Pap. roy. Soc. Tas.*, **90,** 157.
IRVING, E., and GREEN, R., 1957, *Mon. Not. R. astr. Soc. geophys. Suppl.*, **7,** 347.
KHAN, M. A., 1960, *Geophys. J.*, **3,** 45.
PARRY, J. H., 1957, Thesis, University of Cambridge.
RAYLEIGH, LORD, 1880, *Phil. Mag.*, **10,** 77 ; 1919, *Ibid.*, **37,** 321.
STOTT, P. M., and STACEY, F. D., 1960, *J. geophys. Res.*, **65,** 2419.
VERHOOGEN, J., 1959, *J. geophys. Res.*, **64,** 2441.
WATSON, G. S., 1956, *Mon. Not. R. astr. Soc. geophys. Suppl.*, **7,** 160.

'Conservative Climb' of a Dislocation Loop due to its Interaction with an Edge Dislocation†

By F. Kroupa‡ and P. B. Price§
Cavendish Laboratory, Cambridge, England

[Received August 12, 1960]

Abstract

A new type of dislocation motion, called 'conservative climb', has been observed in zinc platelets deformed in tension inside an electron microscope. Circular, prismatic dislocation loops are often forced to climb out of their glide cylinders by their repulsive interaction with edge dislocations. It is observed that the area inside a loop is conserved during its movement, from which it is concluded that the climb occurs, not by self-diffusion, but by the transfer of vacancies around the loop by pipe diffusion. Calculations of the interaction energy, of the total forces on the loop, and of the forces per unit length on the elements of the loop show that conservative climb can be expected to occur when the temperature is not too low and the separation of loop and edge dislocation is small.

During a transmission electron microscope study of the formation and climb of dislocation loops in deformed zinc crystal platelets (Price 1960), an unusual type of dislocation motion was observed, which has not previously been considered. A number of crystals were deformed on a tensile straining stage (Fisher 1959) inside the electron microscope, and it was often observed that during pyramidal glide dislocation loops were generated by moving screw dislocations with a Burgers vector in the direction $\mathbf{c}+\mathbf{a}=\frac{1}{3}[\bar{1}\bar{1}23]$. Figure 1 (*a*)|| is a transmission micrograph showing loops with a [0001] Burgers vector which are lying in the basal plane in a row along the path taken by the screw dislocation (not shown in the figure) from which they were formed. The basal plane is parallel to the plane of the micrograph. Also in the micrograph is an edge dislocation with a Burgers vector $\mathbf{a}=\frac{1}{3}[\bar{1}\bar{1}20]$. (For the method of determining the Burgers vectors, see Price (1960).) One end of the dislocation, which is situated mainly on the basal plane, ends at the crystal surface at A. During straining it was observed that the dislocation, in attempting to glide past the loops, forced one of them to move slowly sideways as shown in the sequence of fig. 1 (*a*), (*b*) and (*c*). In fig. 1 (*c*) it has also begun to displace another one of the loops. The area inside the loops appeared to be conserved during the motion, so that there was no net flow of vacancies to or from the loops. This type of loop movement as a result

---

† Communicated by the Authors.

‡ Permanent address: Institute of Physics, Prague, Czechoslovakia.

§ Permanent address: General Electric Research Laboratory, Schenectady, New York, U.S.A.

|| Figure 1 is shown as a plate.

of interaction with a moving dislocation was observed several times and will be called 'conservative climb' to distinguish it from ordinary climb, which involves vacancy diffusion. The purpose of this note is to give a qualitative explanation for conservative climb in terms of classical elasticity theory.

Let us consider the interaction between a circular edge dislocation loop and an infinite, straight dislocation whose glide plane is parallel to the plane of the loop. We assume an infinite isotropic medium characterized by the shear modulus μ and the Poisson constant ν. The loop lies in the plane $z=0$ (fig. 2) with its centre at the origin of coordinates, with radius R and with Burgers vector $\mathbf{b}^0$ along the z axis. The straight dislocation, 1, is located at y_1, z_1, extends along the x axis and has a Burgers vector $\mathbf{b}^1$.

Fig. 2

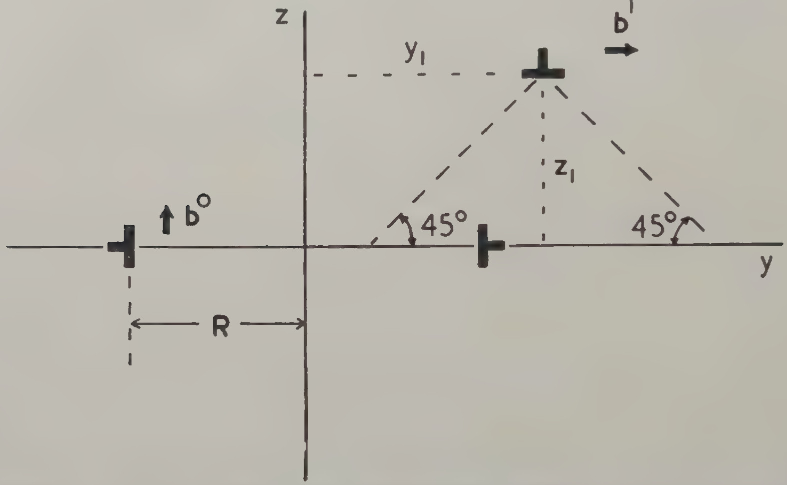

Circular edge dislocation loop and infinite straight edge dislocation.

If $\mathbf{b}^1$ is along the x axis (i.e. if the dislocation is pure screw), the interaction energy of loop and line is zero and the total force on the loop is zero. We now consider the case of a pure edge dislocation with $\mathbf{b}^1$ along the y axis (fig. 2). The components of the stress tensor, σ_{ij}', for the dislocation 1 are given in the book by Cottrell (1953), with his coordinates x, y, z replaced by $y-y_1, z-z_1, x$. The interaction energy E^{01}, was obtained by integrating the expression $E^{01}=\mathbf{b}^0\iint_A \sigma_{zz}^1(x, y, 0)dx\,dy$ over the area, A, of the loop. The result,

$$E^{01}=(\mu\mathbf{b}^0\mathbf{b}^1/(1-\nu))RZ\{1-\{2(Y^2+Z^2-1)+2\sqrt{[(1+Y^2+Z^2)^2-4Y^2]}\}^{-1/2}$$
$$\times[(Y^2+Z^2-Y)((Y-1)^2+Z^2)^{-1/2}+(Y^2+Z^2+Y)((Y+1)^2+Z^2)^{-1/2}]\}, \quad (1)$$

is plotted in fig. 3 as a function of Y, for $Z=1$ and $Z=0{\cdot}1$, where $Y=y_1/R$ and $Z=z_1/R$.

The total forces on the loop were found from the expressions $F_x{}^0=0$, $F_y{}^0=\partial E^{01}/\partial y_1$, $F_z{}^0=\partial E^{01}/\partial z_1$. $F_y{}^0$, the force tending to cause climb, is plotted in fig. 3 as a function of Y for $Z=1$ and $Z=0{\cdot}1$. $F_z{}^0$, the force tending to drive the loop out of the crystal by glide (not plotted in the figure), has a maximum value which is smaller than that of $F_y{}^0$ and occurs at a different value of Y.

Fig. 3

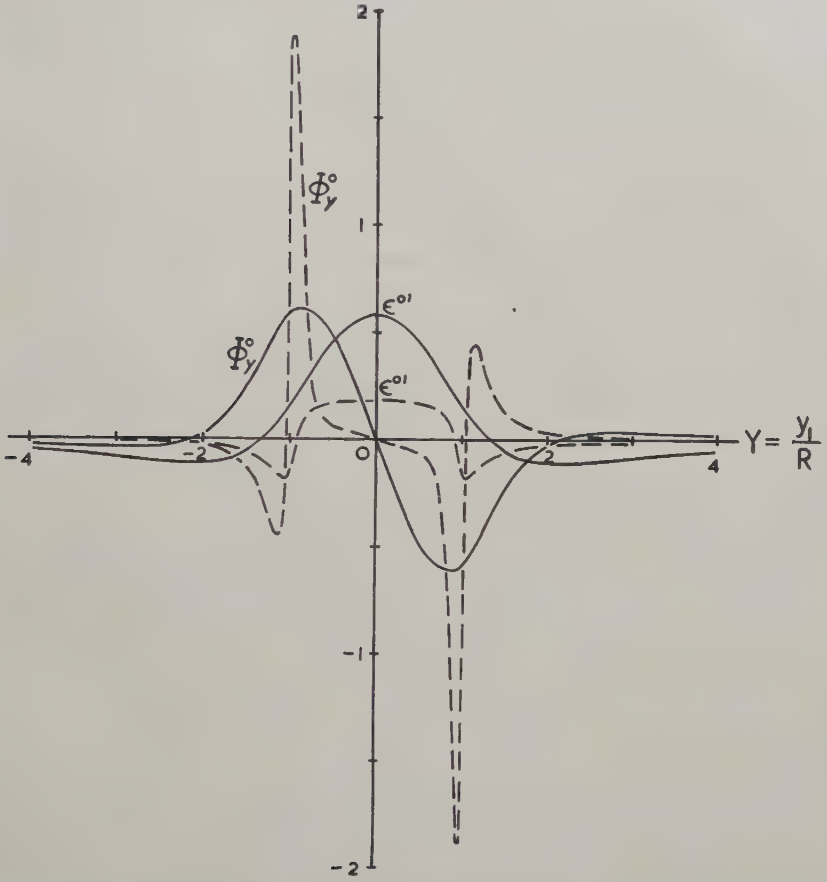

Interaction energy, ϵ^{01}, and total force, $\Phi_y{}^0$, on the loop as a function of Y, with $\epsilon^{01} = E^{01}/[\mu \mathbf{b}^0\mathbf{b}^1 R/2(1-\nu)]$, $\Phi_y{}^0 = F_y{}^0/[\mu \mathbf{b}^0\mathbf{b}^1/2(1-\nu)]$. The full lines are for $Z=1$ and the broken lines for $Z=0{\cdot}1$.

The force per unit length, $\mathbf{f}^0$, on every element of the loop was obtained by applying the Peach–Koehler formula (Peach and Koehler 1950). At the point $(R\cos\theta, R\sin\theta, 0)$ the components of $\mathbf{f}^0$ are

$$\left.\begin{aligned} f_x{}^0 &= \frac{\mathbf{b}^0 D^1}{R} \frac{Z[(\sin\theta - Y)^2 - Z^2]}{[(\sin\theta - Y)^2 + Z^2]^2} \cos\theta, \\ f_y{}^0 &= \frac{\mathbf{b}^0 D^1}{R} \frac{Z[(\sin\theta - Y)^2 - Z^2]}{[(\sin\theta - Y)^2 + Z^2]^2} \sin\theta, \\ f_z{}^0 &= \frac{\mathbf{b}^0 D^1}{R} \frac{(\sin\theta - Y)[(\sin\theta - Y)^2 - Z^2]}{[(\sin\theta - Y)^2 + Z^2]^2} \sin\theta, \end{aligned}\right\} \quad . \quad . \quad (2)$$

where $D^1 = \mu \mathbf{b}^1/2\pi(1-\nu)$. The radial forces, given by $f_r{}^0 = [(f_x{}^0)^2 + (f_y{}^0)^2]^{1/2}$, depend only on $\sigma_{zz}{}^1$, which is zero along a plane at 45° to the glide plane of dislocation 1 (see fig. 2) and changes sign across this plane. For example, when $Y = Z = 1$, that is, when the dislocation is a distance R above one edge of the loop, the plane intersects the loop at $y = 0$ and the forces are directed toward the centre on one side and away from the centre on the other side, as shown in fig. 4. The lengths of the arrows in the drawing are proportional to the magnitude of the forces.

Fig. 4

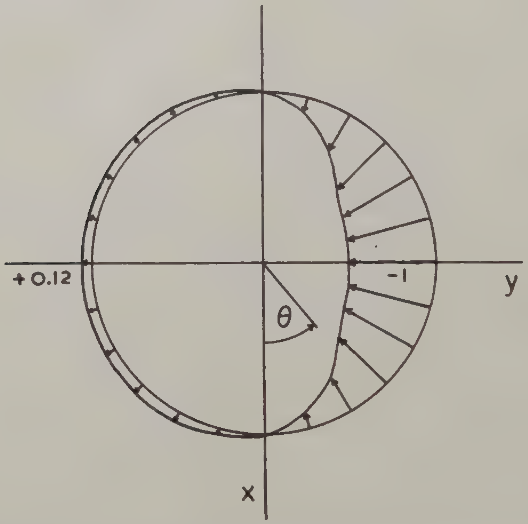

Radial forces, $\phi_r{}^0$, on the elements of the loop for $Y = Z = 1$, with $\phi_r{}^0 = f_r{}^0/[\mu \mathbf{b}^0 \mathbf{b}^1/2\pi(1-\nu)R]$.

We now apply these results to the electron microscope observations, assuming that they are qualitatively the same when the dislocation 1 is finite and the medium is crystalline, anisotropic, finite and bounded by a thin oxide film. The Burgers vectors $\mathbf{b}^0$ and $\mathbf{b}^1$ are directed along the **c** axis and an **a** axis and have the values 4·94 Å and 2·66 Å respectively. The x, y plane is the basal plane of the platelet. If the glide plane of the dislocation is far from the plane of the loop (Z large), the total force on 1, $-F_y{}^0$, may be small enough for it to glide past the loop. If Z is not large, the dislocation will be unable to surmount the energy barrier and will be held up near the loop and exert a repulsive force on it.

Since $F_z{}^0 < F_y{}^0$, it is not surprising that prismatic glide of the loop was not the predominating process, especially when the Peierls force and the repulsive force of the oxide layer at small distances are considered. The total forces on the loop favour conservative climb, and if the temperature is not too low it should be quite easy for this to occur at a reasonable rate by the transfer of vacancies from one end of the loop to the other by pipe diffusion along the core of the dislocation. Since the Burgers vector of the loop is quite large—almost 5 Å—the activation energy for this process should be much smaller than for the movement of vacancies through a perfect lattice.

The large total force F_y^0 and the conservative climb of the loop are due to the large gradient of the stress component σ_{zz}^1. (The average gradient of σ_{zz}^1 in the region of the loop is $\sim 10^5$ kg/mm^2/mm for $Z=1$ and $\sim 10^6$ kg/mm^2/mm for $Z=0{\cdot}1$.) Although we have made observations and calculations for only one special case of conservative climb, there is no reason to doubt that this type of dislocation motion is a general one as a result of the interaction of closed prismatic loops with each other and with other dislocations, provided a suitable stress gradient is available.

ACKNOWLEDGMENT

We are indebted to the British Council for a scholarship (F. K.) and to the U.S. National Science Foundation for a post-doctoral Fellowship (P. B. P.).

REFERENCES

Cottrell, A. H., 1953, *Dislocations and Plastic Flow in Crystals* (Oxford: Clarendon Press).
Fisher, R. M., 1959, *Rev. Sci. Instrum.*, **30**, 925.
Peach, M., and Koehler, J. S., 1950, *Phys. Rev.*, **80**, 436.
Price, P.B., 1960, *Phil. Mag.*, **5**, 873.

The Stability of a Wavefunction under a Perturbation†

By G. G. Hall

Department of Mathematics, Imperial College, London, S.W.7

[Received August 22, 1960]

Abstract

The concept of the stability of a wavefunction under a perturbation is defined and the properties which distinguish stable wavefunctions are deduced. The stability of approximate wavefunctions is particularly examined and a number of general results stated. Self-consistent wavefunctions are shown to be stable under one-electron perturbations. The concept enables many hitherto isolated results to be unified and extended. In particular a new method of calculating nuclear magnetic shielding constants for atoms is given. The concept also suggests means of improving an approximate wavefunction so that the derived estimate of some property is made more accurate.

§ 1. Introduction

The application of quantum mechanics to the study of atoms and molecules is made difficult by two related obstacles. The first is that the number of problems, for which exact solutions in terms of familiar functions can be found. is very severely limited and the second is that there are few theorems which can be used to simplify the evaluation of properties or to estimate the accuracy of approximations. Almost all calculations have to be made using approximate wavefunctions and the theoretical values of properties involve inaccuracies. It is very difficult to estimate these inaccuracies theoretically and their behaviour, judged from agreement with experiment, is often erratic. There have been several examples published in which the accuracy of the wavefunctions, as judged by the minimum energy criterion, bears no relation to the accuracy of the estimate of some derived property. Sometimes a change in a wavefunction, which produces no appreciable improvement in the energy, may make a large difference to the estimate of a property.

In this paper the concept of the stability of a wavefunction under a perturbation is introduced and used to illuminate some of these difficulties. Much of the erratic behaviour is associated with the use of instable wavefunctions. A number of different methods of making wavefunctions stable is also discussed.

§ 2. Definition of Stability

The estimation of many atomic and molecular properties can be considered in terms of perturbation theory. The unperturbed equation is usually taken as the non-relativistic Schrödinger equation and the perturbation may be a relativistic term, some additional internal operator, a change in one of the terms already present or a term representing the interaction of the system with some external field. The perturbed Schrödinger equation is written

---

† Communicated by the Author.

$$(H+\lambda P)\psi=W\psi \quad . \quad . \quad . \quad . \quad . \quad . \quad . \quad . \quad (2.01)$$

where λ is a parameter governing the strength of the perturbation P, and the unperturbed equation has eigenfunctions ϕ_n satisfying

$$H\phi_n=W_n\phi_n, \quad n=0,1,\ldots \quad . \quad . \quad . \quad . \quad . \quad . \quad (2.02)$$

In most applications only the ground-state solution of (2.01) is needed. This equation can be generalized by considering a Hamiltonian

$$H(\lambda), \quad . \quad . \quad . \quad . \quad . \quad . \quad . \quad . \quad . \quad . \quad . \quad (2.03)$$

whose eigenfunctions are known for some non-zero λ_0. This generalization is easily carried out and need not be given here. The quantities of interest are usually the coefficients of λ and λ^2 in $W(\lambda)$. It will be assumed that the operators H and P are of such a kind that the energy levels $W(\lambda)$ are differentiable functions of λ at least at $\lambda=0$. A discussion of conditions sufficient to ensure this has been given by Kato (1951).

If the eigenfunction $\psi(\lambda)$ in (2.01) is normalized, so that

$$\int\psi^*\psi\,d\tau=1 \quad . \quad . \quad . \quad . \quad . \quad . \quad (2.04)$$

for all λ, then the energy can be expressed as

$$W(\lambda)=\int\psi^*(H+\lambda P)\psi\,d\tau. \quad . \quad . \quad . \quad . \quad . \quad (2.05)$$

In general, therefore, since ψ depends on λ,

$$\frac{dW}{d\lambda}=\int\psi^*P\psi\,d\tau+\int\frac{d\psi^*}{d\lambda}H\psi\,d\tau+\int\psi^*H\frac{d\psi}{d\lambda}\,d\tau, \quad . \quad . \quad (2.06)$$

but for certain wavefunctions

$$\int\frac{d\psi^*}{d\lambda}H\psi\,d\tau+\int\psi^*H\frac{d\psi}{d\lambda}\,d\tau=0, \quad . \quad . \quad . \quad . \quad . \quad (2.07)$$

and so

$$\frac{dW}{d\lambda}=\int\psi^*P\psi\,d\tau\equiv\langle P\rangle. \quad . \quad . \quad . \quad . \quad . \quad . \quad . \quad (2.08)$$

Such wavefunctions will be called *stable*. More generally, if ψ is only an approximate wavefunction, (2.05) is the corresponding approximate energy and this ψ also will be called stable at λ_0 if it satisfies (2.07) for some $\lambda=\lambda_0$. If ψ is not normalized the corresponding equations to (2.07) and (2.08) are

$$\int\frac{d\psi^*}{d\lambda}(H-W)\psi\,d\tau+\int\psi^*(H-W)\frac{d\psi}{d\lambda}d\tau=0, \quad . \quad . \quad (2.09)$$

$$\frac{dW}{d\lambda}=\int\psi^*P\psi\,d\tau\Big/\int\psi^*\psi\,d\tau\equiv\langle P\rangle. \quad . \quad . \quad . \quad (2.10)$$

§ 3. THE STABILITY OF EXACT EIGENFUNCTIONS

The discussion of stability is easier when ψ is an exact solution of (2.01) but there are three different cases to be considered. If, in the first place, the lowest eigenvalue W_0 is non-degenerate then ψ is stable for any perturbation which gives rise to an energy differentiable at $\lambda=0$. This can be proved from the definition by using (2.02), (2.04) and the limiting form of ψ at $\lambda=0$, i.e. ϕ_0, for

$$\begin{aligned}\int\frac{d\psi^*}{d\lambda}H\phi_0\,d\tau+\int\phi_0{}^*H\frac{d\psi}{d\lambda}\,d\tau &= W_0\int\frac{d\psi^*}{d\lambda}\phi_0\,d\tau+W_0\int\phi_0{}^*\frac{d\psi}{d\lambda}d\tau\\ &= W_0\frac{d}{d\lambda}\int\psi^*\psi\,d\tau\\ &=0, \qquad \qquad (3.01)\end{aligned}$$

where the derivatives are taken at $\lambda=0$.

When W_0 is degenerate and the degeneracy persists in the presence of the perturbation then, even though the energy varies smoothly, the individual wavefunctions can be discontinuous since the choice of basis functions in the degenerate sub-space may vary from point to point. To overcome this difficulty it is usual to introduce the operator or operators necessary to label the degenerate wavefunctions uniquely and to consider only those wavefunctions in which these labels are kept constant. Thus the simultaneous eigenfunctions of the energy and these additional operators are uniquely defined and so, according to the first part, can be differentiated with respect to λ and will satisfy (3.01).

When W_0 is degenerate and the degeneracy is split by the perturbation then the wavefunctions can be discontinuous but only at $\lambda=0$. Thus the derivative $d\psi/d\lambda$ exists except possibly at $\lambda=0$ which is the point involved in (3.01). If the degeneracy at $\lambda=0$ is resolved by defining ψ there by

$$\psi(0)=\underset{\epsilon\to 0}{\mathrm{Lt}}\,\psi(\epsilon), \qquad \qquad (3.02)$$

then this difficulty is avoided. Thus the perturbation is regarded as virtually present even when $\lambda=0$. The usual modification of perturbation theory consists in choosing the zero-order degenerate wavefunctions so that the matrix elements of the perturbation are diagonalized. These are already the functions necessary for (3.02) and consequently are the stable wavefunctions. If the splitting is only partial it will be necessary to combine the techniques above. The significant feature of this case is that the stable zero-order wavefunctions depend on the perturbation and, in general, will differ according to the perturbation. When two perturbations are applied simultaneously the stable zero-order wavefunctions may even vary as the magnitudes of the perturbations vary.

The calculation of the dipole moment of the hydrogen atom in its first excited state gives an illustration of the influence of the degeneracy. In the non-relativistic theory the first excited state has 4-fold degeneracy with wavefunctions which can be labelled 2s, $2p_x$, $2p_y$, $2p_z$. Each of these functions gives a symmetrical distribution of charge and so has no dipole moment. This does not imply, however, that the atom has no dipole moment since these are not the stable zero-order wavefunctions in the presence of an electric field and an electric field is required for a dipole moment to be observed. The electric field E in the z direction produces an additional term in the Hamiltonian so that the Schrödinger equation becomes

$$(H-Ez)\psi=W\psi \quad . \quad . \quad . \quad . \quad . \quad . \quad . \quad . \quad (3.03)$$

and the dipole moment is defined as

$$\mu=-\left(\frac{\partial W}{\partial E}\right)_{E=0} \quad . \quad . \quad . \quad . \quad . \quad . \quad . \quad . \quad (3.04)$$

The stable wavefunctions are, then, those linear combinations of 2s, $2p_x$, $2p_y$, $2p_z$, which diagonalize z and these are the digonal hybrids

$$\sqrt{\tfrac{1}{2}}(\mathrm{s}\pm \mathrm{p}_z) \quad . \quad . \quad . \quad . \quad . \quad . \quad . \quad . \quad . \quad (3.05)$$

and the degenerate pair p_x and p_y. For these stable wavefunctions equation (2.08) leads to the simpler formula

$$\mu=\langle z\rangle. \quad . \quad . \quad . \quad . \quad . \quad . \quad . \quad . \quad . \quad (3.06)$$

The hybrid functions (3.05) no longer have symmetrical distributions of charge but have dipole moments of ± 7·6 Debyes. (For further details see Van Vleck (1932), p. 204.)

§ 4. The Stability of Approximate Wavefunctions

The definition of the stability of a wavefunction under a perturbation by means of eqn. (2.07) applies equally well to approximate wavefunctions. Indeed its importance is even greater since it gives a new method of discussing the probable accuracy of the properties deduced from an approximate wavefunction.

There are a small number of examples in which it is possible to find approximate wavefunctions which are completely stable in the sense of satisfying (2.07) exactly. Thus both the exact and the approximate wavefunctions may be eigenfunctions of the perturbing operator for all λ and consequently will satisfy

$$\frac{\partial\psi}{\partial\lambda}=0 \quad . \quad . \quad . \quad . \quad . \quad . \quad . \quad . \quad . \quad . \quad (4.01)$$

which ensures (2.07). Practical examples of this include perturbations depending only on angular momentum operators.

In general, for most approximate wavefunctions and most perturbations, only approximate stability can be attained even when there is no degeneracy present. The basic method of finding wavefunctions which are stable to a good approximation is to introduce into the approximate wavefunction parameters which enable it to adjust to the presence of the perturbation. Thus if the approximate wavefunction is

$$\psi(\lambda)=\psi(\mu_1,\ \mu_2,\ \ldots,\ \mu_n), \qquad (4.02)$$

where the parameters μ_i depend on λ, and if these parameters are determined by minimizing the unperturbed energy so that they satisfy

$$\int \frac{\partial\psi^*}{\partial\mu_i} H\psi\, d\tau + \int \psi^* H \frac{\partial\psi}{\partial\mu_i}\, d\tau = 0, \quad i=1,\ 2,\ \ldots,\ n, \qquad (4.03)$$

then by using this and

$$\frac{d\psi}{d\lambda} = \sum_i \frac{\partial\psi}{\partial\mu_i}\frac{d\mu_i}{d\lambda} \qquad (4.04)$$

eqn. (2.07) is satisfied. The degree of stability will depend on the success with which these parameters μ_i can be used to represent the change in ψ due to the perturbation even though it is the *unperturbed* energy which is minimized. The method may be described as determining the wavefunction by treating the perturbation as latent and the resulting stable wavefunction has the significance that it enables the effects due to the perturbation and those due to the approximations to be isolated at least to zero order in the wavefunction and first order in the energy. Similar effects in higher order terms have been discussed by Dalgarno and Lewis (1956) and Schwartz (1959). If there are degeneracies present the procedures above need to be combined and this can be done by minimizing the perturbed energy so that

$$\int \frac{\partial\psi^*}{\partial\mu_i}(H+\lambda P)\psi\, d\tau + \int \psi^*(H+\lambda P)\frac{\partial\psi}{\partial\mu_i}\, d\tau = 0 \qquad (4.05)$$

since this implies stability at any λ and hence also at the limit $\lambda\to 0$. This expression should also be used for a non-degenerate wavefunction if there is a degeneracy induced by the perturbation, i.e. if the energy becomes degenerate for some particular $\lambda_0 \neq 0$. Sometimes the degeneracy is prevented by the non-crossing rule but still the form of the wavefunction changes very rapidly with λ and (4.05) must be used.

In one important particular instance of this basic method the parameters are linear and the trial wavefunction is a linear combination with arbitrary coefficients of some fixed functions (the Ritz method). For many perturbations a suitable set of functions is the set suggested by Hassé (1930) and Lennard-Jones (1930), viz.

$$\psi_0,\quad P\psi_0,\quad P^2\psi_0, \ldots, \qquad (4.06)$$

where ψ_0 is a good approximation to the unperturbed wavefunction. The use of this set is analogous to the power method of finding matrix eigenvectors. Corresponding to this another useful criterion for stability can be written as

$$\int (P\psi_0)^* H\psi_0\, d\tau + \int \psi_0{}^* H(P\psi_0)\, d\tau = 0. \qquad (4.07)$$

Another linear set which is often useful consists of the functions

$$\psi(\lambda_0),\quad d\psi(\lambda_0)/d\lambda,\quad d^2\psi(\lambda_0)/d\lambda^2, \ldots. \qquad (4.08)$$

It may be more convenient to use this set than to permit λ to vary freely particularly when the dependence on λ is non-linear. With a sufficient number of terms the set is equivalent to a Taylor expansion in λ and so leads to a stable wavefunction.

§ 5. SIGNIFICANCE OF SELF-CONSISTENT WAVEFUNCTIONS

A self-consistent wavefunction has the significance of being stable under certain perturbations. If the Hamiltonian for an atom or a molecule had the form of a sum of one-electron operators then, in the absence of degeneracy, a single determinant of orbitals would be an exact wavefunction. Such a wavefunction would also be stable under a perturbation which was the sum of one-electron operators. Since the true Hamiltonian also contains electron repulsion terms the single determinant is only an approximation. The best single determinant wavefunction

$$\Psi=\mathrm{Det}\{\psi_1(1), \quad \psi_2(2), \dots\}, \qquad . \quad . \quad . \quad . \quad . \quad . \quad (5.01)$$

where ψ_i are spin-orbitals, functions of both space and spin, is defined by the equation

$$\delta\int \Psi^*(H-W)\Psi\, d\tau=0, \qquad . \quad . \quad . \quad . \quad . \quad . \quad . \quad (5.02)$$

in which W is the approximate energy and δ acts only on the various ψ_i. By the turnover rule or some equivalent procedure, this equation simplifies to

$$\delta\int \psi_1^*(1)\psi_2^*(2)\dots(H-W)\Psi\, d\tau=0 \qquad . \quad . \quad . \quad . \quad (5.03)$$

and, by treating the variation of individual functions, the set of equations

$$\int \psi_1^*(1)\dots\delta\psi_i^*(i)\dots(H-W)\Psi\, d\tau=0, \quad i=1,\ 2,\ \dots \qquad (5.04)$$

is obtained. The coefficient of the arbitrary variation $\delta\psi_i$ must then vanish and this condition is the usual differential equation for the self-consistent functions ψ_i. Thus, for the self-consistent ψ_i, eqn. (5.04) is satisfied for arbitrary $\delta\psi_i$. If the system is now subject to a perturbation of one-electron form

$$P=\sum_i \mathrm{p}(i) \qquad . \quad . \quad . \quad . \quad . \quad . \quad . \quad . \quad . \quad . \quad (5.05)$$

the first term in eqn. (4.07), after modification as in (2.09) for lack of normalization, can be similarly simplified to become

$$\int P\Psi^*(H-W)\Psi\, d\tau=\sum_i\int \psi_1^*(1)\dots[\mathrm{p}(i)\psi_i^*(i)]\dots(H-W)\Psi\, d\tau \qquad (5.06)$$

and since each term of this has the form of eqn. (5.04) the sum vanishes. The second term in (4.07) is the Hermitean conjugate of this and so the whole equation is satisfied. Thus the self-consistent wavefunction is stable under any one-electron perturbation provided that there is no degeneracy present.

The degeneracy due to the spin restricts the states which can be described by a single determinant which is an eigenfunction of S^2, to those in which all the orbitals are doubly occupied and those whose singly-occupied orbitals all have the same spin factor. In addition, any degeneracy due to the spatial symmetry has to be resolved in a similar way.

§ 6. APPLICATION TO ENERGY CALCULATIONS

The idea of using stable wavefunctions to discuss various perturbations is of special value in energy calculations. It enables some familiar results to be generalized and related to a few basic theorems.

The simplest of these results is the quantum mechanical virial theorem (for full references see Löwdin (1959)). It states that the mean values of the total potential energy and the total kinetic energy of any atom or molecule are in the ratio $2:-1$. An approximate wavefunction, even if its total energy is close to the true eigenvalue, does not necessarily give this same ratio. The theorem is proved, in the usual way, by introducing a variable scale-factor into the trial wavefunction. The equation for the optimal scale-factor is of the form (2.07) and consequently any function in the optimal scale is stable with respect to scale and so gives the correct ratio. Another method of finding a stable wavefunction is by the Ritz method using the functions (4.06) or (4.08). In the helium isoelectronic sequence, for example, with the wavefunction a simple product of orbitals of the form

$$\psi = \exp(-r) \quad . \quad . \quad . \quad . \quad . \quad . \quad . \quad . \qquad (6.03)$$

the scale can be adjusted exactly by scaling or approximately by using

$$\psi_1 = (1-\delta r)\exp(-r), \quad . \quad . \quad . \quad . \quad . \quad . \quad . \qquad (6.04)$$

which is a Ritz-type function with δ as linear parameter and the second function is

$$\frac{\partial}{\partial\lambda}\left[\exp(-\lambda r)\right]_{\lambda=1} \quad . \quad . \quad . \quad . \quad . \quad . \quad . \quad . \qquad (6.05)$$

in accordance with (4.08) when λ is a scale factor. The equivalence between these can be demonstrated by attempting to apply both. The energy found using ψ_1 and the optimal scale for each value of Z, the nuclear charge, is, in reduced Hartree units,

$$W = -\left(Z - \tfrac{5}{16} - \tfrac{3}{32}\delta^2 - \tfrac{9}{64}\delta^3 + \tfrac{27}{512}\delta^4 + \ldots\right)^2 / \left(1 + \tfrac{3}{4}\delta^4 + \ldots\right). \qquad (6.06)$$

This is insensitive to δ and is least for $\delta = 0$. Thus, when the scale is optimized, the extra freedom introduced by the parameter δ in ψ_1 does not improve the wavefunction since this type of improvement has already been used in the scaling. A similar situation is found in many more elaborate calculations in which scaling is used and its symptom is extreme insensitivity to a parameter or the presence of an over-complete set (Löwdin 1956).

Another well-known result is the theorem due to Hellmann and Feynman (1939), according to which the force on a nucleus can be expressed as the sum of forces of classical electrostatic type from the electronic cloud and the remaining nuclei. This theorem is derived by considering a displacement of the nucleus as a perturbation. Many approximate wavefunctions do not satisfy the theorem since they are not stable under this perturbation. Hurley (1954) has shown that the theorem is satisfied if 'floating' trial wavefunctions are used. This is not the only type of stable wavefunction. Since the perturbation is of the one-electron type self-consistent wavefunctions will also be stable in the circumstances discussed in § 4. Approximate stability can also be attained by including in a Ritz-type trial wavefunction terms which correspond to an infinitesimal change of nuclear position.

Any other parameter in the Hamiltonian can be treated as variable and will yield corresponding results. Thus if one nuclear charge Z in an atom or molecule is allowed to vary then the theorem is deduced from (2.08) that the total potential energy $\langle L \rangle$ due to the electrons and that nucleus is given by

$$\langle L \rangle = Z \partial W / \partial Z, \quad . \quad . \quad . \quad . \quad . \quad . \quad . \quad . \quad (6.07)$$

where W is the energy of the atom or the electronic energy of the molecule in the Born–Oppenheimer approximation. Equation (6.07) will also apply to approximate wavefunctions as long as they are stable under the perturbation of a change in Z. Since this is another one-electron perturbation the self-consistent wavefunctions will be stable. The major effect of a change in Z is to change the scale of the wavefunction and consequently for an atom the use of the optimal scale will make the wavefunction closely stable. The difficulties of convergence that arise when $\langle L \rangle$ is calculated using unscaled functions have been noted by Hylleraas and Skavlem (1950).

For an atom in a ^1S state the nuclear magnetic shielding constant σ is very closely related to this potential energy. Lamb (1941) has shown that

$$\sigma = \frac{\alpha^2}{3} \sum_i \left\langle \frac{1}{r_i} \right\rangle, \quad . \quad . \quad . \quad . \quad . \quad . \quad . \quad . \quad . \quad (6.07)$$

when α is the fine structure constant. Thus by analogy with (6.06) the simpler relation

$$\sigma = -\frac{\alpha^2}{3} \partial W / \partial Z \quad . \quad . \quad . \quad . \quad . \quad . \quad . \quad . \quad (6.08)$$

can be given. This equation needs some correction if W is the experimental energy and relativistic corrections are appreciable. Its importance is that σ can be deduced from W without any quantum mechanical calculation. For the two electron series, Hylleraas and Midtdal (1956) have given the energy formula, in H_R,

$$W = -Z^2 + 5Z/8 - 0{\cdot}157\,655 + 0{\cdot}008\,535 Z^{-1} - 0{\cdot}000\,34 Z^{-2}$$
$$- 0{\cdot}000\,82 Z^{-3} - 0{\cdot}002\,445 Z^{-4} \quad . \quad . \quad . \quad . \quad (6.09)$$

and this yields

$$\sigma = \tfrac{1}{3}\alpha^2(2Z - 5/8 + 0{\cdot}008\,535Z^{-2} - 0{\cdot}000\,68Z^{-3} - 0{\cdot}002\,46Z^{\;4} - 0{\cdot}009\,78Z^{-5}. \qquad (6.10)$$

The probable error of σ should be the same as that for W which is about 0·00001 for $Z \geqslant 2$. The values given by this formula are shown in table 1, along with those calculated by Ormand and Matsen (1959) and Hylleraas and Skavlem (1950).

Table 1. Calculated nuclear magnetic shielding constants ($\sigma \times 10^5$)

	H^-	He	Li^+	Be^{++}
Hylleraas and Skavlem		5·9938		
Ormand and Matsen	2·3475	5·9856	9·5396	13·091
This paper	2·432811	5·993347	9·541983	13·091305

The kinetic energy associated with the different nuclei and with the electrons can also be deduced from the total energy by treating the masses as variable parameters. The electronic kinetic energy is given by

$$\langle T_e \rangle = m^{-1}\partial W/\partial(m^{-1}) = -m\partial W/\partial m \qquad (6.11)$$

and the kinetic energy of the nucleus of mass M by

$$\langle T_M \rangle = -M\partial W/\partial M. \qquad (6.12)$$

The hydrogen-like atoms, for example, have a total energy proportional to the reduced mass μ and these equations lead immediately to the result

$$\langle T_M \rangle / \langle T_e \rangle = m/M. \qquad (6.13)$$

§ 7. APPLICATION TO DIPOLE MOMENT CALCULATIONS

When a molecule is placed in a uniform electric field of strength E in the z direction its Hamiltonian will contain the perturbing operator

$$P = -E\sum_i z_i. \qquad (7.01)$$

Since this operator is unbounded for large values of the variables the system is not strictly quantized but nevertheless, as Kato (1951) has shown, psuedo-eigenvalues may be defined and calculated by perturbation methods. The dipole moment of the molecule is defined, as in (3.04), by differentiating the energy with respect to E since this corresponds to the process needed to measure the dipole moment. This derivative reduces to $\langle z \rangle$ only for a stable wavefunction. For a trial wavefunction to yield a good estimate of the dipole moment from $\langle z \rangle$ it is necessary, as in § 4, that it should contain parameters which would enable it to adjust the molecule continuously to the presence of the field. When the wavefunction is built from atomic orbitals the approximate effect of the field is to mix each orbital with one which is z times itself (cf. 4.06). Thus the adjustment of the 2s can be represented by including 2p$_z$ among the orbitals but the 1s function requires what has been called a Kp$_z$ function, i.e. a p$_z$ function whose radial dependence makes it largest in the K shell. Similarly the 2p functions will require Ld functions.

The importance of using stable wavefunctions can be illustrated from some recent calculations on LiH. These are summarized in table 2. It can be seen that the changes in the dipole moment as the wavefunction becomes more stable are considerable and out of proportion to the corresponding improvements in the energy. For more complete stability it may be necessary to include Ld functions on the Li.

Table 2. Dipole moment of lithium hydride

Atomic functions used		$\langle z \rangle$ in	energy in	Reference
on Li	on H	Debyes	ev	
1s, 2s	1s	−0·87	(−206·98)†	Hurst *et al.* (1957)
1s, 2s, 2p$_z$	1s	−6·04	(−208·01)†	
1s, 2s, 2p$_z$, 2pπ	1s	−6·05	−217·51	Karo and Olsen (1959)
1s, 1s, 2p$_z$	1s, Kp	−5·86	−217·07	Platas and Matsen (1958)

† Energy value calculated from data in reference.

REFERENCES

DALGARNO, A., and LEWIS, J. T., 1956, *Proc. roy. Soc.* A, **233,** 70.
FEYNMAN, R. P., 1939, *Phys. Rev.*, **56,** 340.
HASSÉ, H. R., 1930, *Proc. Camb. phil. Soc.*, **26,** 542.
HURLEY, A. C., 1954, *Proc. roy. Soc.* A, **226,** 170.
HURST, R. R., MILLER, J., and MATSEN, F. A., 1957, *J. chem. Phys.*, **26,** 1092.
HYLLERAAS, E. A., and SKAVLEM, S., 1950, *Phys. Rev.*, **79,** 117.
HYLLERAAS, E. A., and MIDTDAL, J., 1956, *Phys. Rev.*, **103,** 829.
KARO, A. M., and OLSON, A. R., 1959, *J. chem. Phys.*, **30,** 1232.
KATO, T., 1951, *J. Fac. Sci. Tokyo. Univ.*, **6,** 145.
LAMB, W., 1941, *Phys. Rev.*, **60,** 817.
LENNARD-JONES, J. E., 1930, *Proc. roy. Soc.* A, **129,** 598.
LÖWDIN, P. O., 1956, *Advanc. Phys.*, **5,** 1; 1959, *J. Mole. Spect.*, **3,** 46.
ORMAND, F. T., and MATSEN, F. A., 1959, *J. chem. Phys.*, **30,** 368.
PLATAS, O., and MATSEN, F. A., 1958, *J. chem. Phys.*, **29,** 965.
SCHWARTZ, C., 1959, *Ann. Phys.*, **6,** 170.
VAN VLECK, J. H., 1932, *The Theory of electric and magnetic susceptibilities* (Oxford: Clarendon Press).

Creep and Stress Relaxation in Alpha-brass at Low Temperatures†

By P. Feltham
Department of Metallurgy, The University, Leeds

[Received May 24, 1960]

Abstract

Creep of vacuum annealed polycrystalline 65/35 alpha-brass was studied at constant stress in the range 77–300°K, close to the yield point, at elongations not exceeding 3%. The tensile strain ϵ increased logarithmically with time, and the characteristic strain $s_{cr} \equiv d\epsilon/d \log_{10} t$, given by the slope of the creep curves in semi-logarithmic representation, decreased approximately linearly with increasing temperature, from 29×10^{-4} at 77°K to 11×10^{-4} at 300°K. The creep was correlated with logarithmic stress relaxation, and the relation $s_{cr} = -s_{rel}/\chi$ was established, where $\chi \equiv d\sigma/d\epsilon$ is the coefficient of work-hardening, and $s_{rel} \equiv d\sigma/d \log_{10} t$ the slope of the corresponding curve obtained with stress relaxation at constant elongation. Both the creep and the relaxation are ascribed to a process of residual slip propagation in which the migration of edge dislocations impeded by the drag of conservatively moving jogs is rate determining. The driving force on the jog is the component of the line tension of the dislocation, which impels the jog in the direction of its Burgers vector; the effective stress on the dislocation is the difference between that necessary to tear it from its locked site and the stress due to the intragranular sub-structure, which opposes its movement through the lattice in the unlocked state. At temperatures exceeding about 300°K, when dislocation locking is weak, both s_{cr} and s_{rel} tend to very small values.

§ 1. Introduction

In a recent paper on the low-temperature stress relaxation of polycrystalline copper and alpha-brasses containing 10–35% Zn, at plastic strains of up to 2% (Feltham 1961), the tensile stress was shown to relax from its initial value σ_0 according to the logarithmic law

$$\sigma_0 - \sigma = s_{rel} \log_{10}(1 + \nu t), \quad . \quad . \quad . \quad . \quad . \quad . \quad . \quad . \quad (1)$$

where ν is independent of the time, t, and s_{rel}, the most characteristic time-independent parameter of the relaxation, given by

$$s_{rel} = -d\sigma/d \log_{10} t, \quad . \quad . \quad . \quad . \quad . \quad . \quad . \quad . \quad . \quad (2)$$

increased approximately linearly with decreasing temperature. At any given temperature in the range investigated (77–300°K) s_{rel} was found to have a minimum at a composition close to Cu_3Zn, which suggested that the rate determining process was influenced by short-range order of the $AuCu_3$ type, occurring in the immediate vicinity of the cores of dislocations.

The main object of the present work was to study the creep of alpha-brass, again at plastic strains close to the yield point, and in the same temperature range as in the case of stress relaxation, for the functional form of the creep law and the temperature dependence of the characteristic parameters were expected to give a more specific indication of the nature of the rate process operative in the creep and in the associated relaxation. Also, existing theoretical treatments of low-temperature creep in metals (Nabarro 1952, Mott 1953, Täubert 1959), and experimental studies (Davis and Thompson 1950, Wyatt 1953, Conrad 1958, Thornton and Hirsch 1958, Michelitsch 1959) were anticipated to be of considerable assistance in the interpretation of the results.

---

† Communicated by the Author.

§ 2. Material and Method

Several rods of 65/35 brass, each 13 cm long and of 2 mm diameter, were together wrapped in thin brass foil of the same composition and then annealed at 730°c for $\frac{1}{2}$ hour in an evacuated silica tube, in which they were also allowed to cool after withdrawal from the furnace. The resulting grain size was approximately $4{\cdot}5 \times 10^{-3}$ cm, as in the rods of brass from the same stock previously used in the work on stress relaxation. Zinc losses during annealing were insignificant.

Fig. 1

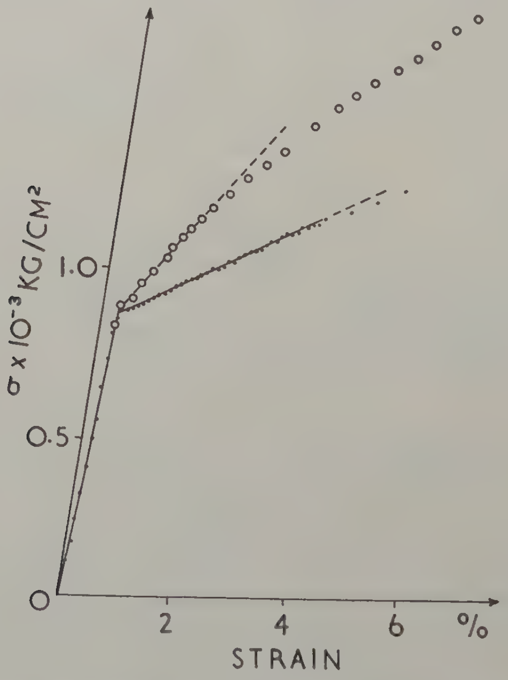

Stress–strain curve of 63/35 alpha-brass at room temperature. Grain size approximately $4{\cdot}5 \times 10^{-3}$ cm. Lower curve: annealing temperature 730°c; upper curve: annealing temperature 800°c. (Extensometer drum chart.)

After hard soldering the specimens into self-aligning grips the gauge length was 9·5 cm. An account of the precautions taken in making the test pieces, as well as the analysis of the brass have been given previously (Feltham 1961).

The stress–strain curve of an annealed specimen extended at room temperature is shown by the lower curve in fig. 1, and was obtained by direct transcription from the drum chart of the extensometer. The tensile yield stresses, σ_y, were close to the corresponding ones determined by Feltham and Copley (1960) with the same type of brass annealed at 800°c for 12 min, given in table 1. However, the initial part of the work-hardening curve was flatter than obtained by them, shown by open circles in fig. 1. The steep portion found on annealing at 800°c is absent; it appears to occur only in conjunction with a polygonized substructure, which does not develop readily below about 750°c (Doo 1960). The flat type of curve was also observed by Feltham and Copley in specimens annealed to the same grain size as at 800°c, but at a lower temperature (600°c).

Table 1. Creep and relaxation data for 65/35 alpha-brass

°K	77	200	273	289	299
$\sigma_y \times 10^{-3}$ kg/cm²	14·3	10·0	—	8·0	—
$G \times 10^{-5}$ kg/cm²	4·50	4·35	4·21	4·20	4·18
s_{rel} kg/cm²	26	19	12	11	10
$s_{\mathrm{cr}} \times 10^4$	29	23	15	12	11
$(s_{\mathrm{cr}}/s_{\mathrm{rel}}) \times 10^4$ kg⁻¹ cm²	1·1	1·2	1·2	1·1	1·1
$G/(s_{\mathrm{rel}}/s_{\mathrm{cr}})$	50	53	52	46	46

With the exception of the first 0·03% of plastic strain, when the hardening rate is anomalously low due to a slight yield-point elongation, a constant work-hardening coefficient, χ, was found up to about 2% of strain at all temperatures, with

$$40 < G/\chi < 50, \qquad (3)$$

where G is the shear modulus given in table 1. All tabulated data were obtained from creep observed at total plastic strains between 0·03 and 2%.

Specimens, completely submerged in liquid nitrogen, solid carbon dioxide in alcohol, or melting ice-plus-water, maintained at a constant level in a 35 cm long tubular cryostat, were mounted in a Hounsfield Tensometer. The '125 lb' beam was used. If, at stresses exceeding the yield point, a strain increment (generally between 0·03 and 0·6%) was applied to the specimen by the manual operation of the drive of the machine, the stress tended to relax, and the level of the mercury in the capillary of the load indicator diminished with time unless the stress was maintained constant at the initial value by the continuation of the straining of the specimen. This was done by means of the manual control of the 'fine' drive of the reduction gear of the machine. A 360° protractor was mounted concentrically with the coarse drive, and was used for the measurement of the strain as function of the time; a 1° rotation was equivalent to an extension of the specimen by about 9 μ.

Some difficulty was experienced in holding the stress constant during the first few seconds after the sudden application of a new stress increment, particularly at 77°K, when the initial rates of relaxation were high. Again, after about 200 sec the creep rate required to maintain the stress at its initial value was so small that the manual control of the stress was no longer fine enough to give a smooth compensation for the residual relaxation. Apart from these limitations the method was found suitable for determining the time-extension relations, and results were reproducible.

Fig. 2

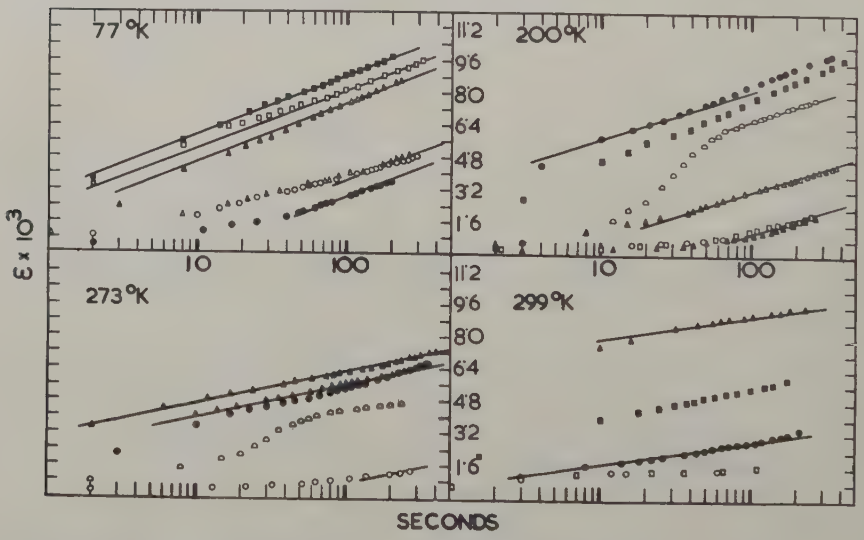

Creep curves of 65/35 alpha-brass annealed at 730°C, at plastic strains within about 3% of the yield point. Semi-circular symbols denote anomalous curves obtained in the yield-point elongation range up to about 0·03% total plastic strain. Curves denoted by other empty symbols refer to creep at plastic strains of 0·03–2%, and the full symbols refer to curves obtained above 2% of total plastic strain.

Creep curves are shown in fig. 2. All, at any given temperature, were obtained with the same specimen. After the determination of a curve due to one stress increment a new small load was added, the strain–time curve was again recorded, and so on. The extension was in each case measured with the zero at the point on the stress–strain curve from which the new increment was applied.

§ 3. EXPERIMENTAL RESULTS

The principal features of the creep, apparent from fig. 2, were its logarithmic form, and the effect of temperature on the time-independent parameter s_{cr} in the equation

$$\epsilon = s_{\mathrm{cr}} \log_{10}(1+\nu t), \quad . \quad . \quad . \quad . \quad . \quad . \quad . \quad . \quad . \quad (4)$$

which was found suitable for the representation of the tensile creep strain. In fact, within the ranges of time amenable to observation by means of the equipment used, the simpler form

$$\epsilon = s_{\mathrm{cr}} \log_{10} \nu t \quad . \quad . \quad . \quad . \quad . \quad . \quad . \quad . \quad . \quad (5)$$

was adequate. Values of the strain s_{cr} obtained from the relation

$$s_{\mathrm{cr}} = d\epsilon / d \log_{10} t, \quad . \quad . \quad . \quad . \quad . \quad . \quad . \quad . \quad . \quad (6)$$

representing the slopes of the parallel lines drawn through some of the representative curves in fig. 2, are shown in table 1. Large values of s_{cr} occur at low temperatures and vice versa. Reproducibility was best at total plastic strains of 0·03–2%. Anomalous curves were obtained at strains of less than about 0·03%, presumably because yielding was not taking place homogeneously throughout the entire length of the specimen and, as will be apparent later, because of the low coefficient of work-hardening near the yield point. Such curves are indicated by semi-circular points in fig. 2. Somewhat high values of s_{cr} were also found at total plastic strains exceeding 2%, again probably because of a decrease in the work-hardening rate below the level in the range 0·03–2% of strain. These anomalies were not pronounced; the strains at which they occurred exceeded those of the 'normal' range by at most $1\frac{1}{2}$%, i.e. giving a total of $3\frac{1}{2}$%.

The occurrence of delay times, if the strain increments were less than about 0·03%, apparent for example in the lowest curves at all temperatures, appears to be a general feature associated with 'source-looking' in stochastic processes of deformation. An interpretation of the phenomenon has recently been given by Yokobori (1959).

The time-independent frequency ν in eqn. (5) (and also in eqn. (15)) can be determined from the intercepts of the creep curves with the strain axis in fig. 2. At any given temperature its magnitude increases with the stress increment; a detailed study of the effect of changes of stress and temperature on ν was not however made.

§ 4. THEORY

4.1. *The Relation between Creep and Stress Relaxation*

In order to be able to discuss both the creep and the corresponding low-temperature stress relaxation of alpha-brasses jointly, we shall first establish a general relation between them. Now, the rate of change of the applied stress with time may be expressed in terms of the relaxation at constant strain and the variation due to work hardening:

$$\frac{d\sigma}{dt}=\frac{\partial\sigma}{\partial t}+\frac{\partial\sigma}{\partial\epsilon}\frac{d\epsilon}{dt}, \qquad (7)$$

which, for stress relaxation at constant strain, reduces to

$$\frac{d\sigma}{dt}=\frac{\partial\sigma}{\partial t}, \quad \frac{d\epsilon}{dt}=0, \qquad (8)$$

while for creep under constant stress

$$\frac{\partial\sigma}{\partial t}=-\chi\frac{\partial\epsilon}{dt}, \quad \frac{d\sigma}{dt}=0. \qquad (9)$$

χ is the coefficient of work-hardening, which we shall assume to be independent of time and strain in the part of the stress strain curve used, so that

$$\frac{\partial\sigma}{\partial\epsilon}=\frac{d\sigma}{d\epsilon}=\chi=\text{const.} \qquad (10)$$

On eliminating $\partial\sigma/\partial t$ between eqns. (8) and (9), and multiplying both sides by t, one obtains

$$\frac{d\sigma}{d\log_{10}t}=-\chi\frac{d\epsilon}{d\log_{10}t}, \qquad (11)$$

so that, with a constant value of χ, logarithmic creep and logarithmic stress relaxation are conjugates, in accord with our observations.

Further, on substituting for the differential coefficients from eqns. (2) and (6), eqn. (11) yields

$$s_{\mathrm{rel}}/s_{\mathrm{cr}}=\chi. \qquad (12)$$

The ratios G/χ (table 1), where G is the shear modulus, were determined by the use of eqn. (12) with s_{cr} values measured in the present work, and s_{rel} as given for the same type of brass by Feltham (1961). They agree well with the corresponding ones obtained with χ's derived directly from the stress–strain curves (eqn. (3)).

4.2. *The Equation of Logarithmic Creep*

Application of the theory of rate processes to creep gives for the shear rate

$$\frac{d\gamma}{dt}=NAb\nu_0\exp(-U/kT), \qquad (13)$$

where N is the number of dislocation elements per unit volume contributing to the creep, A is the area swept out by one such element after activation, b the Burgers vector, and ν_0 an atomic frequency. The tensile creep rate would be given by

$$\frac{d\epsilon}{dt}=a\frac{d\gamma}{dt}, \qquad (14)$$

where a is a constant fraction of the order $\frac{1}{2}$–$\frac{1}{3}$.

In logarithmic creep the apparent activation energy may be expressed with sufficient accuracy, within the intervals of time readily amenable to experimental study of the flow, by

$$U(t)=kT\ln(\nu t), \quad \text{with} \quad \nu=NAb\nu_0/2{\cdot}3s_{\mathrm{cr}}, \qquad (15)$$

and if the assumption is made that it depends linearly upon the effective shear stress acting on the dislocation (e.g. Thornton and Hirsch 1958), one obtains

$$kT\ln(\nu t)=U_0-v(\tau-\tau_g), \qquad (16)$$

where U_0 is independent of stress and time. The effective shear stress is equal to the difference between the applied shear stress τ and the average opposing internal shear stress τ_g, both resolved in the slip direction. The product $v(\tau-\tau_g)$ is a function of the time; v is generally termed the activation volume. If the shear stresses are replaced by corresponding tensile stresses, then in eqn. (16)

$$v(\tau-\tau_g)=q(\sigma-\sigma_g), \qquad (17)$$

with

$$\tfrac{1}{2}>q/v>\tfrac{1}{3}.$$

From eqns. (16) and (17):

$$\frac{d\sigma}{d\ln t}=-\frac{kT}{q}, \qquad (18)$$

which, with eqns. (2) and (12), yields

$$s_{\mathrm{rel}}=\frac{2{\cdot}3\,kT}{q} \qquad (19)$$

and

$$s_{\mathrm{cr}}=\frac{2{\cdot}3\,kT}{q\chi}. \qquad (20)$$

As may be seen from eqns. (19) and (20), the assumption that the activation energy is linear in the effective stress (which we shall show to be consistent with the results obtained), and the relation between s_{cr} and s_{rel} facilitate the evaluation of q, and hence of the activation volume v, as well as of the stress-dependent part of $U(t)$, i.e.

$$Q\simeq Q(\sigma_{\mathrm{y}})=q(\sigma_{\mathrm{y}}-\sigma_g), \qquad (21)$$

where we have replaced σ by σ_{y}, as the former was always within a few per cent of the yield stress in the experiments. Values of Q calculated from the relation†

$$Q=(2{\cdot}3kT/s_{\mathrm{rel}})(\sigma_{\mathrm{y}}-\sigma_g), \qquad (22)$$

obtained by substituting for q from eqn. (19) into eqn. (21), are given in table 2, together with s_{rel} and σ_{y} taken respectively from the data of

---

† As $T\rightarrow 0$ creep will be observable at a finite time only if also $Q\rightarrow U_0$ (eqn. (16)). U_0 is therefore the energy supplied by the line tension in moving a jog without thermal activation (see § 4.4). If it is assumed that $\sigma_g(T)=\sigma_{\mathrm{y}}(400°\mathrm{K})G(T)/G(400)$, the values of Q in table 2 are decreased by 3–10%.

Table 2. Activation energies derived from eqns. (22) and (23); given in kcal/g atom

Brass		Cu	90/10	80/20	70/30	65/35
77°K	Q	5·3	8·0	5·6	5·0	9·9
	Q_j	5·0	7·6	5·3	4·7	8·5
200°K	Q	7·3	9·9	5·9	6·3	10·6
	Q_j	6·2	8·4	5·0	5·3	8·8
299°K	Q	7·0	9·9	7·7	4·6	11·0
	Q_j	5·5	7·7	5·9	3·5	8·3

Feltham (1961) and Feltham and Copley (1960). The stresses σ_g are shown in fig. 3, and were found by extrapolating the σ_y/T curves of Feltham and Copley from 300°K to the virtually temperature-independent part at 400°K; hence $\sigma_g = (\sigma_y)_{400°K}$. A similar method of deriving σ_g in low-temperature creep has also been employed by Thornton and Hirsch (1958). We shall return to the discussion of the probable significance of σ_g below.

Fig. 3

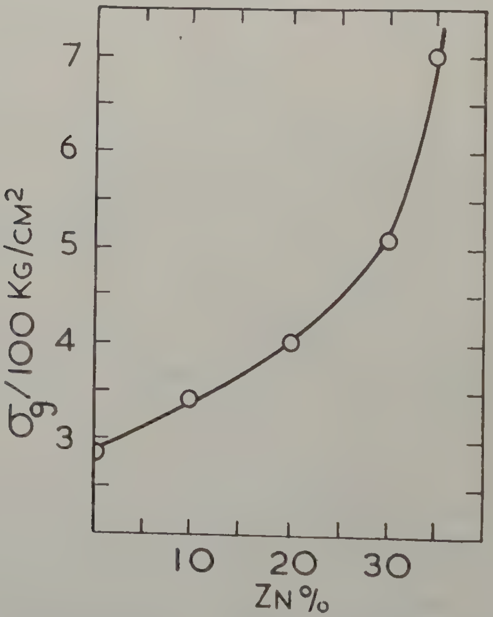

The intragranular elastic stress σ_g. Values indicated by points are equal to the tensile yield stresses of the brasses at 400°K, and were obtained by extrapolation from the data of Feltham and Copley (1960).

4.3. *The Rate Process*

The values of Q in table 2 may be in error by as much as $\pm 10\%$, particularly those referring to room temperature, where σ_g approaches σ_{y} closely (eqn. (22)). It is nevertheless apparent that Q is not appreciably temperature dependent, which implies (eqns. (16) and (21)) that with t equal to a few seconds $\ln(\nu t)$ in eqn. (16) must be close to zero. Values of ν found by Feltham (1961) in the work on stress relaxation referred to above were of the order of 10/min, which, on substituting into eqn. (16) shows that for small t, i.e. with $\sigma \simeq \sigma_{\mathrm{y}}$ we can write

$$Q \simeq U_0 \qquad . \quad . \quad . \quad . \quad . \quad . \quad . \quad . \quad . \quad . \qquad (23)$$

irrespective of temperature within the range studied. The small values of ν are probably due to the small number of dislocation elements per unit volume contributing to the creep, and to the small area swept out by each such element after activation (eqn. (15)). Similar low values of the corresponding parameter were found by Davis and Thompson (1950) in precipitation hardened alloys.

The actual magnitude of Q in copper, for example, is close to the activation energy determining the temperature dependence of the activation volume q in high temperature creep, i.e. 6·6 kcal/g atom, which Feltham (1957) associates with the conservative migration of jogs in dislocations. The lattice defect in the re-entrant corner of a jog in an undissociated edge dislocation resembles a small vacancy, which the dislocation must drag along on moving (Maddin and Cottrell 1955). A somewhat more complex defect would exist in an extended jog. Feltham (1957) suggested that the activation energy for jog migration should take the form

$$Q = Q_j[1-(T/T_{\mathrm{m}})] \qquad . \quad . \quad . \quad . \quad . \quad . \quad . \quad . \qquad (24)$$

where the constant Q_j is equal to Q at 0°K, and T_{m} is the melting point of the metal. The values of Q_j obtained by means of eqn. (24) are also shown in table 2; T_{m} was in each case taken to be solidus temperature of the particular brass. For any given brass Q_j can be seen to be constant within the limits of experimental error.

The mean values of Q_j, shown in fig. 4, show a definite minimum close to the composition Cu_3Zn. If jog migration is rate determining this could be interpreted as signifying a reduction of the misfit energy associated with the jog defect due to the interaction of the defect with solute atoms, enhanced by short range order localized in its immediate vicinity. It should be noted that Q_j does not appear to depend in an obvious manner on the stacking-fault energy, and it cannot therefore be attributed readily to processes such as the mutual intersection of dislocations as visualized by Thornton and Hirsch (1958), or to cross-slip, the break-down of Cottrell–Lomer barriers, the formation of constrictions at the points of intersection of extended dislocations, and other processes requiring the recombination of extended dislocations.

In relation to the short-range order it is interesting to note that Masumoto *et al.* (1952) obtained evidence of short-range order in alpha-brasses at low temperatures by specific-heat measurements, and found that ordering ceased to take place at temperatures above about 360°K, i.e. at about the same temperature at which the $s_{\rm rel}$ versus T curves of alpha-brasses appear to converge to a common, low, value (Feltham 1961).

Fig. 4

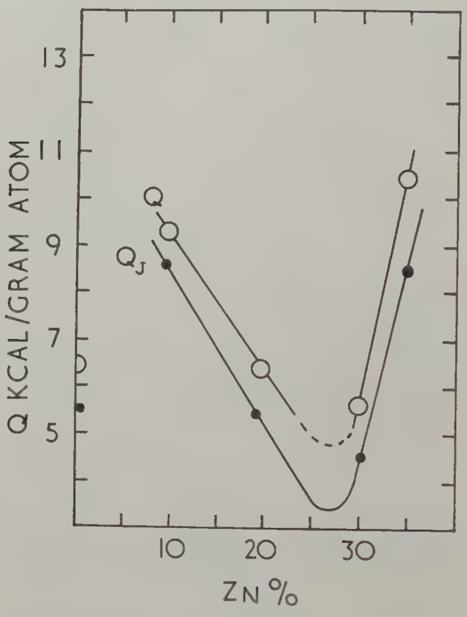

Mean values of the activation energies given in table 2.

Feltham and Copley (1960) suggest that the strong temperature dependence of σ_y below about 300°K results from a special form of Cottrell locking of dislocations, in which the tendency to the formation of short-range order near dislocation cores becomes instrumental in confining partial dislocations to close-packed crystallographic directions, and that ordering is most pronounced in brasses with compositions close to Cu_3Zn. They also show that σ_g (eqn. (22)) does depend somewhat upon the intragranular sub-structure resulting from any given heat treatment. This, and the observation that σ_g increases uniformly with the zinc content, and hence with decreasing stacking-fault energy (fig. 3), as well as the small temperature dependence of σ_y above about 300°K, suggest that a significant part of the internal stress σ_g at temperatures of the order of 300–400°K may be due to the interaction between stacking faults and solute atoms (and vacancies), of the type considered by Suzuki (1957) and Flinn (1958).

We believe that the foregoing observations, particularly the derivation of constant Q_j values from eqn. (24) are consistent with the assumption that the driving force of the activated process in the low-temperature creep and relaxation considered is the effective shear stress acting on the dislocation after it has broken away from its locked position, i.e. the strongly temperature sensitive part of the yield stress, represented by the bracketed term in eqn. (22). The locking is virtually ineffective in brasses above about 360°K. In copper the creep and relaxation are very small at all temperatures in the range, and the effective stress probably derives from the pinning of dislocations by residual impurities and vacancies.

4.4. *The Activation Volume*

An estimate of v (eqn. (16)) can be obtained by considering the migration of a jog in an edge dislocation. Neglecting the dissociation of the dislocation, the force F on the jog J (fig. 5) is

$$F = 2T' \sin \alpha,$$

where α is the angle between the tangent to the circular dislocation arc at J and the radius of curvature, ρ, passing through J, l is the mean spacing between adjacent jogs, and T' the line tension of the dislocation:

Fig. 5

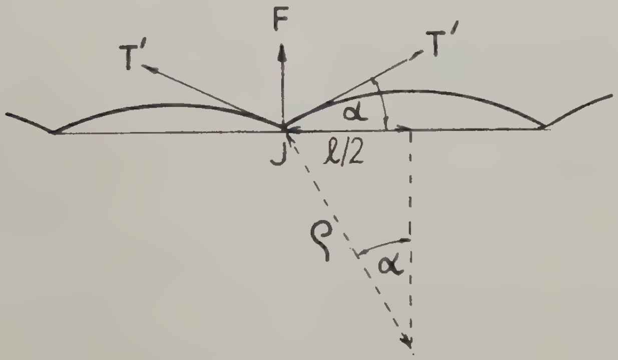

Schematic representation of the resultant force F acting on the jog J. The dislocation is bowed out into arcs by the effective shear stress $\tau - \tau_g$.

$$T' = \rho b(\tau - \tau_g).$$

As $\sin \alpha = l/2\rho$, we have

$$F = (\tau - \tau_g)bl,$$

and hence

$$Q = (\tau - \tau_g)b^2 l,$$

or with

$$\tau - \tau_g = \tfrac{1}{3}(\sigma - \sigma_g)$$

and $\sigma = \sigma_{\mathrm{y}}$:

$$l_{\mathrm{y}}/b = 3Q/(\sigma_{\mathrm{y}} - \sigma_g)b^3,$$

which, on substituting measured values, gives for 65/35 alpha-brass $l_{\mathrm{y}}b/ \simeq 200$ at 77°K, and approximately 500 at room temperature.

ACKNOWLEDGMENT

I am indebted to Mr. Trevor Myers for assistance with the experiments.

REFERENCES

CONRAD, H., 1958, *Acta Met.*, **6**, 339.
DAVIS, M., and THOMPSON, N., 1953, *Proc. phys. Soc. Lond.* B, **63**, 847.
DOO, V. Y., 1960, *Acta Met.*, **8**, 106.
FELTHAM, P., 1957, *Phil. Mag.*, **2**, 584; 1961, *J. Inst. Met.*, **89**, 210.
FELTHAM, P., and COPLEY, G. J., 1960, *Acta Met.*, **8**, 542.
FLINN, P. A., 1958, *Acta Met.*, **6**, 631.
MADDIN, R., and COTTRELL, A. H., 1955, *Phil. Mag.*, **46**, 735.
MASUMOTO, H., SAITO, H., and SUGIHARA, M., 1952, *Sci. Rep. Res. Insts Tôhoku Univ.* A, **4**, 480.
MICHELITSCH, M., 1959, *Z. Metallk.*, **50**, 548.
MOTT, N. F., 1953, *Phil. Mag.*, **44**, 742.
NABARRO, F. R. N., 1952, *Advanc. Phys.*, **1**, 269.
SUZUKI, H., 1957, *Dislocations and Mechanical Properties of Crystals* (New York: John Wiley and Sons), p. 361.
TÄUBERT, P., 1959, *Abh. dtsch. Akad. Wiss. Berl.* (*Ser. Math. Phys., Techn.*), No. 7.
THORNTON, P. R., and HIRSCH, P. B., 1958, *Phil. Mag.*, **3**, 738.
WYATT, O. H., 1953, *Proc. phys. Soc. Lond.* B, **66**, 459.
YOKOBORI, T., 1959, *Kolloidzschr.*, **166**, 20.

Interactions between Dislocations with Burgers Vectors at 120° in Crystals of Silver Bromide†

By J. T. Bartlett and J. W. Mitchell‡
H. H. Wills Physics Laboratory, University of Bristol

[Received July 12, 1960]

Abstract

A detailed analysis is given of examples of the combination, in crystals of silver bromide, of two dislocations on intersecting glide planes with Burgers vectors at 120°. The observations provide direct evidence for the occurrence of pencil glide in which slip can occur on any plane containing a ⟨110⟩ lattice vector.

§ 1. Introduction

We have recently described a method for sensitizing crystals of silver bromide which allows surface terraces and dislocation lines introduced during the earliest stages of plastic deformation to be made visible simply by exposing the crystals to radiation from a medium pressure mercury vapour lamp (Bartlett and Mitchell 1960 a). This permits the glide planes of the dislocations to be determined with reasonable accuracy. The Burgers vectors of the dislocations can then be deduced if the direction of the effective shear stress can be inferred. This method has already been used to show that two dislocations with Burgers vectors of $\frac{1}{2}a\langle 110\rangle$ can combine in a silver bromide crystal to form a single dislocation with a Burgers vector of $a\langle 100\rangle$ (Bartlett and Mitchell 1960 b).

In the present work we have made a detailed study of two cases of the interaction between dislocations on intersecting glide planes with Burgers vectors at 120°. Many cases of such interactions have been observed near the surfaces of silver bromide crystals.

This interaction, in which the intersecting dislocations are unable to form Lomer–Cottrell dislocations, has been discussed by Whelan (1959) in terms of the Thompson nomenclature (Thompson 1953) with particular reference to stainless steel which deforms by glide on {111} planes. He observed frequent examples of the interaction when dislocations piled up on one glide plane were intersected by a dislocation lying on another glide plane. The position with silver chloride and silver bromide which deform by pencil glide (Nye 1949) is more complicated. Here, as we have established by direct observations both in our previous work and in the present work, any plane containing a ⟨110⟩ lattice vector, the pole of which does not lie in the immediate neighbourhood of the pole of a {100} plane can act as a glide plane. To emphasize this, we present two examples of the particular interaction to be discussed here in which different pairs of glide planes are involved. For the description of the interactions, we prefer to use indices to define the Burgers vectors and the glide planes of the dislocations as the Thompson notation is less convenient when the glide planes are not {111} planes. We use an arrow to show the positive sense of the dislocation line and write the Burgers vector beside the arrow.

---

† Communicated by the Authors.

‡ Now at the Department of Physics, University of Virginia, Charlottesville, Virginia.

Fig. 2

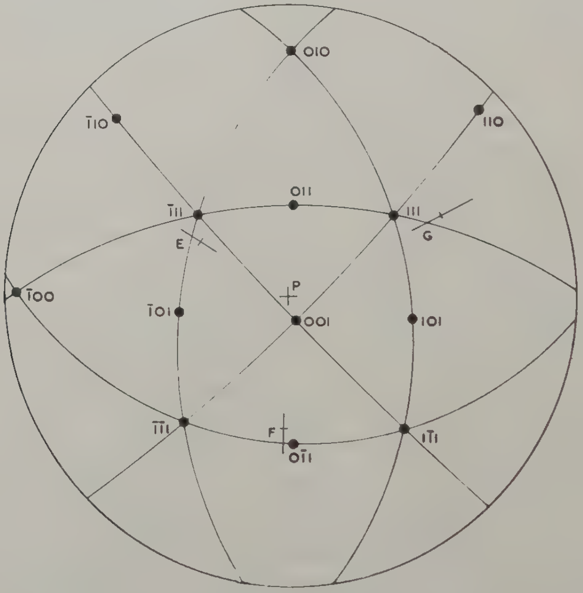

Stereographic projection of the crystal of fig. 1.

§ 2. Experimental Observations

Full details of the experimental methods have been given in two previous papers (Bartlett and Mitchell 1960 a, b) and nothing further need be added here. The systems of dislocations form networks in three dimensions and considerable difficulty has been experienced in producing a satisfactory record at the necessary high magnification. This problem has been partially resolved, where necessary, by taking a series of photomicrographs with the microscope focused successively on planes at an increasing depth below the surface. The sharply focused sections were then cut out from enlargements of the negatives and assembled to form a mosaic.

The first interaction which we will describe is shown in the photomicrograph of fig. 1†. The orientation of the crystal was determined from a back-reflection Laue x-ray diffraction photograph and the pole of the surface, P, is plotted in the stereographic projection of fig. 2. We have found that the glide planes which we determine experimentally are always near planes containing a $\langle 110 \rangle$ lattice vector. This can be seen on the stereogram where we have plotted the poles of the glide planes. The orientations of the glide planes were deduced from observations with the microscope of the relative positions of the surface terraces and of the corresponding dislocation lines with respect to the known orientation of the crystal. The lengths of the arcs represent the error in the observations. We therefore conclude that the two approximately parallel dislocations were introduced by glide on a pair of planes with poles very near the pole, E, of the $(\bar{3}23)$ planes. As the specimen was deformed by the application of very small tensile stress, the dislocations must have a Burgers vector of $\frac{1}{2}a[101]$. They are crossed by a third dislocation on a $(0\bar{1}1)$ plane with a pole at F on the stereogram. This dislocation has a Burgers vector of $\frac{1}{2}a[0\bar{1}\bar{1}]$. It combines with the other two dislocations lowering the elastic strain energy to form a dislocation with a Burgers vector of $\frac{1}{2}a[1\bar{1}0]$ along the line of intersection of the glide planes ; this is a [533] direction which is represented by the point G on the stereogram. This deduction is consistent with the experimental observations, the error in which is indicated by the length of the arc at G. The glide plane of the resultant dislocation would be a $(33\bar{8})$ plane but the dislocations meeting at the nodes could not move simultaneously on their three intersecting glide planes so that the nodes are effectively immobile. The results of the analysis of this interaction are summarized in the diagram of fig. 3.

A second interaction of the same type is shown in the photomicrograph and diagrams reproduced as figs. 4, 5 and 6. In this crystal, dislocations with Burgers vectors of $\frac{1}{2}a[01\bar{1}]$ and $\frac{1}{2}a[\bar{1}01]$ on $(\bar{1}11)$ and (212) glide planes, respectively, are involved. The poles of these glide planes are indicated, as before, by E and F in the stereogram. The dislocations combine to form a dislocation with a Burgers vector of $\frac{1}{2}a[\bar{1}10]$ along the line of intersection of the two glide planes which is a $[\bar{1}\bar{4}3]$ direction. This is shown at G on the stereogram. The glide plane of the combined dislocation would therefore be a (335) plane. The validity of this analysis of the interaction was confirmed by the analysis of further interactions between these dislocations and other intersecting dislocations in the surrounding area. At A in fig. 6, the dislocation on the (212) plane interacts and annihilates with a dislocation with the same Burgers vector on a $(1\bar{1}1)$ plane. The pole of this plane is plotted on the stereogram at H. At B and C in fig. 6, the dislocations on the $(\bar{1}11)$ and (212) planes are intersected by a third dislocation on a $(\bar{1}\bar{1}1)$ plane

---

† Figures 1 and 4 are shown as plates.

Fig. 3

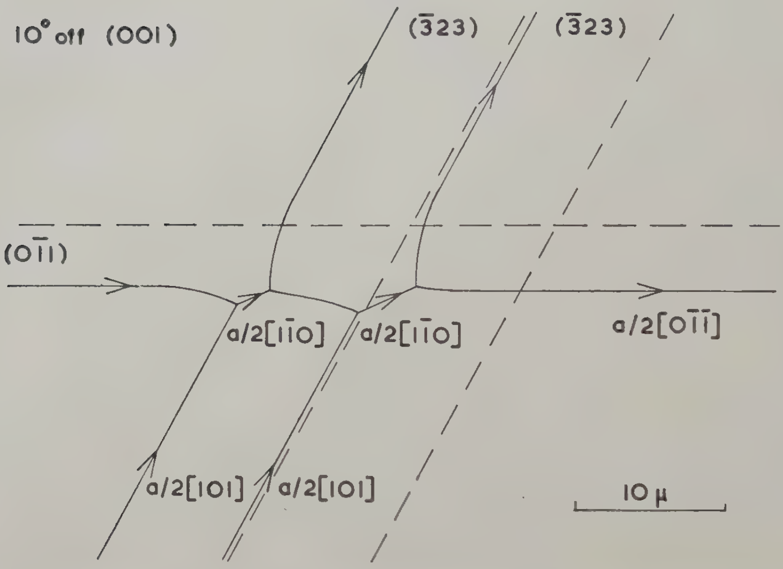

Diagram showing the Burgers vectors and glide planes of the dislocations in fig. 1. The dotted lines are the projections on the plane of the diagram of the traces of the intersections of the glide planes with the surface of the crystal.

Fig. 5

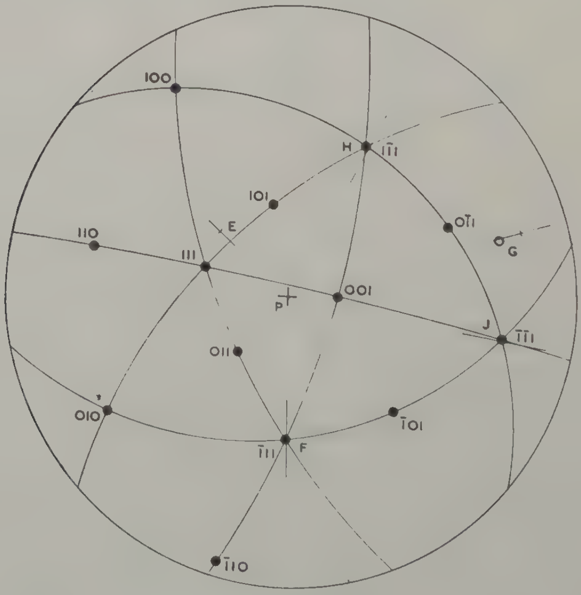

Stereographic projection of the crystal of fig. 4.

represented by J in the stereogram with a Burgers vector of $\frac{1}{2}a[\bar{1}0\bar{1}]$. A further example of an interaction between two dislocations with Burgers vectors at 120° therefore occurs at B, while the two dislocations meeting at C combine to form a segment with a Burgers vector of $a[\bar{1}00]$ (see Bartlett and Mitchell 1960 b).

The one possible alternative assignment of Burgers vectors was excluded as being inconsistent with deformation by the application of a tensile stress.

Fig. 6

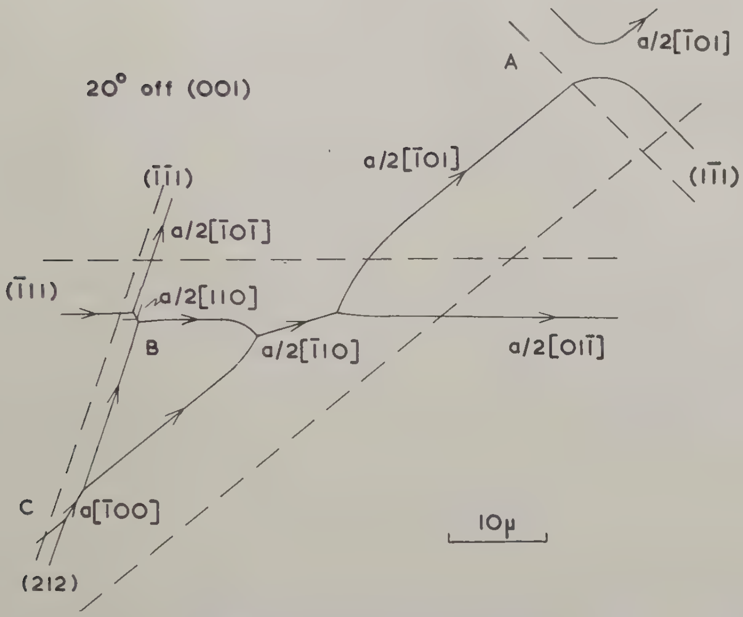

Diagram corresponding to fig. 4.

Acknowledgments

This work was begun during the tenure of a Research Studentship in the University of Bristol awarded to J. T. Bartlett by the Department of Scientific and Industrial Research. It was completed while he was holding a Research Fellowship in the Department of Physics of the University of Virginia. The work in Bristol was supported by a grant from Kodak, Ltd., and, in Virginia, by the United States Atomic Energy Commission. All this assistance is gratefully acknowledged.

References

Bartlett, J. T., and Mitchell, J. W., 1960 a, *Phil. Mag.*, **5**, 445; 1960 b, *Ibid.*, **5**, 799.
Nye, J. F., 1949, *Proc. roy. Soc.* A, **198**, 190.
Thompson, N., 1953, *Proc. phys. Soc., Lond.*, **66**, 481.
Whelan, M. J., 1959, *Proc. roy. Soc.* A, **249**, 114.

Thermal Expansion of Aluminium at Low Temperatures†

By Eva Huzan, C. P. Abbiss and G. O. Jones
Department of Physics, Queen Mary College (University of London),
London, E.1

[Received July 22, 1960]

Abstract

The thermal expansion of aluminium has been determined by a sensitive optical method between 100°K and 15°K; that is, down to temperatures below $\Theta_D/20$. At the lowest temperatures the Grüneisen parameter shows a significant rise. The results are discussed from the point of view of the theory of lattice vibrations.

§ 1. Introduction

In the past few years there has been renewed interest in the thermal expansion of crystals at low temperatures (Rubin *et al.* 1954, Bijl and Pullan 1954, 1955, Barron 1955, Domb and Zucker 1956, Figgins *et al.* 1956, Simmons and Balluffi 1957, Blackman 1958, Dheer and Surange 1958, Gibbons 1958). The importance of the coefficient of thermal expansion

$$\alpha=\frac{1}{V}\left(\frac{\partial V}{\partial T}\right)_p$$

is that it is one of the three independent derivative thermodynamic parameters which are experimentally accessible. In the dynamical theory of crystal lattices its importance is that it leads to information about the variation with volume of the frequency distribution of lattice vibrations.

The expansion coefficient α is best studied via the Grüneisen parameter $\gamma=\alpha V/c_v\kappa_T$ which is of course constant for simple isotropic solids over a wide range of temperature. On the Debye model this implies the Grüneisen assumption that for all frequencies (ν_j) the quantities $\gamma_j(=-d\ln\nu_j/d\ln V)$ are equal and given by $\gamma=-d\ln\Theta_D/d\ln V$. There have been few attempts to predict theoretically the variation of α at low temperatures and only that by Barron makes use of a proper lattice theory.

Experimentally, the situation seems to be that for simple isotropic solids γ remains nearly constant at least down to $\Theta_D/10$. Below these temperatures the facts are still uncertain because the values of α to be measured ($\approx 10^{-6}$ for aluminium, say) are so small. In a previous paper (Figgins *et al.* 1956) measurements were reported on aluminium using X-ray diffraction for the measurements of lattice parameter. This method gave good results down to $\Theta_D/10(\approx 40°\text{K})$, and it is, of course, an absolute method. In the present paper we describe measurements using a new optical method giving good results below $\Theta_D/20$ and capable of use at still lower temperatures.

---

† Communicated by the Authors.

§ 2. EXPERIMENTAL METHOD

Previous methods for the measurement of α at low temperatures have included the use of X-ray diffraction (Figgins *et al.* 1956, Simmons and Balluffi 1957), an optical lever (McLennan *et al.* 1931), interferometric techniques (Rubin *et al.* 1954) and capacitative dilatometers (Bijl and Pullan 1955, Dheer and Surange 1958).

The present method makes use of the optical lever principle, but employs a microptic autocollimator (Hilger and Watts), a kinematically designed twin-strip mechanism (Geary 1954), and an optical system designed to eliminate all errors due to incidental movement or to thermal expansion of parts of the apparatus other than the test specimen. The ultimate sensitivity in measuring the linear thermal expansion of a 5 cm specimen corresponds for the optical lever used to a displacement of about 30 Å, that is, defines an α of 1×10^{-6} with an accuracy of about 20% with a temperature interval of 1°K.

The apparatus is shown schematically in fig. 1. Expansion of the test specimen relative to a control specimen causes the rotation of a mirror attached to a twin-strip mechanism held between them. The two specimens are mounted on a glass plate, and a second mirror, inclined at about 90° to the first, is carried by the control specimen. The autocollimator, having an ultimate sensitivity of 0·3″ of arc, indicates the angle between the mirrors through the separation between the images formed by the two beams of light passing between the mirrors in opposite directions. To the first order the separation between the images depends only on the angle between the mirrors and is not affected by incidental rotations or movements in the system. The field of view of the instrument is only 10′ of arc so that to keep the images suitably placed it is necessary to make adjustments from outside, using control rods which can be disengaged. In separate experiments at room temperature the device was checked for linearity.

The assembly is set up in an evacuated cryostat with anti-vibration mountings. By means of helium as exchange gas the comparator system can be brought into thermal equilibrium with the cryostat, whose temperature is controlled by balancing the Joule–Kelvin cooling of hydrogen against electrical heating.

The comparator is absolute in the sense that it measures the relative expansion of two specimens of the same metal at different temperatures and does not depend upon the expansion coefficient of another material. There is however a temperature gradient near the specimen so that it is

Fig. 1

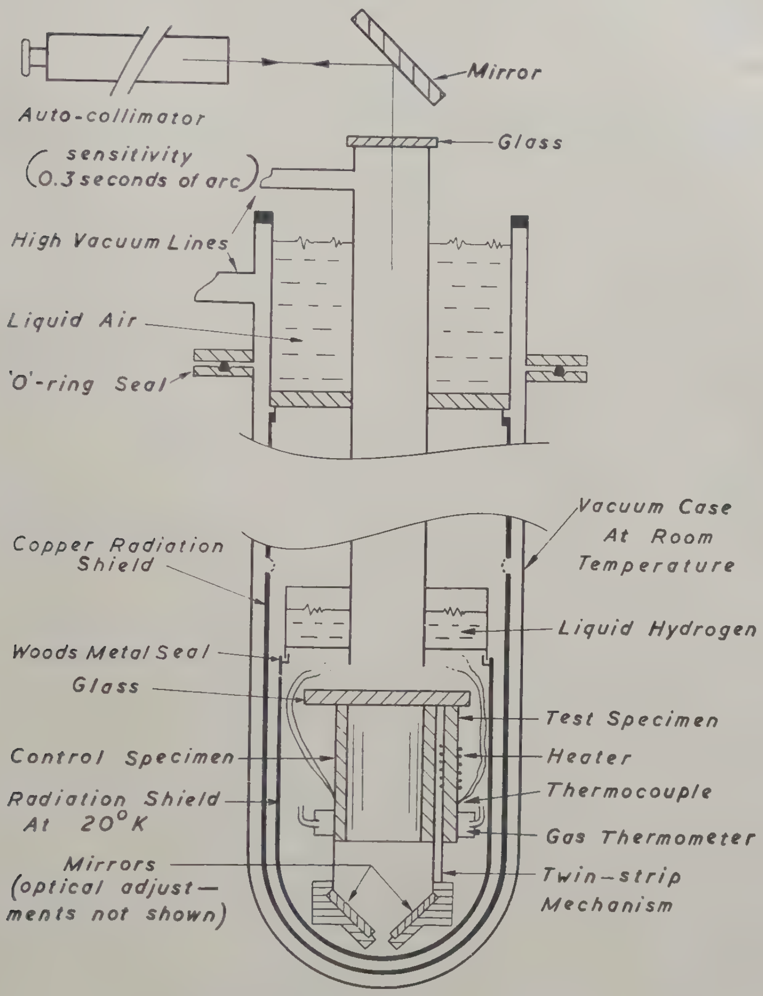

Schematic diagram of apparatus.

essential to use a dynamic method—somewhat similar to that used in the ‘ discrete heating ’ method of determining specific heats—in which temperatures and deflections are continuously watched.

Temperatures were determined using copper–constantan thermocouples calibrated at the steam, ice, oxygen and hydrogen points and at the hydrogen triple point. At the lowest temperatures helium gas thermometers, arranged differentially, may also be used.

The sensitivity of the optical lever depends critically upon the separation of the strips and so was determined *in situ* by making use of a value of α at room temperature of $7{\cdot}05 \times 10^{-5}\,\mathrm{deg}^{-1}\,\mathrm{C}$ taken from the tabulated data of Nix and McNair (1941). Cooling the mechanism from room temperature to 20°K cannot alter the sensitivity by more than $\frac{1}{2}$%.

The aluminium was stated to be at least 99·99% pure (British Aluminium Company), and was poly-crystalline.

§ 3. Results

The results are shown in fig. 2, where each circle represents a separate experimental determination. Because of the difficulty of measuring small values of α with accuracy a greater number of experiments were performed at the lowest temperatures. We believe that the values

Fig. 2

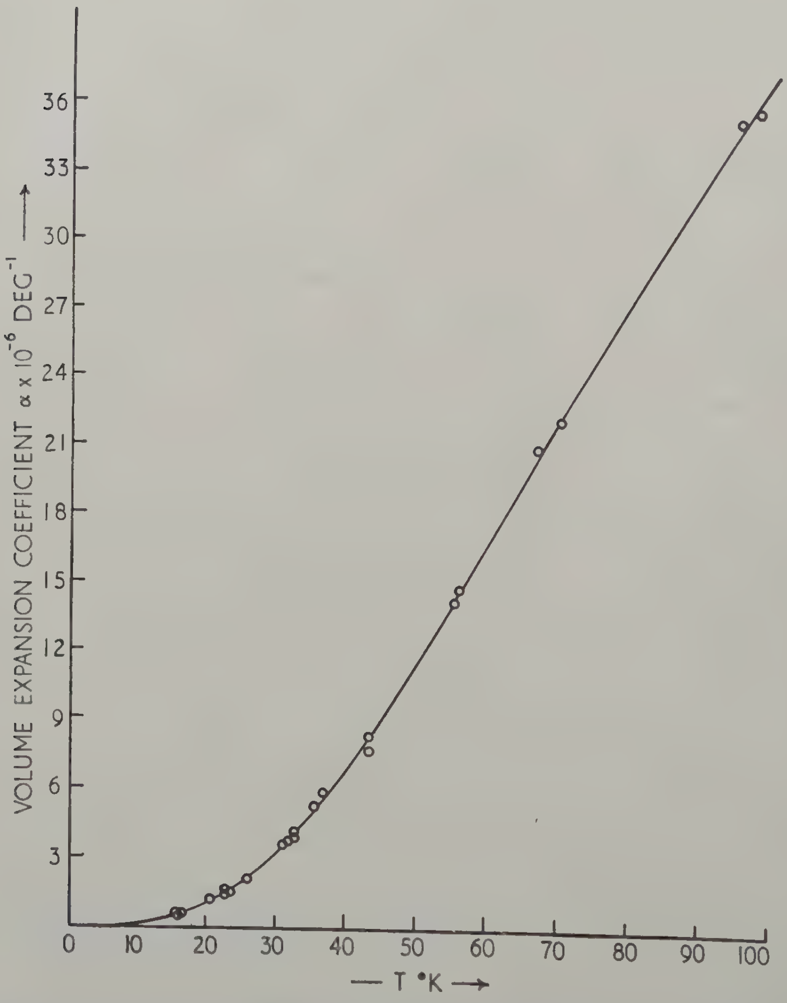

Coefficient of thermal expansion of aluminium as a function ot temperature: results of the present investigation.

represented by the curve as drawn are accurate to within about ±1·5% at 100°K, and ±30% at 15°K.

Fig. 3

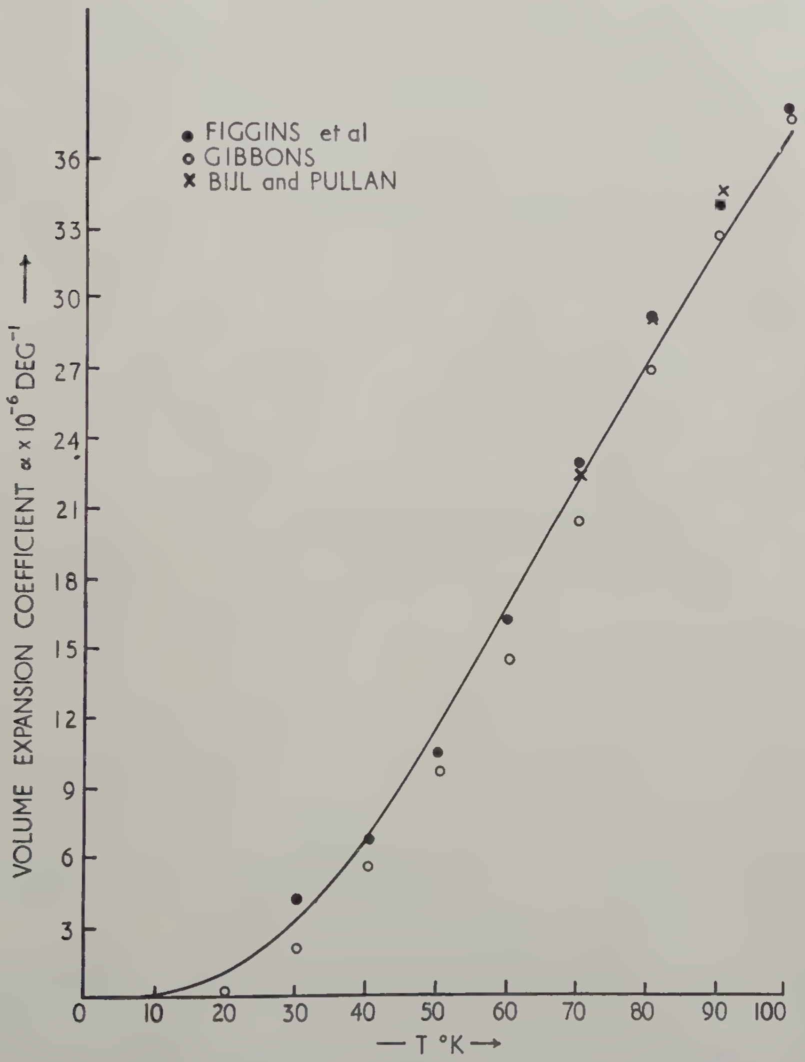

Coefficient of thermal expansion of aluminium: comparison of present results with those of other workers.

In fig. 3 the same curve is drawn, with values plotted from the results of Bijl and Pullan (1956, private communication), Figgins *et al.* (1956) and Gibbons (1958). The only other published results on aluminium near $\Theta_D/20$ are those of Gibbons and it will be seen that our results are in disagreement with his at low temperatures.

In order to obtain a value of the Grüneisen parameter characteristic of the lattice only, we have used the formula

$$\gamma_l = \left(\frac{\alpha V}{\kappa_T} - \frac{2}{3} c_e\right) \Big/ (c_v - c_e)$$

(Bijl and Pullan 1955) where c_e is the electronic specific heat. As can be seen in fig. 4, we find a marked rise in γ_l below $\Theta_D/10$ which we believe to be well outside experimental uncertainty. Rounded values of α and γ_l at intervals of 5° or 10° are shown in the table, together with the data used in the computations, and their sources.

Fig. 4

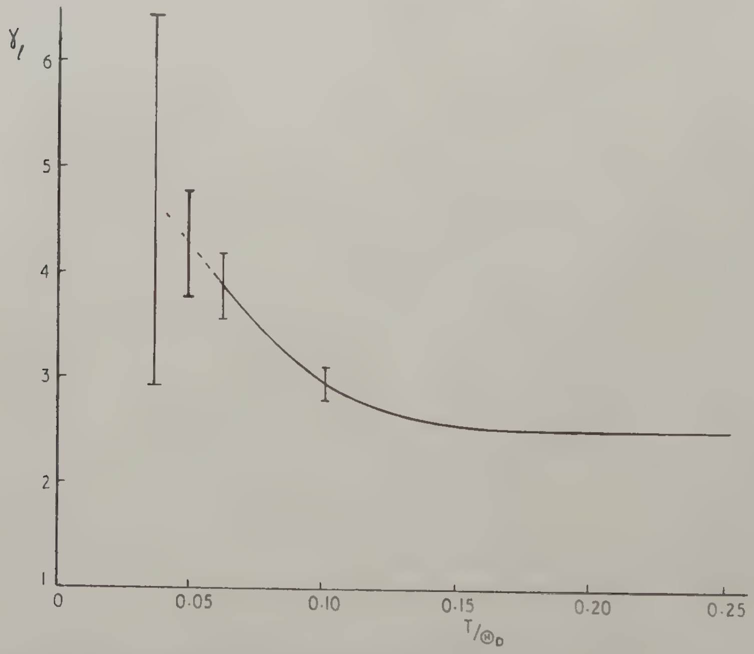

Variation with temperature of the Grüneisen parameter (γ_l) of aluminium.

§ 4. Discussion

The theory of Barron computes γ as a weighted average of the γ_j taken over the different modes of vibration, and using a central force model predicts a drop in γ near $0{\cdot}2\Theta_D$. A general treatment making use of the Debye–Brillouin model and leading to restricted conclusions is that of Bijl and Pullan (1954). They adopt the method of assuming the same cut-off wavelength for longitudinal and transverse waves and thus two different cut-off frequencies. This leads to the existence of a high-temperature and a low-temperature limit for γ, and they conclude that the low-temperature limit will be the greater†. An attempt is made

---

† The definitions of γ employed by Bijl and Pullan and ourselves are not identical, but their conclusion must apply to both cases.

Rounded values of α and γ_l with data used in computations

T °K	T/Θ_D ($\Theta_D = 400$°K)	α deg$^{-1} \times 10^{-6}$	κ_T cm^2 dyne^{-1} 10^{-12}	V cm^3 g atom^{-1}	c_v erg g atom^{-1} deg$^{-1} \times 10^6$	c_e	$\dfrac{\alpha V}{c_v \kappa_T}$	γ_l
15	0·037	$0{\cdot}3_5 \pm 0{\cdot}1$	1·13	9·869	0·92	0·206	3·3	$4{\cdot}1 \pm 2$
20	0·050	$1{\cdot}0 \pm 0{\cdot}1$	1·13	9·869	2·26	0·274	3·9	$4{\cdot}3 \pm 0{\cdot}5$
25	0·062	$1{\cdot}8_5 \pm 0{\cdot}1$	1·13	9·869	4·68	0·342	3·5	$3{\cdot}8 \pm 0{\cdot}3$
30	0·075	3·3	1·13	9·870	8·49	0·410	3·4	3·5
35	0·088	$4{\cdot}8_5$	1·13	9·870	13·88	0·478	$3{\cdot}0_5$	3·1
40	0·100	$6{\cdot}7_5 \pm 0{\cdot}2$	1·13	9·870	20·92	0·547	2·82	$2{\cdot}8_5 \pm 0{\cdot}2$
50	0·125	11·6	1·13	9·871	38·15	0·684	2·65	2·68
60	0·150	$16{\cdot}9_5$	1·14	9·872	57·52	0·821	2·56	2·58
70	0·175	22·3	1·14	9·874	77·22	0·949	2·50	2·53
80	0·200	27·4	1·14	9·877	96·13	1·094	2·47	2·48
90	0·225	32·4	1·15	9·880	113·54	1·231	2·45	2·47
100	0·250	$37{\cdot}3 \pm 0{\cdot}5$	1·15	9·884	129·43	1·368	2·48	2·50

References: Θ_D: Walker 1956; κ_T: Sutton 1953; V: Figgins *et al.* 1956; c_v: Giauque and Meads 1941; c_e: Howling *et al.* 1955.

to compute the effective contribution γ_l of the lattice only by assuming that the electronic contribution corresponds to the free-electron value of $\frac{2}{3}$ for γ_e. We have used the same procedure, and it is worth noting that at the lowest temperatures the differences between γ and γ_l are significant, as may be seen in the table. The main result of the present work is that γ_l rises at the lowest temperatures, as suggested by Bijl and Pullan.

The deficiencies in the present theoretical situation are particularly obvious for the case of metals and it is worth considering whether any improvement can be made by empirical means. It does not seem possible at present to improve on the somewhat over-simplified procedure of extracting γ_l from the data by assuming a value for γ_e. It is however possible to insert certain data on the variation of elastic constants with pressure due to Lazarus (1949). On the assumption that the γ_j take constant values $\gamma_{\text{long.}}$ and $\gamma_{\text{trans.}}$ for the longitudinal and transverse modes of vibration respectively in the Debye–Brillouin model this leads to a variation of γ_l with temperature given by

$$\gamma_l=\frac{2\gamma_{\text{trans.}}\,c_v(\Theta_{\text{trans.}}/T)+\gamma_{\text{long.}}\,c_v(\Theta_{\text{long.}}/T)}{2c_v(\Theta_{\text{trans.}}/T)+c_v(\Theta_{\text{long.}}/T)},$$

where

$$\gamma_{\text{trans.}}=\tfrac{1}{2}\left\{\frac{c_{11}-\frac{4}{3}c_{44}}{c_{44}}\,\frac{dc_{44}}{dp}-1\right\},$$

$$\gamma_{\text{long.}}=\tfrac{1}{2}\left\{\frac{c_{11}-\frac{4}{3}c_{44}}{c_{11}}\,\frac{dc_{11}}{dp}-1\right\},$$

and

$$\frac{3}{{\Theta_{\text{D}}}^3}=\frac{1}{\Theta^3_{\text{long.}}}+\frac{2}{\Theta^3_{\text{trans.}}}\quad;\quad\frac{\Theta_{\text{trans.}}}{\Theta_{\text{long.}}}=\left(\frac{c_{44}}{c_{11}}\right).$$

Using Lazarus's figures, this leads to an increase of γ_l with falling temperature, the low-temperature limit being about 8% higher than the high-temperature limit. The main rise in γ_l takes place below $0{\cdot}3\Theta_{\text{D}}$ but above $0{\cdot}1\Theta_{\text{D}}$ where the rise in our experimental values begins to appear. There is thus no more than a rough qualitative agreement between this semi-empirical conclusion based on the Debye–Brillouin model and our own results.

ACKNOWLEDGMENTS

We are grateful to Dr. R. O. Davies for helpful discussions and for the calculation of γ from data on elastic constants, to Mr. D. J. Craven and Mr. J. Wynn for their help in the measurements, and to the British Oxygen Company for the award of a studentship to one of us (C.P.A.).

Note added in proof.—Our results are in good agreement with those of D. B. Fraser as reported to the VIIth International Conference on Low Temperature Physics (September 1960). The question of the effective value of γ_e has recently been discussed by Klemens (1960) and Gross and

Olsen (1960). The latter have determined the pressure shift in the superconducting transition temperature of aluminium and estimate $\gamma_e \approx 10$. Our results at the lowest temperatures can be interpreted in terms of a constant $\gamma_e \approx 6$ rather than $\frac{2}{3}$.

REFERENCES

BARRON, T. H. K., 1955, *Phil. Mag.*, **46,** 720.
BIJL, D., and PULLAN, H., 1954, *Phil. Mag.*, **45,** 290; 1955, *Physica,* **21,** 285.
BLACKMAN, M., 1958, *Phil. Mag.*, **3,** 831.
DHEER, P. N., and SURANGE, S. L., 1958, *Phil. Mag.*, **3,** 665.
DOMB, C., and ZUCKER, I. J., 1956, *Nature, Lond.*, **178,** 484.
FIGGINS, B. F., JONES, G. O., and RILEY, D. P., 1956, *Phil. Mag.*, **1,** 747.
GEARY, P. J., 1954, *Flexure Devices* (B.S.I.R.A.), p. 8.
GIAUQUE, W. F., and MEADS, P. F., 1941, *J. Amer. chem. Soc.*, **63,** 1899.
GIBBONS, D. F., 1958, *Phys. Rev.*, **112,** 136.
GROSS, D., and OLSEN, J. L., 1960, *Cryogenics,* **1,** 91.
HOWLING, D. H., MENDOZA, E., and ZIMMERMAN, J. E., 1955, *Proc. roy. Soc.* A, **229,** 86.
KLEMENS, P. G., 1960, *Phys. Rev.*, **120,** 843.
LAZARUS, D., 1949, *Phys. Rev.*, **76,** 545.
McLENNAN, J. C., ALLEN, J. F., and WILHELM, J. O., 1931, *Trans. roy. Soc. Can.*, **25,** III, 1.
NIX, F. C., and MACNAIR, D., 1941, *Phys. Rev.*, **60,** 597.
RUBIN, T., ALTMAN, H. W., and JOHNSTON, H. L., 1954, *J. Amer. chem. Soc.*, **76,** 5289.
SUTTON, P. M., 1953, *Phys. Rev.*, **91,** 816.
SIMMONS, R. O., and BALLUFFI, R. W., 1957, *Phys. Rev.*, **108,** 278.
WALKER, C. B., 1956, *Phys. Rev.*, **103,** 547.

The Transition to the Metallic State†

By N. F. Mott
Cavendish Laboratory, Cambridge

[Received January 10, 1961]

Abstract

An account is given of the theory that a crystalline or non-crystalline array of atoms will make a transition from the metallic to the non-metallic state as the interatomic distance is varied. Experimental evidence relevant to the theory is summarized. Wigner's (1938) suggestion that an electron gas might crystallize at sufficiently low densities is examined, and an experiment suggested by which it might be tested.

§ 1. Introduction

In a number of papers (Mott 1949, 1952, 1956, 1958, Mott and Stevens 1957), the present author has put forward the hypothesis that a crystalline array of hydrogen-like atoms, or more generally atoms in which there is an incomplete shell, may not necessarily show metallic conduction, by which is meant a conductivity which does not vanish at the absolute zero of temperature. The hypothesis states, moreover, that as the lattice parameter of the crystalline array is increased, there will at the absolute zero of temperature be a *sharp* transition from a metallic state, with a finite or infinite conductivity at the absolute zero, to a non-metallic state in which it will *not* conduct at the absolute zero and in which there is a finite activation energy for conduction. Much earlier Wigner (1938) suggested that an electron gas of low concentration might 'crystallize', the electrons becoming localized. These hypotheses have proved controversial and are not, I believe, universally accepted. There is however a good deal of new experimental evidence in the favour at any rate of the first, and the purpose of this paper is to restate this hypothesis, to summarize the evidence and to suggest an experiment by which Wigner's proposal could be tested.

§ 2. Theory of the Transition to the Metallic State (Divalent Metals)

Since A. H. Wilson's papers of 1931, an insulator has been described by a Slater determinant formed from Bloch wave-functions $\psi_k(\mathbf{r})$ such that the wave vectors $\mathbf{k}$ are all within totally occupied Brillouin zones. Thus in a simple case, for instance a divalent cubic metal, one might envisage a full zone (β) and an empty zone (α) as shown in fig. 1, with an activation energy

---

† Communicated by the Author.

E needed to excite an electron from the full to the empty zone. As one compresses the crystal, decreasing the lattice parameter from its equilibrium value b_1, one would expect both bands to widen so that E would tend to zero at a value of b equal to b_0. For values of b smaller still the bands overlap and the model predicts metallic conduction; thereafter the number of free electrons increases uniformly.

The first point that we must make about this model is that the predicted continuous increase in the number of free electrons and holes from the value zero is not possible. An electron and a positive hole will attract each other with a force behaving at large distances r like $e^2/\kappa r^2$, where κ is a dielectric constant. With a Coulomb force of this kind, the electron and hole will always, when in the state of lowest energy, form pairs (excitons, like positronium), with binding energy of order

$$e^4 m^*/2\hbar^2\kappa^2, \qquad (1)$$

Fig. 1

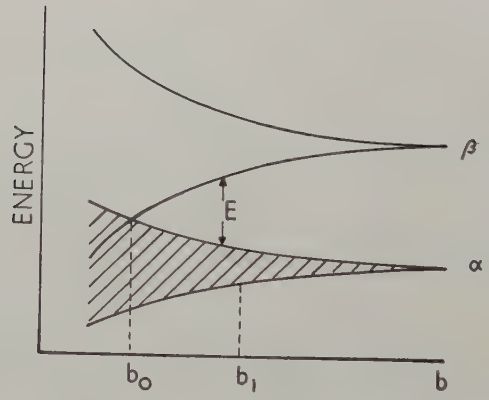

Showing a full zone (α) and an empty zone (β) varying with the interatomic distance b.

where m^* is their reduced mass. They will not therefore be able to carry a current at the absolute zero of temperature. It is only possible to escape from this conclusion if there is a considerable concentration, n per unit volume, of free carriers; the Coulomb field will then be replaced by one derived from the potential energy

$$-(e^2/\kappa r)\exp(-qr), \qquad (2)$$

where q is a screening constant given in the Thomas–Fermi approximation by (Mott and Jones 1936, Chap. II):

$$q^2 = 4me^2n^{1/3}/\kappa\hbar^2. \qquad (3)$$

A screened potential of this type does not necessarily lead to any bound states. We therefore predict that the number of free carriers (electron and holes) varies discontinuously† with b, as shown in fig. 2.

§ 3. THEORY OF THE TRANSITION TO THE METALLIC STATE (MONOVALENT METALS)

We turn to the consideration of materials which, according to the Wilson model, ought to be conductors for all values of b; the simplest is an arrangement of one-electron centres (hydrogen atoms) arranged on a cubic close-packed cubic or similar lattice. According to the Wilson model, the zone will be half full and the material a metallic conductor for *all* values of b, as in fig. 3, though the effective mass will increase with b.

Fig. 2

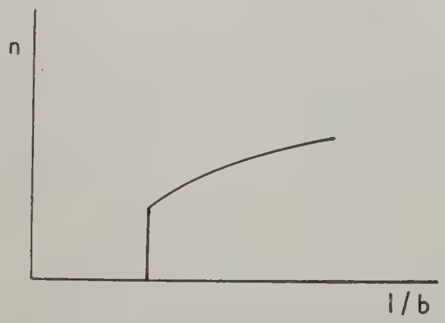

Plot of the predicted number of free electrons of (say) a divalent metal against the reciprocal of the distance b between the atoms.

Now for large values of b this is against common experience and, one might say, common sense. Suppose that the overlap between the centres is small. Then clearly one would expect a current at low temperatures only if one or more of the electrons were missing. Into the 'hole' so formed an electron from the neighbouring site could move and the process could continue; the hole would behave like a carrier of high effective mass. But if all centres are occupied by an electron, then for a current to flow it is necessary to ionize at least one atom and to put the electron back on a *distant* atom; two free carriers are thereby obtained. The work necessary for this is to a first approximation $I-E$, where I is the ionization energy and E the electron affinity. Thus an activation energy of this order is necessary for conduction. We want to emphasize that the presence of polar states in the wave function, such as one finds to some extent in the hydrogen molecule however small the overlap between atomic orbitals, does *not* lead to conductivity; this point will be considered further in § 4.

---

† The assumption that n changes discontinuously may break down if κ tends to infinity at the transition value of b. This can only occur if the energy of the *optically allowed* transition from the full to the empty zone tends to zero.

These findings accord with what we know about the conductivity of some of the transition metal oxides (e.g. NiO, Morin 1954). This particular oxide has a cubic structure; the nickel ions (Ni^{2+}) should have the configuration $3d^8$; according to the Wilson model, the 3d band should be partly filled. Nevertheless this oxide when pure is an insulator and transparent; it conducts only when activated, say by Li^+ ions replacing some Ni^{2+} ions, with consequent formation of Ni^{3+} ions to preserve neutrality of charge. This shows that the nickel ions overlap sufficiently to allow some current to pass, but that the oxide only shows conductivity when Ni^{3+} ions are present.

Fig. 3

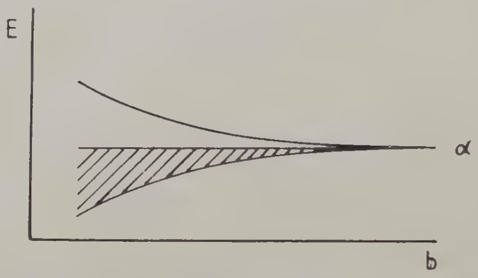

Showing a half full zone for a monovalent metal varying with the interatomic distance *b*.

We consider therefore that in the array of one-electron centres, as in the array considered in § 2, free carriers are only possible if they are present in such numbers as to give a screening constant q big enough to prevent the formation of pairs. We come therefore again to the conclusion that, as the interatomic distance b is varied, there must be a *sharp* transition between a non-metallic state which can carry no current at the absolute zero and one in which a large number of electrons are free. Since the latter is the well-known metallic state, it is reasonable to expect all the electrons to be free. A very approximate estimate can then be made of the value of b at which the transition will occur.

If the potential energy of a positive charge and an electron is

$$-(e^2/\kappa r)\exp(-qr),$$

the condition that pairs will not form is (Friedel 1952, Blatt and Weisskopf 1952)

$$q > 1{\cdot}0/(\hbar^2\kappa/me^2). \qquad (4)$$

We do not know the effective masses of the 'hole' or the electron under discussion; m should be the reduced mass of these which we shall take equal to the electronic mass. Using formula (3) for q, (4) then gives

$$n^{1/3}a_H > 0{\cdot}25, \qquad (5)$$

where

$$a_H = \hbar^2\kappa/me^2.$$

If we are dealing with an array of hydrogen atoms, the 'background' dielectric constant is of course unity and we see that free electrons do not form until the interatomic distance is two or three multiples of the hydrogenic radius. If the centres are impurity centres in semiconductors, κ should be the dielectric constant of the semiconductor, and m should be an *effective* mass of an electron (or hole) in its conduction band.

Formula (5) is doubtless dimensionally correct but the derivation of the numerical constant contains too many crude assumptions to be taken very seriously. It is, however, interesting to apply it to bismuth, where the number of free electrons and holes is certainly small, about 10^{-5} per atom (Smith 1959). On the other hand, the effective masses are small, and the background dielectric constant κ, due to the very nearly full bands, is likely to be large. There can be little doubt that (5) is satisfied.

§ 4. A More Detailed Discussion of the Non-conducting Wave Function

A detailed discussion of the non-conducting wave function and a proof that a system described by it does not conduct may be given as follows (Mott 1956, 1958). We consider a crystalline array of N one-electron (hydrogen) atoms. For an electron moving in a periodic field due to N atoms, there are N Bloch wave functions $\psi_k(\mathbf{r})$ possible in the first band for each spin direction. The usual description of the wave function of a monovalent metal is a determinant or sum of determinants using *half* these wave functions, the half with the lowest energy. These wave functions describe a state which can carry a current because the excited states of the system lie very close to the ground state, being separated from it by an energy which tends to zero as N tends to infinity. It is thus possible, for energies of the whole system very near to that of the ground state, to set up *complex* wave functions, which can describe a state with a current.

Fig. 4

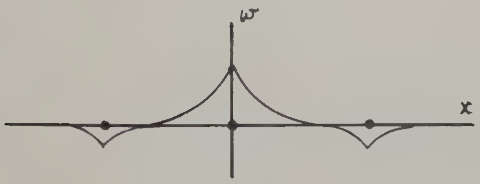

Localized (Wannier) wave functions w overlapping neighbouring atoms; atoms shown by dots

It is, however, possible from the N wave functions in the first band to set up a set of orthogonal wave functions, the Wannier (1937) or Löwdin (1950) functions $w_n(\mathbf{r})$ which are *localized*, one on each atomic site; here the suffix n denotes the site. Such Wannier functions are shown in fig. 4.

They decay exponentially as one moves away from the site in question, but there can be considerable overlap onto neighbouring sites.

It must be emphasized that to set up Wannier functions for each lattice point, one must make use of *all* the Bloch wave functions in the band. We may use these Wannier functions to describe a state of the system which is antiferromagnetic or ferromagnetic and is non-conducting. If the material is antiferromagnetic we may set up for each site a wave function

$$w_n(\mathbf{r})\,\chi_\alpha(\sigma) \quad \text{or} \quad w_n(\mathbf{r})\,\chi_\beta(\sigma),$$

the functions χ_α, χ_β being spin wave functions for the two spin directions, and from these we may form a single determinant to describe the state of the whole system. The properties of this wave function are:

(*a*) It is real, and therefore does not describe a state carrying a current.

(*b*) The only state with the same or nearly the same energy is that in which all the spin directions are interchanged, except states formed by the excitation of spin waves, which are believed not to carry a current.

(*c*) If it is treated as an approximation to an exact wave function, we see that the first excited state with zero spin will have an energy of order $I-E$ (several electron volts) above the ground state.

(*d*) Since the wave functions $w_n(\mathbf{r})$ overlap, polar states are present, in the sense that the wave function allows the presence of two electrons on one atom; but since the wave function is real this cannot lead to a current. The polar states therefore do *not* lead to mobile charge carriers so long as the state of the crystal is correctly described by this kind of wave function. This is because the holes and electrons in the lowest state wave function are bound to each other in space.

For crystals containing *two* electrons per atom, it is well known that the determinant formed from Bloch wave functions and that formed from localized (e.g. Wannier) functions are identical, both describing a non-conducting state; but for crystals with *one* electron per atom they are not the same. The above considerations show that the two approximate wave functions then correspond to two different states of the crystal with different exact wave functions, one conducting (and with an electronic specific heat linear in T and with other metallic properties), and the other non-conducting. They are thus not alternative zero-order descriptions of the exact function; they correspond to different states of the system, the true ground state (at the absolute zero) in each case being that with the lower energy. The wave function formed from Wannier functions will clearly give the lowest energy for large interatomic distances; the existence of metals leads us to believe that the other gives the lower energy for small interatomic distances.

We have assumed up to this point that the non-conducting wave function describes an antiferromagnetic arrangement of spins. There are other possibilities—that it may be ferromagnetic or paramagnetic without any long-range order in the directions of the spins. We do not know of any non-conducting material corresponding to the second case, nor whether such a case can exist. For ferromagnetic non-conducting materials the argument would be the same as that given above; one can set up a single determinant as a first approximation to the wave function, so that the wave function is real and cannot describe a state in which a current flows.

In either the ferromagnetic or antiferromagnetic case, by reversing the spin of one or more electrons and setting up the wave functions corresponding to a spin wave one can obtain excited states with excitation energies tending to zero as N tends to infinity. One can therefore set up complex wave functions. But it is assumed† that a spin wave cannot carry a current, the current vector corresponding to a wave function describing a spin wave being zero. This theoretical prediction corresponds to the observed fact that typical antiferromagnetic materials show an exponential increase in conductivity (as $\exp(-W/kT)$) as the temperature is raised, while the energy of spin waves excited is believed to be proportional to T^4 (Anderson 1950).

Finally, we want to emphasize that the sharp transition described here is only expected in an *infinite* lattice. It goes without saying that for a finite number of atoms there will be a *gradual* decrease in the weight of the ionized states in the wave function as the interatomic distance is increased, or in other words a gradual transition from the LCAO model to the London–Heitler model.

§ 5. SLATER'S MODEL FOR SUBSTANCES OF THE NICKEL–OXIDE TYPE

Slater (1951) has suggested that antiferromagnetic substances of the nickel–oxide type should be described by Bloch wave functions and their non-conducting properties described as follows. Any electron described by a Bloch wave function will, in terms of the Hartree–Fock equation, be repelled considerably less by electrons with spins in the parallel direction than by electrons with spins in the antiparallel direction. Therefore in a crystal in the antiferromagnetic state each electron will move in a crystalline field on which is superimposed that of a superlattice. This field of a superlattice will split the first zone of a cubic lattice into two, each containing $\frac{1}{2}N$ states for each spin direction. With one electron per atom, the first zone could be completely full and the second empty. The material would then be an insulator.

The suggestion that the band model can lead to a non-conducting state in this way is certainly correct. It can also lead to localized magnetic moments, both antiferromagnetic or ferromagnetic, and with integral or non-integral spin. This seems first to have been emphasized by Lidiard (1954). A recent paper by Friedel *et al.* (1961) discusses the transition metals in terms of these concepts, and shows that, always retaining the band model and if necessary non-integral moments, localized moments may survive above the transition point. This suggests that as one increases the interatomic distance of an array of one-electron atoms, the first thing that happens may be the appearance of localized moments without the disappearance of conductivity.

---

† If this assumption is false, our argument falls to the ground.

What is misleading in Slater's model is the following. It suggests incorrectly that the crystal will show metallic conductivity above the Néel temperature or in other words that the activation energy required to destroy the long-range antiferromagnetic order and that to produce carriers of current are of the same order of magnitude. In fact the former will depend on some overlap integral giving the strength of the exchange or superexchange interaction, which will tend to zero as b tends to infinity. The activation energy for conduction, on the other hand, tends to $I-E$.

Fig. 5

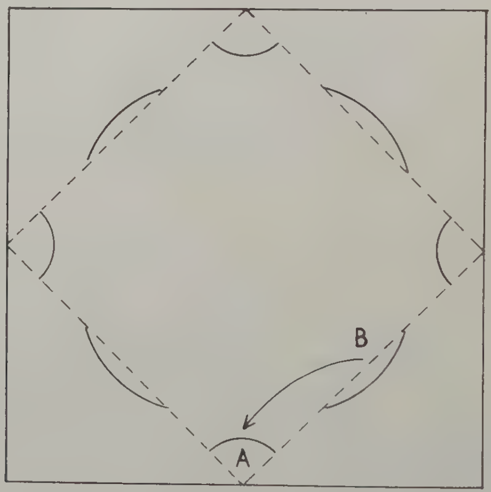

A Brillouin zone split in two by a superlattice, giving sub-zone boundaries shown by the dotted lines.

Nonetheless, Slater's model of the non-conducting state must be the same as that set out in § 4 at the absolute zero of temperature. It is interesting to note that it, too, predicts a discontinuous change in n, the number of free electrons. This may be seen as follows.

Figure 5 shows schematically a Brillouin zone split into two by the superlattice lines due to an antiferromagnetic arrangement of spins. Then suppose that the material is still a conductor and there is a small overlap n_B at B into the second zone and an equal number of holes in the first zone at A. What we have to show is that a *small* number is impossible. This is because the states within the dotted zone near its boundary are those in which the wave function of an electron has its maxima in those atoms with the same spin and nodes in the planes containing atoms with opposite spin. The n_B electrons at B are electrons which spend most of their time in atoms with opposite spin.

Thus if the n_B electrons are transferred to A, the moment on each atom will be increased by about $n_B\mu$, where μ is the Bohr magneton, and the width of the energy gap along the dotted lines will be increased by a term proportional to n_B. Thus the energy of the whole system will be lowered by a term proportional to n_B. On the other hand, the work done to transfer the electrons is proportional to $n_B{}^{5/3}$, since their Fermi energy is proportional to $n_B{}^{2/3}$. Thus, if n_B is small enough, energy must be gained in transferring electrons from B to A. This model, therefore, shows that a *discontinuous* change in the number of free electrons is to be expected at the value of b for which the non-conducting state occurs.

Other discussions in the literature on the transition to the metallic state are given by Des Cloiseaux (1959), Frood (1960) and Coldswell-Horsfall and Maradudin (1960). These will not be discussed here.

§ 6. INTERATOMIC DISTANCE AT WHICH THE TRANSITION OCCURS

A rough estimate of this has been given in § 4, based on the concentration of electrons at which screening is strong enough to prevent pair formation. Although this gives satisfactory results, it should not perhaps be taken too seriously. Neither should a treatment based on the Slater model given by the author (Mott 1956).

Ideally, it should be possible both to calculate the energy of a degenerate electron gas in the field of an array of ions, and the energy of an array of overlapping hydrogen-like atoms with an antiferromagnetic spin arrangement. With the positive charge smeared out this has been done by Carr *et al.* (1961); the accuracy is however doubtful, since they use the method of Gell-Mann and Brueckner (1957) which converges badly for a low value of the electron density. One would expect curves of the form shown in fig. 6. ABC is the normal curve for the energy of metallic electrons in an array of hydrogen-like atoms, calculated for instance by the Wigner–Seitz method with full allowance for correlation; ED is for the antiferromagnetic array of hydrogen-like atoms. Since the curve is meant to represent the lowest state of the whole system, the dotted parts have no physical meeting, but are just extrapolations of hypothetical calculations. The transition should occur when the two curves cross. It is an assumption that dE/db is discontinuous there, but if there is a discontinuity in the number of free electrons it would be surprising if it were not. Moreover, we give in § 7.1 some evidence that it is discontinuous.

If this is so a sharp transition should also occur at finite temperatures at the value of b for which *free* energy curves similar to those in fig. 6 cross. Since the entropy of the electrons in a metal increases as T and that due to spin waves among localized electrons as T^3, a rise in temperature will favour the metallic state and increase the value of b for which the transition occurs. A suitable analysis would be the following: let

$$E_M(V-V_0)/V_0,\ E_{NM}(V-V_0)/V_0$$

be the energies per electron at $T=0$ in the metallic and non-metallic states at a volume V per atom differing slightly from the transition volume V_0.

Fig. 6

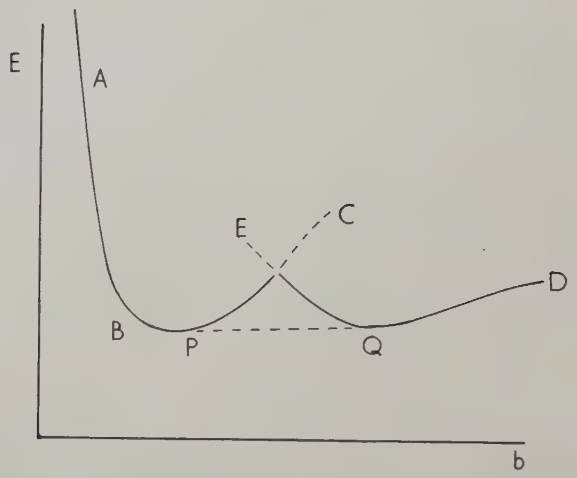

Energy of the metallic state (ABC) and the non-metallic (ED) as a function of interatomic distance b (schematic).

Fig. 7

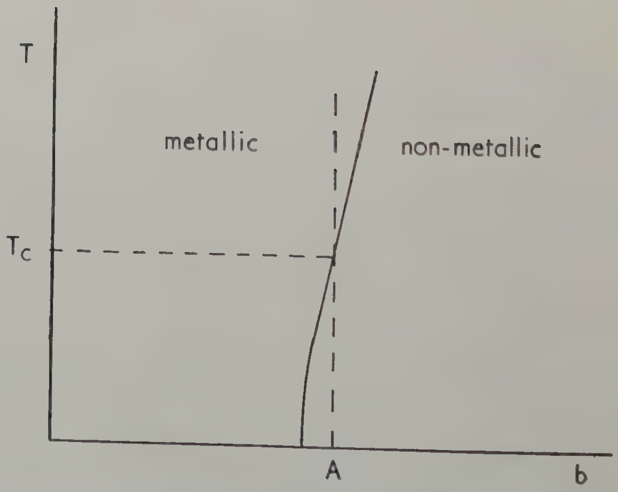

The full line shows the boundary in a b, T diagram between the non-metallic and metallic states. A crystal with a value of b denoted by A in the figure will make the transition at the temperature T_c.

Let E_F be the Fermi energy in the metallic form, so that the electronic specific heat is

$$\tfrac{1}{2}\pi^2 k^2 T/E_F.$$

Then, neglecting the spin wave term in T^4, the difference in free energy between the two forms is

$$(E_M - E_{NM})(V - V_0)/V_0 - \tfrac{1}{2}\pi^2 k^2 T^2/E_F. \quad . \quad . \quad . \quad . \quad (6)$$

We therefore expect a boundary between the two forms as shown in fig. 7.

These ideas will be applied to certain oxides in the next section.

§ 7. APPLICATIONS

7.1. *Oxides and Sulphides of the Transition Metals*

A recent paper by Morin (1961) classifies these materials into metals and non-metals according to the degree of overlap between the 3d functions. He considers not only that the direct overlap between 3d functions with e_g symmetry is important, but also that partly filled orbitals are formed in which electrons are shared between these and the $2p-\pi$ orbitals of oxygen, and that overlap between these may have a comparable effect. Figure 8 shows his division into metals and non-metals plotted according to his estimate of the overlap integrals of the two types. Some of the oxides listed as metals only show metallic conductivity at reasonably high temperatures, there being a *sharp* transition to the metallic state as the temperature is raised with a rise in conductivity which may be as large as 10^6 (Morin 1959 a). Figure 9, taken from Morin's paper, shows the behaviour of the vanadium and titanium oxides. We consider that such oxides must lie near the transition line in fig. 7, e.g. at A, and that the transition occurs at T_c where the isotherm (dotted line) crosses the dividing line between the two phases. Essentially this explanation is given by Morin (1959 b), though he expresses it in terms of the splitting of a band by an antiferromagnetic arrangement of spins, which is Slater's (1951) model.

There are, however, difficulties in too simple an interpretation of the transition. There is first the low conductivity in the 'metallic' region, smaller by about 1000 than in true metals. The conductivity of a metal should be given by

$$\sigma = ne^2 \tau / m_{\mathrm{eff}}$$

where τ is the time of relaxation and m_{eff} the effective mass. If we write $\tau = l/v$ where l is the mean free path and v the velocity at the Fermi surface, then

$$\sigma = ne^2 l / m_{\mathrm{eff}} v.$$

Now $m_{\mathrm{eff}} v/h$, the wave vector at the Fermi surface, must be of the same order as for a metal; the low conductivity can thus only be explained by the assumption that l is of the order of the lattice parameter. Several tentative suggestions may be made about this. The coupling between the electrons and an ionic lattice may be greater than in normal metals, though we should be surprised if this made a very large difference to the mean free path.

There may be localized spins of the kind suggested by Friedel *et al.* (1961), which would give a high electrical resistivity nearly independent of temperature (de Gennes and Friedel 1958). Perhaps this is the most probable explanation. Morin (1959 b) ascribes it simply to a very narrow band. We cannot accept this, because we do not think there could be a transition to the metallic state under these conditions.

Fig. 8

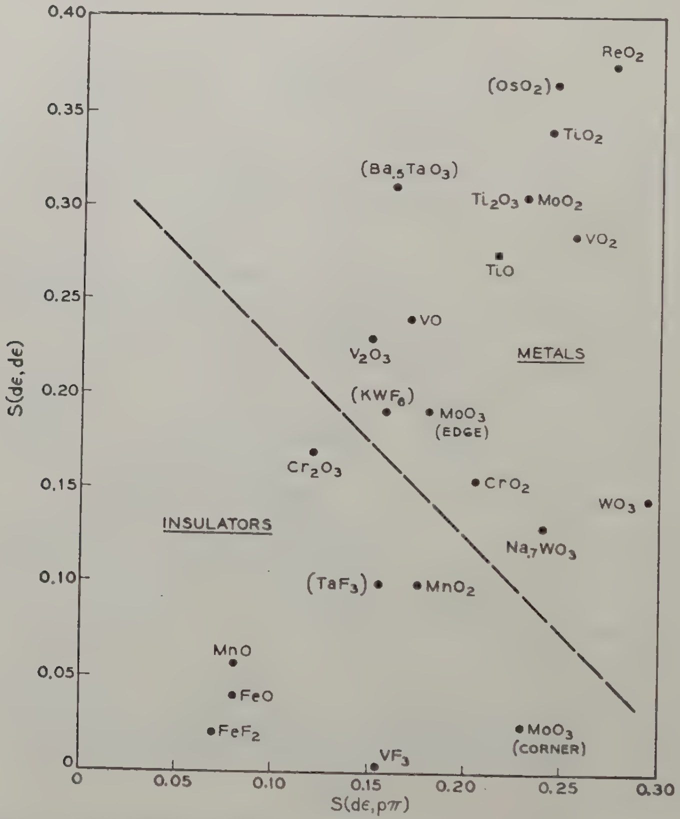

Comparison of the overlap integrals $S(d\epsilon, d\epsilon)$ and $S(d\epsilon, p\pi)$ for a number of compounds (Morin 1960). The dotted line is an arbitrary one which, in fact, separates metals from insulators.

Then we must ask how near the point A in fig. 7 must be to B. We suppose that all the energies E_{M}, E_{NH} and E_{F} are likely to be of order $me^4/2\hbar^2\kappa^2$. Unless κ is particularly large, and there is no reason to believe it to be for an oxide, this should be of the order of an electron volt. If so, $(V-V_0)/V_0$ must be of the order 10^{-3}. It seems unlikely that a transition would be observed for a number of oxides if A had to be as near to B as this. On the other hand, for V_2O_3 a phase change has been observed at the transition point, (Paoletti and Pickart 1959) and we suggest that the forces holding the metal ions in position in the lattice of oxide ions may change somewhat at the transition point and that there may be a considerable change in vibrational entropy. If the vibrational frequency is of order kT/h, and

Fig. 9

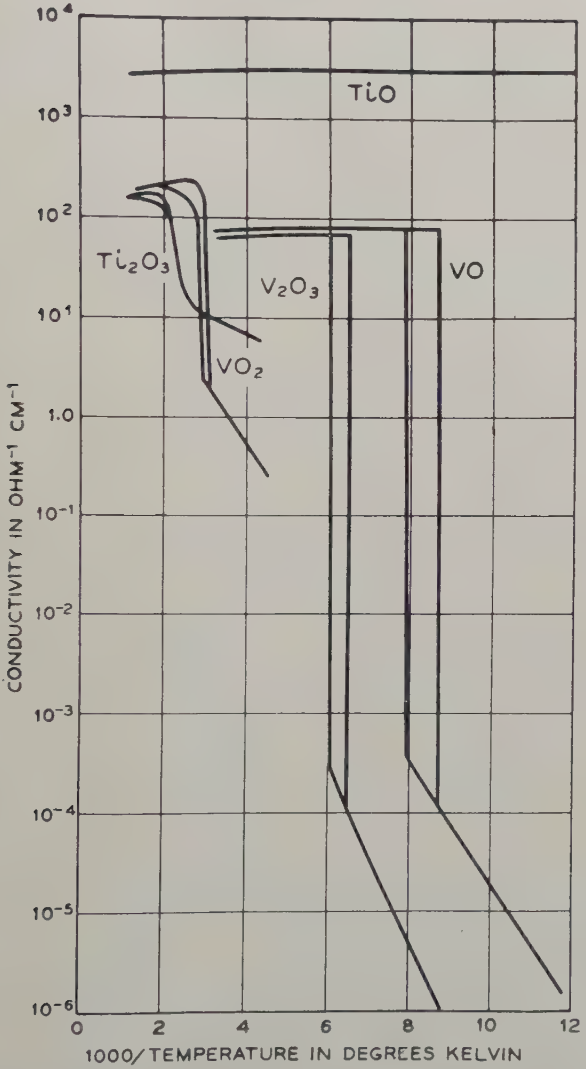

Conductivity of certain oxides as a function of temperature (Morin 1959 a).

changes by a factor of order 2, we expect an entropy change of order k and thus a free energy change of order kT. Under these conditions $(V-V_0)/V_0$ should be of order a few per cent. A pressure of 100 000 atmospheres should, if this is the case, lower the transition temperature by a factor of order 2.

7.2. *Highly-doped Semi-conductors*

The rapid drop in the resistance of most extrinsic semi-conductors that occurs when the concentration of impurity exceeds a certain value is well known, and has been described by the author (1956) as a transition to the metallic state. Above a certain concentration of impurity, it is found

(i) that the Hall constant indicates that the number of free electrons is equal to the number of centres;

(ii) that the conductivity at low temperatures is independent of the temperature, and tends to a finite value as T tends to zero. The mean free path, though of the order of the distance between centres, is roughly independent of concentration (Mott and Twose 1961);

(iii) that the magnetic susceptibility, at any rate of n-type germanium, is that expected of a degenerate electron gas, the carriers having the effective mass appropriate to the semi-conductor. In particular, if N is the number of centres per unit volume, the susceptibility is proportional to $N^{1/3}$ and is independent of temperature (Bowers 1957, Bowers and Yafet 1958, 1960, Yafet 1959).

As a means of investigating the transition to the metallic state, doped semi-conductors suffer from two disadvantages.

(*a*) The centres are not in a crystalline array, but in general are completely disordered (far more so than the metal atoms in a liquid metal).

(*b*) At any rate in germanium and silicon and probably in other semi-conductors, when the mean distance b between centres exceeds the assumed critical value, one does *not* find a simple state of affairs where weakly interacting one-electron centres allow conductivity only with an activation energy $I-E$ (which would be near to the energy I required to excite an electron into the conduction band). This is because the position is complicated by the presence of minority centres (acceptors in n-type conductors). These will receive electrons, and the resulting unoccupied donors can, by tunnel effect, receive electrons from neighbouring donors, thus allowing a current to pass. However as pointed out first by the present author (1956; see also Price 1957, Miller and Abrahams 1960 and Mott and Twose 1961), this impurity conduction in compensated semi-conductors cannot be independent of temperature. As the temperature T tends to zero, the conductivity will tend to zero as $\exp(-W/kT)$ where W is an activation energy due to the charged minority centres. Mott (1956) first considered the case when the compensation ratio K, defined by

$$K=N_{\min}/N_{\mathrm{maj}}$$

is very small; here $N_{\min}$ and N_{maj} are the concentrations of minority and majority centres. He stated that in this case one should have

$$W=e^2/\kappa R$$

where R is the mean distance from a minority to the nearest majority centre. W is then simply the energy required to remove the 'hole' on a majority centre to an infinite distance from the charged minority centre.

As K increases, W decreases rapidly as predicted by Price and by Miller and Abrahams, and observed by Fritzsche and Cuevas (1960).

The transition is fairly sharp, as shown in fig. 10. To the right of the drop the conductivity is independent of temperature.

Fig. 10

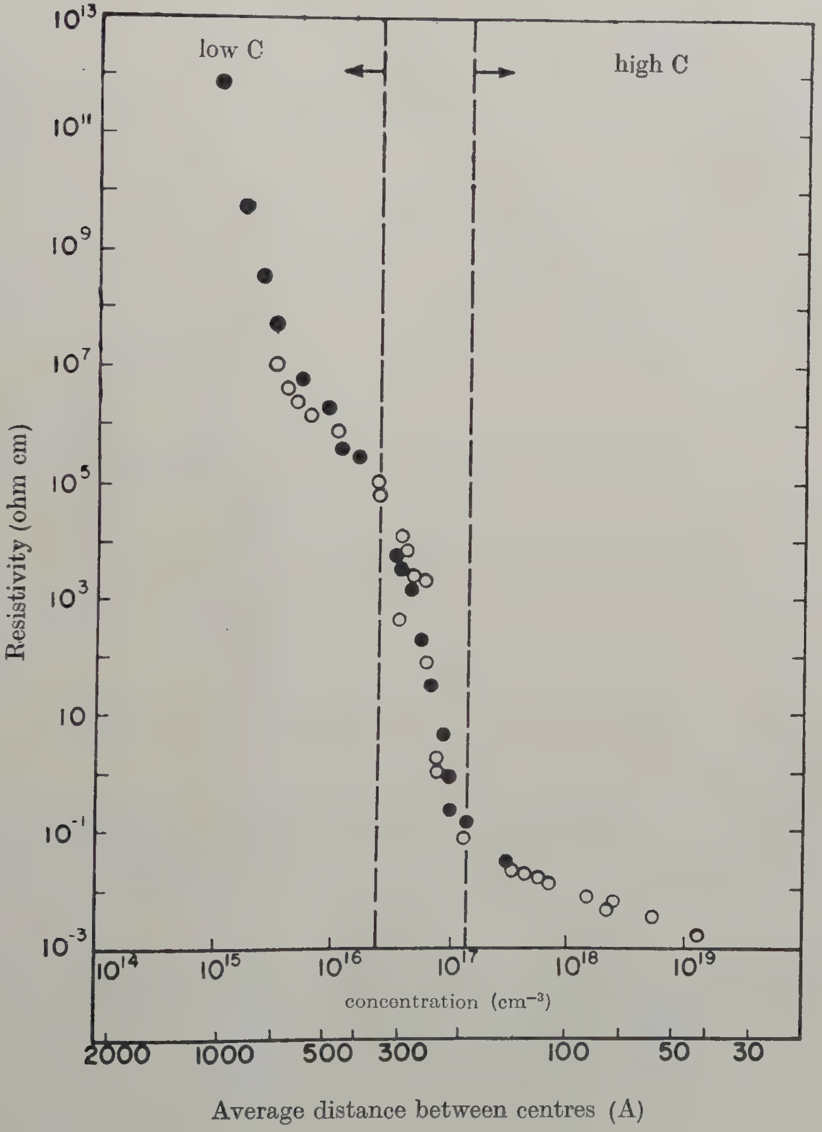

Dependence of the resistivity of germanium at 2·5°K on impurity concentration. Full dots : n-type antimony-doped ; open circles : p-type gallium-doped. From Fritzsche 1959.

We expect, according to the crude estimate of § 3, that the critical density N for semiconductors that are elements should be given by

$$N^{1/3} a_{\mathrm{H}} = 0\cdot 25$$

where

$$a_{\mathrm{H}} = \kappa \hbar^2 / m_{\mathrm{eff}} e^2.$$

Fritzsche and Cuevas (1960) have shown that the critical concentration depends little on compensation between values of K of 0·04 and 0·4, not by more than 10%. An exact experimental value of $N^{1/3} a_{\mathrm{H}}$ is difficult to obtain because the wave functions of the centres are not hydrogen-like; approximately the results for Ge and Si suggest a value of about 0·2 (Mott and Twose 1961).

For semi-conductors which are not elements it is not quite clear what value of the dielectric constant should be taken. In the metallic state the force between the electrons will be $e^2/\kappa_0 r^2$ where κ_0 is the high-frequency dielectric constant, but in the non-metallic state the charged centres however will polarize the ionic lattice round them. Further investigation of this problem will be necessary†.

7.3. *Heavily Compensated Semi-conductors and Wigner's Hypothesis*

If K, the compensation constant, is nearly equal to unity, an interesting case may arise which would enable one to investigate whether Wigner's assumption that a free electron gas can 'crystallize' is true or not. One will then have many more majority centres than electrons. If the distance between majority centres is large enough, then (Anderson 1958) the states for these electrons are localized. In other words, the wave functions for any one of these states decays exponentially with distance from one of the centres. As N_{A} increases, however, and overlap between the wave functions of the centres becomes strong, the states of a single electron become delocalized, the wave functions extending throughout the lattice. We thus have a gas of $n(=N_{\mathrm{D}}-N_{\mathrm{A}})$ electrons per unit volume moving in the field of a random distribution of positive and negative point charges, the mean distance between them being small compared with $n^{-1/3}$. This seems to us the nearest approach available experimentally to the original Sommerfeld model of a metal, a gas of electrons moving in a uniform distribution of positive charge ('jellium').

If Wigner (1938) is right, then at the absolute zero of temperature these electrons ought to crystallize, say in a body-centred cubic lattice, if the quantity $n^{1/3} a_{\mathrm{H}}$ is greater than some critical value‡. We shall make a very rough estimate of this critical value. We denote by r_0 the radius such that $4\pi n r_0^3/3 = 1$; then in the non-metallic state each electron is thought to move in the field of a sphere of this radius filled with a uniform distribution of positive charge, and thus with a potential energy

---

† Compare McIrvine (1960) who has given an empirical formula relating N to the dielectric constant for several materials.

‡ For intermediate values it is always possible that an ordered antiferromagnetic arrangement of spins would arise, as envisaged by Friedel *et al.* (1961).

$$V(r) = -\tfrac{1}{2}\frac{e^2}{r_0}\left(1 - \frac{r^2}{r_0^2}\right),$$

where r is the distance from the centre of the sphere. Wigner ascribes to each electron a fixed potential energy $-\frac{1}{2}e^2/r_0$ and a zero-point energy $3\hbar\omega/2$, where

$$\omega = \sqrt{(e^2/mr_0)}.$$

This will be correct for large interatomic distance, but near the transition point it may be better to set for the potential energy the average over the sphere

$$\int_0^{r_0} V(r)\, 4\pi r^2\, dr/(4\pi r_0^3/3) = -2e^2/5r_0,$$

and for the zero point energy that of a particle in a spherical cavity of radius r_0, namely $\pi^2\hbar^2/2mr_0^2$.

For the metallic phase, since each sphere is occupied by all the electrons, the Hartree approximation will give half the above contribution to the potential energy, namely

$$-2e^2/10r_0.$$

The zero point energy is now the Fermi energy, namely

$$\frac{3}{5}\frac{\pi^2\hbar^2}{2mr_0^2}\left(\frac{3}{2\pi}\right)^{4/3}.$$

The transition will thus occur when

$$\frac{1}{5}\frac{e^2}{r_0} \simeq 0{\cdot}7\frac{\pi^2\hbar^2}{2mr_0^2}$$

or

$$r_0 \simeq 20\, a_{\mathrm{H}}.$$

While this paper was in proof, Dr. Carr showed the author the manuscript of a more detailed calculation along these lines (Carr *et al.* 1961). They find energy curves cutting when $r_0/a_{\mathrm{H}} \sim 3$, though they appear to assume, contrary to our belief, that there is a continuous transition from one form to the other.

If the phenomenon is to be observed, the density of centres must be big enough for bound states to disappear. According to an extension of Anderson's (1958) work due to Twose (Mott and Twose 1961) this should occur when Ra_{H} is of the order 3·6, where $N = 3/4\pi R^3$ is the density of majority centres. In germanium this would mean that the density of centres must be greater than about $10^{17}\,\mathrm{cm}^{-3}$.

Actually it may be doubted whether a crystallization with long distance order could ever be observed. The energy of melting might be expected to be of the order of $1/100$ of $e^2/\kappa r_0$ and thus only a few hundredths of a degree in germanium. Also the random field due to the charged centres might lead to a polycrystalline arrangement, even at the absolute zero. But a sharp transition between a normal *liquid* at low concentrations and the condensed electron gas at high concentration might occur. Perhaps the most straightforward way to observe any such effect would be a change in the magnetic susceptibility.

The transition can be compared to that between liquid helium I and II; the fact that the repulsion between helium atoms falls off as a higher power of the distance than the zero point energy and a lower power for electrons means that the super fluid (condensed gas) is destroyed by compression in the former case, by expansion in the latter.

Fig. 11

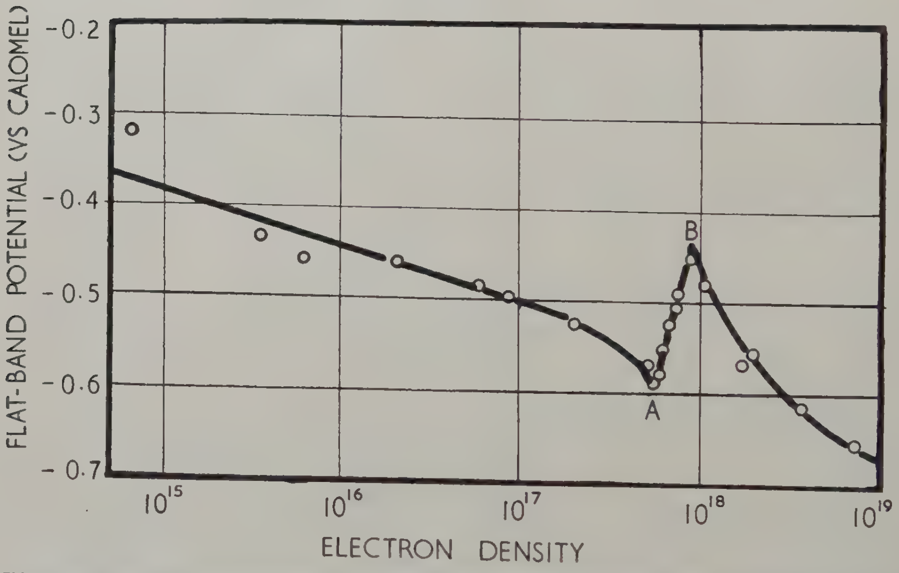

The flat-band potential as a function of electron density for crystals freshly etched in H_3PO_4 (Dewald 1960).

7.4. *Fermi Energy in Zinc Oxide Activated by Indium*

Dewald (1960) has measured the capacity of the interface between an electrolyte and zinc oxide activated by indium, and from these measurements he deduces what he calls the 'flat band potential', i.e. the potential at which there is no Schottky barrier in the surface layer. This gives a measure of the Fermi energy of the electrons in the semi-conductor for various concentrations of the indium, measured against a fixed level determined by the concentration of the electrolyte. His results are reproduced in fig. 10, which shows—with sign reversed—the Fermi energy as a function of concentration. At about the concentration marked A metallic conductivity (i.e. conductivity without temperature-dependence) is known to set in (Thomas 1958). We make the hypothesis that the discontinuity in the Fermi energy at A, its drop to a minimum at B and subsequent rise is due to the same cause as the corresponding behaviour of the total free energy shown in fig. 6. The minimum at B, which should not be sharp if this explanation is correct, should be the point where the free energy of the electron gas is a minimum. The curve suggests that the transition to the metallic state occurs when the electron density is less by a factor 2 than at this minimum. If r_0/r_H is of order 3 for the transition to the metallic state as for germanium, this would suggest that the minimum occurred for $r_0/r_H \sim 2{\cdot}4$. This is considerably larger than the values calculated for metallic hydrogen by Wigner and Huntingdon (1935) and by Stern and Talley (1955), (1·5–1·6), but since the electron in indium is in a p state there is no reason to think these results applicable.

Fig. 12

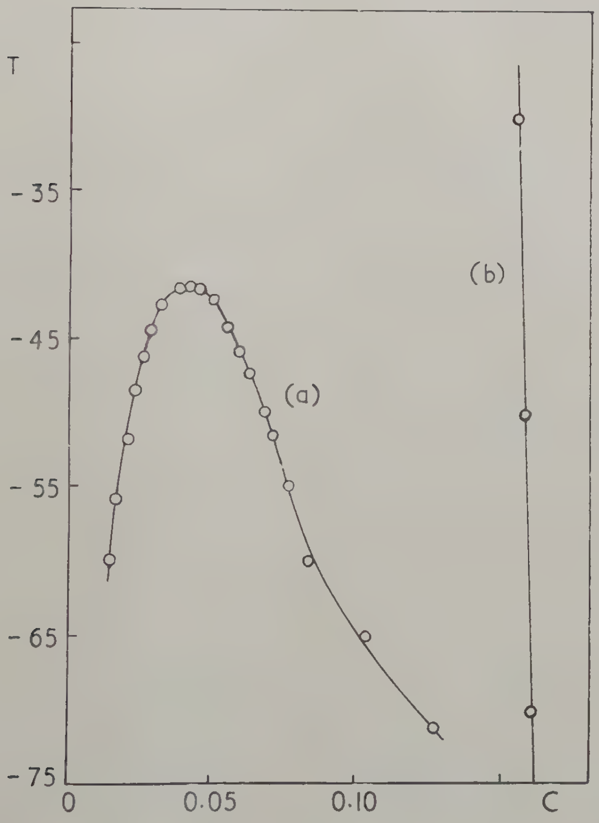

Solubility gap (*a*) and limit of solubility (*b*) for sodium in ammonia, as a function of concentration *c* of ammonia (Bingel 1953). Temperatures in °c.

7.5. *Metal–Ammonia Solutions*

If the centres were free to move about, fig. 6 shows that one would expect a two phase region[†] between the points marked P and Q. This is observed for solutions of sodium in liquid ammonia (Kraus 1953, Bingel 1953), for which the phase diagram is as in fig. 12. Solutions of about 10% sodium in ammonia are probably 'metals' of the type discussed here, the sodium atoms being expanded by the surrounding dielectric constant (its high-frequency value). The free energy of the solutions, including the terms representing the cohesive energy between these centres, must be at a minimum about here.

§ 8. LOCALIZED STATES IN METALS

Several authors recently (e.g. Goodenough 1960) have referred to localized states in transition metals and the present author (Mott and Stevens 1957) and also Lomer and Marshall (1958) make use of this concept in discussing the magnetic electrons in iron. In this section we shall not discuss individual metals in detail, but shall state certain general principles.

We have emphasized that, for an array of one-electron atoms, impurity states in a semi-conductor or inner shells of a transition metal oxide, the question whether the material is 'metallic' or not is one capable of a precise answer. Whether it is a conductor or insulator at the absolute zero of temperature is a physical question and not a matter of the most convenient theoretical model. For inner shells of transition metals, the question can only be answered to the approximation to which one writes down separate many-electron wave functions for the inner and outer electrons. As soon as one takes into account the interaction between them, the question is no longer precise; one can only ask which is the best model. Nonetheless, the question may be worth asking.

Let us then consider a metal in which the atoms have an incomplete inner shell, for instance the rare earth metals. The overlap between the 4f shells is so small that it is most unlikely that a 'metallic' type of wave function would be appropriate or that the 4f shells contribute to the Fermi surface. On the other hand, one will *always* get a metallic type of wave function if the number of electrons in the inner shell is non-integral (as in nickel). Such a state of affairs is possible in, for instance, a rare earth metal. Suppose an extra electron is added to one of the 4f shells. The energies that this electron can have will lie in a narrow band. If the Fermi energy of the conduction electrons lies in this band, it will fill up until the Fermi energy of the narrow 4f band and of the conduction band are the same. If the Fermi energy of the conduction band lies below it, the wave functions of the 4f electrons will remain non-conducting. If it lies sufficiently far below it, however, it may overlap the band obtained by taking an electron out of one of the 4f shells.

[†] I am indebted to Dr. Dewald for pointing this out to me.

If then one were to plot the number N of 4f electrons against the Fermi energy of the conduction electrons, a curve similar to fig. 13 would be expected, n being an integer. In the regions where N is non-integral, one has a band of energy levels and a Fermi surface. A band of energy levels containing only *one* electron per atom is a new concept. If however for n and for $n+1$ electrons the states are non-conducting, it must be a valid one; and s band, for instance, that would normally have two electrons will split into two bands, a p band into six (fig. 14).

Fig. 13

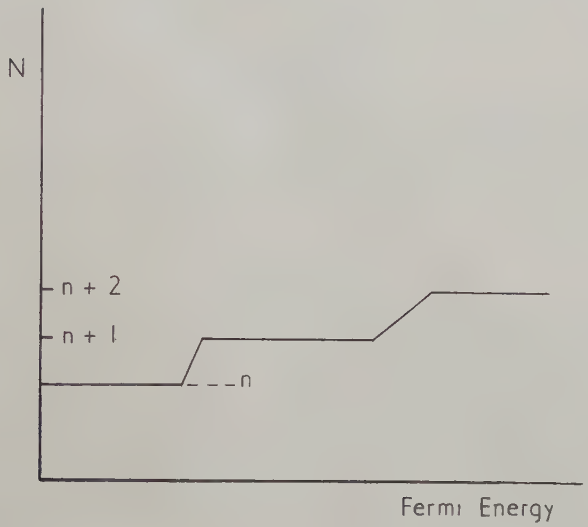

Number of electrons expected in an inner band as a function of the Fermi energy of a metal.

Fig. 14

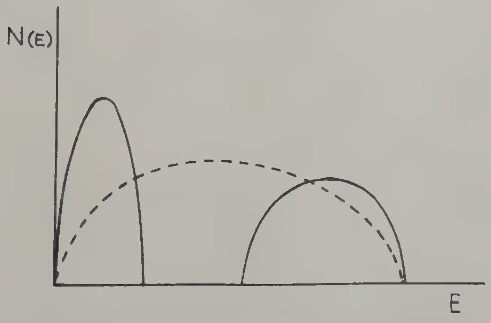

Suggested splitting of an inner band into two (or more) sub-bands when the overlap between atomic orbitals is small.

We may also emphasize that it is only in a metal that we may anticipate that, if a band is narrow enough to have a non-metallic wave function for an integral number of electrons, it will necessarily have a Fermi surface at $T=0$ when the number is non-integral. For non-metals the position is made clear by the behaviour of compensated semi-conductors (§ 7.2); at very low temperatures the carriers are held in position by the corresponding positive charges, and the material is not a conductor.

ACKNOWLEDGMENTS

I would like to express my indebtedness to several of my colleagues with whom I have discussed this subject, particularly J. F. Dewald, H. Fritzsche, V. Heine, W. M. Lomer, W. Marshall, J. F. Morris, A. B. Pippard, J. C. Slater, W. D. Twose.

REFERENCES

ANDERSON, P. W., 1950, *Phys. Rev.*, **79,** 705; 1958, *Phys. Rev.*, **109,** 1492.
BINGEL, W., 1953, *Ann. Phys., Lpz.*, **12,** 57.
BLATT, J. M., and WEISSKOPF, V. F., 1953, *Theoretical Nuclear Physics*, (New York: John Wiley & Sons), p. 55.
BOWERS, R., 1957, *Phys. Rev.*, **108,** 683.
BOWERS, R., and YAFET, Y., 1958, *Phys. Rev.*, **115,** 1165; 1960, *Ibid.*, **120,** 62.
CARR, W. J., COLDSWELL-HORSFALL, R. A., and FEIN, A. E., 1961, *Phys. Rev.* (in the press).
COLDSWELL-HORSFALL, R. A., and MARADUDIN, A. A., 1960, *J. math. Phys.*, **1,** 395.
DE GENNES, P. G., and FRIEDEL, J., 1958, *J. Phys. Chem. Solids*, **4,** 71.
DES CLOISEAUX, J., 1959, *J. phys. Radium*, **20,** 606.
DEWALD, J. F., 1960, *J. Phys. Chem. Solids*, **14,** 151.
FRIEDEL, J., 1952, *Phil. Mag.*, **43,** 153.
FRIEDEL, J., LEMAN, G., and OLSKAWSKI, 1961, *J. Phys. Chem. Solids* (in the press).
FRITZSCHE, H., 1959, *J. Phys. Chem. Solids*, **6,** 69.
FRITZSCHE, H., and CUEVAS, M., 1960, *Phys. Rev.*, **119,** 1238.
FROOD, D. G. H., 1960, *Proc. phys. Soc. Lond.*, **75,** 185.
GELL-MANN, M., and BRUECKNER, K. A., 1957, *Phys. Rev.* **106,** 364.
GOODENOUGH, J. B., 1960, *Phys. Rev.*, **120,** 67.
KRAUS, C. A., 1953, *J. chem. Educ.*, **30,** 83.
LIDIARD, A. B., 1954, *Rep. Progr. Phys.*, **7,** 201.
LOMER, W. M., and MARSHALL, W., 1958, *Phil. Mag.*, **3,** 185.
LÖWDIN, P. O., 1950, *J. chem. Phys.*, **13,** 365.
MCIRVINE, E. C., 1960, *J. Phys. Chem. Solids*, **15,** 356.
MILLER, A., and ABRAHAMS, E., 1960, *Phys. Rev.*, **20,** 745.
MORIN, J. F., 1954, *Phys. Rev.*, **93,** 1199; 1959 a, *Phys. Rev. Letters*, **3,** 34; 1959 b, *Semi-conductors*, Edited by N. B. Hannay (New York : Reinhold), p. 600; 1960, *Proceedings of the Prague Conference on Semi-conductors*, *Czech. J. Phys.* (in the press).
MOTT, N. F., 1949, *Proc. phys. Soc. Lond.*, **62,** 416; 1952, *Progr. Metal Phys.*, **3,** 76; 1956, *Canad. J. Phys.*, **34,** 1356; 1958, *Nuovo Cim. Suppl.*, **7,** 318.
MOTT, N. F., and JONES, H., 1936, *Theory of the Properties of Metals and Alloys*, (Oxford), p. 87.
MOTT, N. F., and STEVENS, K. W. H., 1957, *Phil. Mag.*, **2,** 1364.
MOTT, N. F., and TWOSE, W. D., 1961, *Advanc. Phys* (to be published).

PAOLETTI, A., and PICKART, S. J., 1959, *J. chem. Phys.*, **32,** 308.
PRICE, P. J., 1957, *J. Phys. Chem. Solids*, **2,** 268.
SLATER, J. C., 1951, *Phys. Rev.*, **82,** 538.
SMITH, G. E., 1959, *Phys. Rev.*, **115,** 1561.
STERN, F., and TALLEY, R. M., 1955, *Phys. Rev.*, **100,** 1638.
THOMAS, D. G., 1960, *J. Phys. Chem. Solids*, **9,** 31.
TWOSE, W. D., 1959, Thesis, Cambridge.
WANNIER, G. H., 1937, *Phys. Rev.*, **52,** 191.
WILSON, A. H., 1931, *Proc. roy. Soc.* A, **133,** 450.
WIGNER, E., 1938, *Trans. Faraday Soc.*, **34,** 678.
WIGNER, E., and HUNTINGDON, H. B., 1935, *J. chem. Phys.*, **3,** 764.
YAFET, Y., 1959, *Phys. Rev.*, **115,** 1172.

CORRESPONDENCE

Hammer Tracks from the Photodisintegration of Light Emulsion Nuclei

By W. T. Morton and T. G. Walker
Department of Natural Philosophy, University of Glasgow

[Received September 14, 1960]

If ^{8}Li or ^{8}B is produced in a nuclear disintegration it will decay at rest into two alpha particles through an excited state of ^{8}Be, and so produce a characteristic T-shaped track. These are usually referred to as 'hammer tracks' (Occhialini and Powell 1947, Alvarez 1950). Events of this type in which the initial disintegration was produced by a particle have been investigated by a number of workers (for example, Titterton 1951). In the present investigation a search has been made for hammer tracks originating in the photodisintegration of the light nuclei (carbon, nitrogen and oxygen) of nuclear research emulsions.

Ilford C.2 nuclear research emulsions, 400 microns in thickness, were exposed perpendicular to a bremsstrahlung beam of maximum energy 120 MeV from the Glasgow electron synchrotron. The emulsions were scanned for nuclear disintegrations in which more than two charged particles were emitted. 4300 events of this type were examined and eight hammer tracks identified. A small number of the three-prong events could have been due to the emission of a ^{8}Li or ^{8}B particle from a heavy nucleus of the emulsion (silver or bromide) for which no other charged particle was emitted. These events might be confused with a low energy 3α photodisintegration of ^{12}C and so were neglected. In each of the accepted hammer track events the initial disintegration had also produced a singly charged, or doubly charged particle of energy less than 5 MeV, and it is considered unlikely that these would be emitted simultaneously with a hammer fragment from a heavy nucleus of the emulsion. Hence it seems reasonable to assume that all of the hammer tracks accepted originated in the light nuclei of the emulsion. In the investigation of hammer tracks emitted in reactions induced by neutrons with an energy of 150 MeV, Titterton (*loc. cit.*) reached a similar conclusion. It would be expected that the probability of emission of a hammer fragment from silver or bromine would decrease with energy of the incident particle.

If a ^{8}B particle was emitted from a carbon nucleus, by the conservation of charge, a singly charged particle would also be emitted. Hence, although the ^{8}B would be recorded as a three-prong event, its true nature would be indicated by the sharp change in grain density and possibly also in direction at the position of the initial disintegration. No events of this type were found. This result is in agreement with Titterton who found that the probability of a hammer track resulting from ^{8}Li is higher than that for ^{8}B. In the remainder of this communication all hammer tracks will be assumed to be due to ^{8}Li.

No events were observed which could be assigned to ^{9}Li, which decays into ^{9}Be* followed by a decay at rest into a neutron and two alpha particles (Fry 1953). In this case the two alpha particles would not be collinear.

The energies of the ^{8}Li tracks were found to be 2·2, 3·2, 3·2, 5·1, 6·5, 8·3, 10·5 and 14·5 Mev. Three of the events in which the ^{8}Li particle originated had three prongs, one of which was singly and the other doubly charged. Hence by charge conservation these events are produced by the reaction ^{12}C(γ, ^{3}He p)^{8}Li with a threshold value of 41·2 Mev. The remaining events had four prongs, three of which were due to singly charged particles. These events must also have originated in a carbon nucleus of the emulsion. Since it was not possible to differentiate between protons and deuterons these events were produced either by the reaction ^{12}C(γ, 3pn)^{8}Li with a threshold value of 50·9 Mev or the reaction ^{12}C(γ, 2pd)^{8}Li with a threshold value of 48·7 Mev.

To obtain the incident γ-ray flux the three-prong events were analysed, using the criteria of Goward and Wilkins (1952), for events produced by the photodisintegration of ^{12}C into three alpha particles. Using the cross section given by these authors for that reaction the cross section for the photoproduction of ^{8}Li from ^{12}C averaged over γ-ray energies between 50 Mev and 120 Mev was found to be $(4 \cdot 9 \pm 2 \cdot 0) \times 10^{-30}$ cm^{2}.

ACKNOWLEDGMENTS

The authors wish to thank Dr. P. V. March for useful discussions and Dr. W. McFarlane for operating the synchrotron. One of us (T. G. W.) wishes to thank the Department of Scientific and Industrial Research for a maintenance grant.

REFERENCES

ALVAREZ, L. W., 1950, *Phys. Rev.*, **80,** 519.
FRY, W. F., 1953, *Phys. Rev.*, **89,** 325.
GOWARD, E. K., and WILKINS, J. J., 1952, *Proc. phys. Soc. Lond.* A, **65,** 671.
OCCHIALINI, G. P. S., and POWELL, C. F., 1947, *Nature, Lond.*, **159,** 93.
TITTERTON, E. W., 1951, *Phil. Mag.*, **42,** 113.

A Comparison of Vacancy and Interstitial Loops in Graphite

By G. K. Williamson
Berkeley Nuclear Research Laboratories, Gloucestershire

and C. Baker
Department of Metallurgy, Cambridge University

[Received September 22, 1960]

A recent letter by Amelinckx and Delavignette (1960) suggested the possibility of distinguishing between interstitial and vacancy loops in graphite because the vacancy loop has a component of its Burgers vector in the basal plane whereas the interstitial loop has a Burgers vector parallel to the C axis. Independent work carried out in the Department of Metallurgy, Cambridge, has proved that this is so and has also produced positive evidence for Amelinckx's interpretation of the Burgers vector of the vacancy loops.

Fig. 4

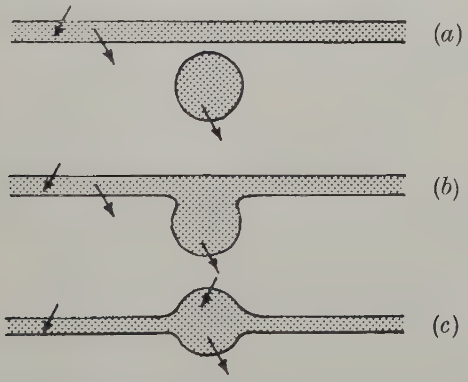

Possible interaction of a loop and a gliding basal plane dislocation to produce the dislocation arrangement shown at F in figs. 1–3 (arrows indicate Burgers vectors).

The photographs shown in figs. 1, 2 and 3† are of quenched and annealed graphite containing vacancy loops. The graphite was heated by direct current in a vacuum, and quenched by switching off. Figures 2 and 3 are dark field photographs of the area shown in fig. 1, taken with $1\bar{2}10$ and $11\bar{2}0$ reflections. The partial Burgers vector of the type

---

† Figures 1–3, 5 and 6 are shown as plates.

$a/3[10\bar{1}0]$ will lie along one of the three projections of the $\{11\bar{2}0\}$ planes on the basal plane and so must go out of contrast on one and only one of the three different $(11\bar{2}0)$ dark field views (Williamson 1960 and Delavignette and Amelinckx 1960). It is necessary to observe the absence of contrast to prove that the component of the Burgers vector in the basal plane is in fact a partial. This does in fact occur for every loop. In the example shown loop A disappears on fig. 2 and loop B on fig. 3. The large loop C at first sight appears on all three dark fields, but this is due to the contrast of dislocations held to its periphery by long-range stress fields, the segment where there are no overlapping dislocations does go out of contrast on fig. 3. Because these loops contain a component in the basal plane, interaction is expected with basal plane dislocations and one type of interaction is shown at F. Figures 1–3 show that the loop has different partial Burgers vectors at opposite sides and a possible mechanism for producing this effect is shown in fig. 4.

Examples of large interstitial loops produced by neutron irradiation ($\sim 3 \times 10^{20}$ nvt) at 300°c are shown in fig. 5. In the case of interstitials a disc of atoms can be inserted as a C layer in an ABAB etc. sequence without producing a high-energy stacking fault. Thus the basal plane component which makes the vacancy loops so easy to observe is missing. Interstitial loops rarely show good contrast and that shown in fig. 5 is produced by tilting the specimen so that the C axis is about 30° away from the electron beam. The contrast effects in this case are clearly very complex and a detailed study has been hindered by the fine scale radiation damage clearly visible in the broad extinction contours. The basal plane dislocations can interact with these loops through their long-range stress fields as in fig. 5. Figure 6 shows the contrast of interstitial loops when the C axis is parallel to the electron beam. This contrast has been discussed in detail by Howie and Whelan (1960) who show that the loops are visible because of the radial displacements perpendicular to the Burgers vector. Under these conditions two concentric loops on either side of the dislocation loop are seen with contrast most intense at those parts of the loop parallel to the reflecting plane and vanishing at points perpendicular to it. This is exactly the contrast observed and in all cases examined the diameter along which there is no contrast is parallel to the reflecting plane.

A fuller account of this work will be published elsewhere.

References

Amelinckx, S., and Delavignette, P., 1960, *Phys. Rev. Letters*, **5**, 50.
Williamson, G. K., 1960, *Proc. roy. Soc.* A, **257**, 457.
Delavignette, P., and Amelinckx, S., 1960, *J. appl. Phys.* (to be published).
Howie, A., and Whelan, M. J., 1960, *European Regional Conference on Electron Microscopy* (to be published).

Evidence of Sub-surface Cross-slip in Fatigued Copper

By A. H. Meleka, W. Barr and A. A. Baker
Metal Physics Section, British Iron and Steel Research Association, London

[Received October 5, 1960]

It is now generally accepted that the formation of extrusions and intrusions on the free surface of fatigued metals leads to the initiation of the ultimate fatigue crack. Particular attention has therefore been given to the possible atomic movements during cyclic stressing responsible for extrusion–intrusion formations. Various mechanisms have been suggested including those due to Cottrell and Hull (1957), and Forsyth (1957) but the one proposed by Mott (1958) appears the most likely. Briefly, it is suggested that during the first half-cycle a dislocation line moves along the slip plane and then cross-slips to an adjacent plane. In the second half-cycle the dislocation glides backwards, then cross-slips to the original plane, and so on. In the presence of a screw component of the dislocation this continuous movement will lead to the formation of an extrusion above the free surface and a cavity below the extrusion. Cross-slip is an essential feature in this mechanism. Although the importance of cross-slip to the phenomenon of fatigue is now generally accepted by most workers in this field, Mott's mechanism has not, as yet, been confirmed by direct observation. We have observed, by using a fine electropolishing technique and by penetrating progressively into the surface of fatigued copper specimens, the existence of cross-slip in those slip bands which eventually lead to crack formation.

Specimens of OFHC copper were fatigued in reversed bending to about half their expected life. The wide slip bands characteristic of fatigue deformation were observed. Upon electropolishing, using the technique developed by Jacquet (1957), most of the surface markings were removed, leaving behind a number of dark bands, the so-called persistent slip bands. The present technique is superior here to standard electropolishing methods for two reasons. Firstly, very thin layers, estimated at 100 Å, can be readily removed; this is particularly useful since early fatigue damage is concentrated in a thin surface layer. Secondly, the persistent slip bands produced by this technique are considerably finer than those obtained by standard electropolishing methods. Persistent slip bands can, therefore, be observed at higher magnifications and fine structural details are revealed.

Figure 1 (*a*)† shows the appearance of a grain after removal of approximately 3 microns ; persistent slip bands on two slip systems can be seen. Successive layers were then removed and fig. 1 (*b*) shows the

---

† Figures are shown as plates.

same field of view after the removal of a further 9 microns. The few persistent slip bands that remain, differ from those in fig. 1 (*a*) in that they deviate from linearity by the presence of short segments inclined to the main slip plane. In the region to the left of fig. 1 (*b*), for example, the segment indicated by the arrow A coincides with the direction of the conjugate slip plane, while that indicated by B coincides with the cross-slip plane. This was confirmed by constructing a stereographic projection based on the sideway shift of the primary slip bands produced by the removal of 9 microns. Other manifestations of cross-slip are indicated and more can be seen elsewhere in the micrograph.

It is interesting to note that cross- and conjugate-slip segments are more in evidence upon deeper penetration into the surface layer. It is likely, as suggested by McEvily and Machlin (1959) that cross-slip provides the means for the easy transport of piled-up material beneath the intrusion to the region beneath the extrusion.

It was further observed that, in certain cases, cross-slip segments were present below the extrusions. Examples of extrusions and the corresponding cross-slip regions are shown in fig. 2 (*a*) and (*b*) respectively. Although this one to one correspondence was observed in a few cases, it is by no means general. Numerous extrusions were observed which could not be related to regions of cross-slip.

Further examples of the abundance of cross-slip in fatigued copper, together with a full account of this work, will be published elsewhere.

REFERENCES

COTTRELL, A. H., and HULL, D., 1957, *Proc. roy. Soc.* A, **242,** 211.
FORSYTH, P. J. E., 1957, *Proc. roy. Soc.* A, **242,** 198.
JACQUET, P. A., 1957, O.N.E.R.A., Note Technique No. 40.
MCEVILY, A. T., and MACHLIN, E. S., 1959, *Proceedings of the Swampscott Conference on Fracture*, p. 450.
MOTT, N. F., 1958, *Acta Met.*, **6,** 195.
THOMPSON, N., WADSWORTH, N. T., and LOUAT, N., 1956, *Phil. Mag.*, **1,** 113.

REVIEWS OF BOOKS

Graphite and its Crystal Compounds. By A. R. Ubbelohde and F. A. Lewis. (Oxford: Clarendon Press, 1960.) [Pp. xii+217.] Price £1 15*s.* 0*d.*

The use of graphite as a moderator in nuclear reactors has given an impetus to the study of this most interesting and versatile material. It is now clear that the properties of graphite are so diverse as to require a monograph for their description. Professor Ubbelohde and Dr. Lewis have now provided such an account. Many of the properties of graphite, such as its increased electrical conductivity when electrons are either added to it, or subtracted from it, depend on its almost unique electronic band structure. Other properties, such as its layer form with normal bond distances within a layer and much larger distances between layers, link it to the peculiar chemistry of aromatic molecules with their π and σ electrons. Yet other properties, such as the bizarre way in which a wide variety of atoms and ions, including such diverse entities as alkali metal atoms, halogen atoms and $AlCl_3$ moleclues are able to prize apart the layers and intercalate themselves between them, thus increasing the interlayer distance from 3·5 Å to as much as 11 Å, depend on the relative weakness of van der Waals forces as compared with valence forces. Much of the reactivity of carbons depends critically on its purity, and so the nature of the residual foreign atoms around the edge is of prime importance. So also are the lattice defects—a matter only recently recognized. All this—and much more—is set out in this book. The explanations are clear, and (almost always) consistent. This, incidentally, is by way of being a minor triumph, since the range of alternative theories suggested from time to time is prodigious. In places the attempt to refer to almost every published paper on graphite gives the book the character of a card index, but anyone working in this field is sure to be grateful for the bibliography of no less than 28 pages. As a reference work on graphite, with all its vagaries and still largely uncomprehended behaviour, this book is unique. It is easy to read and beautifully produced. C. A. C.

Frozen Free Radicals. By G. J. Minkoff. (New York: Interscience Publishers, 1960.) [Pp. 134.] Price $5.00 (£1 18*s.* 0*d.*).

The possibility of freezing or trapping high concentrations of free radicals has been very much in the scientific news over the last year or so, as illustrated by the large-scale research programme recently undertaken by the National Bureau of Standards in Washington on this very subject. Dr. Minkoff was one of the Guest Scientists associated with this project and one suspects that much of this enthusiasm, and many of the ideas developed in the writing of this book, stem from this association. The book has the flavour of a subject that is full of interest and possible practical applications, and is written by an author who is not only an active worker in the field itself, but also has obviously taken a keen interest in all the other lines of development. When considered in ten years' time some parts of the book will undoubtedly appear to have undue emphasis, and others may need modification or correction, but the fact that it is impossible to tell which sections these are at the moment, shows that the monograph is a fair summary of the present position in the development of the subject.

On the other hand, it should not be understood from these remarks that the book only deals with present day work and the more recent advances in free-radical studies. After a short introduction to the subject, a whole chapter is devoted to the early history of free-radical investigations, and forms a very interesting and helpful summary, which is not readily available in many similar monographs. The more recent work is then introduced by a consideration of the experimental techniques, first grouped under the methods of production of radicals, and then the methods of trapping and stabilizing at low temperatures, and finally the methods of detecting and investigating the frozen radicals. Owing to the space available, each of these topics is considered in a rather condensed fashion, but considerable detail is given on the design of low temperature Dewars and cells, including several detailed diagrams, which will prove very useful to any who are entering this field for the first time.

A chapter on the basic principles of the ' trapping mechanism ' then follows, together with a quantitative treatment of both trapping and chain processes. The rest of the book is then devoted to a summary of the results obtained with different types of radicals. This starts with a chapter devoted to the study of individual atoms; hydrogen, oxygen and nitrogen being considered in some detail. The different experimental results are summarized for each case, and it is interesting to see how large a part electron resonance spectra play in the identification of the atomic species. The following chapter deals with diatomic and triatomic radicals in a similar way, while the concluding section summarizes the results on complex organic radicals of both aromatic and aliphatic nature.

The book can certainly be taken as a fair and comprehensive treatment of the whole field of ' frozen free radicals ' as it exists at the moment, although a second edition will undoubtedly be required before too long. There are one or two minor critisisms of careless phrasing in the book, such as the statement that " scattering is less important at *shorter frequencies* ", when it is not immediately evident whether this means ' shorter wavelengths ' or ' smaller frequencies '. These hardly detract from the main content of the book, however.

D. J. E. I.

Beam and Wave Electronics in Microwave Tubes. By Rudolf G. E. Hutter. (New York : D. van Nostrand, 1960.) [Pp. 378.] £3 13*s*. 6*d*.

In the last decade it has become clear that the best description of the operation of microwave valves depends on the application of Maxwellian electrodynamics to the highly complicated system comprising the electron beam in interaction with some kind of slow-wave structure. This model has been the subject of hundreds of articles and several books in several languages. The work under review is an extension of an article in *Advances in Electronics* which appeared in 1954. The new material includes chapters on circuits (about one-third of the book), extensive quotation from the work of Gould on electron waves in crossed electric and magnetic fields, an account of Pierce's mode coupling concept and a chapter on noise. The preface states that the level is that of a university textbook.

The author has decided to ignore many well-known physical facts. For example, most microwave valves in use today use a quasi-cylindrical electron beam formed by some type of magnetic focusing. The trajectories of the electrons depend on the focusing technique and the space-charge wavelength, radio-frequency currents, etc., depend on the trajectories in a very marked way. The behaviour of a beam using Brillouin focusing is thus quite different from that of a confined beam. Yet none of this is mentioned, nor are references given. Again, it is well known that even the simplest case of interaction between a cylindrical beam and a circuit, in which the beam just fills the gaps of a cavity, has to be described using a complete set of orthogonal modes on the beam. The existence of modes of higher order is never mentioned and, as a result, the basic work in Chapters 8 and 9 is never put on a firm theoretical basis. For the same reason, the discussion of energy conversion becomes unrealistic immediately it goes beyond the derivation of an appropriately modified Poynting theorem to consider effects in real tubes. The delicate question of the best description of phenomena on the surface of a rippled beam has recently been discussed, but this is not referred to.

While the author could be excused for not including full treatments of these questions, to omit them entirely is inexcusable and the book cannot be recommended.

A. H. W. B.

Electromagnetic Wave Propagation. Edited by M. DÉSIRANT and J. L. MICHIELS. (London and New York: Academic Press, 1960.) [Pp. xiv+730.] $22.00.

THIS is a collection of 54 papers which were presented in 1958 at a conference in Brussels sponsored by the Postal and Telecommunications Group of the Brussels Universal Exhibition. Five of the papers are in German, four are in French and the rest are in English. Nearly all of them relate to some aspect of radio wave propagation.

About 20 of the papers are theoretical and the topics include diffraction theory, antenna radiation theory, surface waves, ray tracing in the ionosphere, propagation of waves of low and very low frequency, scattering, and the statistics of irregular media. About 27 papers describe measurements or observations, including ground wave propagation, tropospheric scatter, diffraction beyond the horizon, ionospheric backscatter, scattering from meteor trails, the scintillation of radio stars, the reflection of low frequencies from the ionosphere, and 'round the world' echoes. The remaining papers are concerned with analysis of data and with radio engineering techniques.

The contributors include many well known investigators from research centres all over the world. All who are accustomed to watch the current literature on radio wave propagation will need to make a careful study of the contents list of this book.

K. G. B.

An Introduction to the Physics of Mass Length and Time. By NORMAN FEATHER. (Edinburgh University Press, 1959.) [Pp. ix+358.] 18*s*.

PROFESSOR FEATHER'S aim in this book is "to introduce the beginning specialist in physics to those parts of his subject which in any well-designed course he should study first, and to effect that introduction by examining first of all the bases of measurement of the fundamental physical quantities mass, length and time". The term 'beginning specialist' is perhaps misleading, for Professor Feather is writing not only for the future scientist but for all students, whether scientists or not, who wish to acquire a worthwhile grasp of some of the elements of physics, and this of course influences his presentation; in particular, the calculus is not introduced.

After an introductory chapter the author discusses the measurement of length (in both theory and practice) and of time, and he is then in a position to discuss a number of topics in kinematics, including Kepler's laws and Newton's treatment of them. A key chapter on the concepts of force and mass follows, after which rather more than half the book remains in which to make the work "not very different in scope from any elementary *Mechanics and Properties of Matter*".

An historian of science cannot but welcome the frequent efforts to set concepts and laws into their historical context, and here Professor Feather is usually well informed. Most unfortunately he does not recognize that the very attitude to physics which he accepts almost without question was itself the product of intellectual struggles far more profound that those he has occasion to discuss. Physics "may be defined as the body of knowledge derived by making measurements of things"—what pangs attended the birth of that definition!;

and did not the adoption of idealized mathematical quantities constitute a paradoxical method of studying nature? For an understanding of physics such as Professor Feather aims to give, the reader must be made aware of these fundamental historical issues; but it is good to see this attempt to teach physics as a great *human* achievement. M. A. H.

Some Mathematical Methods of Physics. By GERALD GOERTZEL and NUNZIO TRALLI. (McGraw-Hill Book Co., 1960.) [Pp. xiv+300.] £3 6*s*. 0*d*.

THIS book shows how to apply the calculus of operators to problems of theoretical physics. Much of the mathematical technique used in quantum theory is presented here, including the Dirac bracket notation. Yet there is hardly any mention of quantum theory, and all the problems discussed are classical.

The book is in three parts. Part I deals with systems having a finite number of degrees of freedom, such as the loaded string, and the operators are represented by matrices. Part II is concerned with systems having an infinite number of degrees of freedom. The operators are differential operators with boundary conditions, and the problems used for illustration include the vibrating membrane, electrical lines, heat conduction and problems of radiation and scattering. Part III discusses methods of approximation, including perturbation methods and the Rayleigh–Ritz variational principle.

Most students taking a final honours physics course will find this book difficult to understand. It should be more useful to teachers already familiar with the main theme, who want ways of presenting the ideas clearly to students. Readers who master it will be well equipped to tackle an advanced course on mathematical quantum theory. K. G. B.

The Theory of Brillouin Zones and Electronic States in Crystals. By H. JONES. (North-Holland Publishing Company, 1960.) [Pp. 268.] £3 0*s*. 0*d*.

THE bulk of the book is devoted to a thorough discussion of how to specify states in a periodic lattice including topics such as character tables, compatibility relations, screw axes and glide planes, spin–orbit coupling, but only a very incomplete treatment of time-reversal symmetry. The necessary group theory is introduced very well, almost imperceptibly and without tears, in the form directly required by the applications without mathematical frills. One chapter deals with practical methods of calculating band structures discussing three methods in detail.

Chapter 5 is concerned with the large zones in extended k-space, which are often introduced for metals and alloys having a large number of valence electrons per unit cell. Unfortunately the analysis is all based on the nearly free electron approximation (n.f.e.a.) with weak potentials. Since in practice atomic potentials are strong and the n.f.e.a., if carried out, would converge to the 1s energy of the core orbitals, one is left wondering what relevance it all has to real metals. This could easily have been avoided by basing the analysis on the orthogonalized plane wave method, where the structure factors turn up in exactly the same way but where the matrix elements really are small.

The book is clearly written throughout, and fills an important place in the series of monographs into which solid-state theory has now expanded. V. H.

[*The Editors do not hold themselves responsible for the views expressed by their correspondents.*]

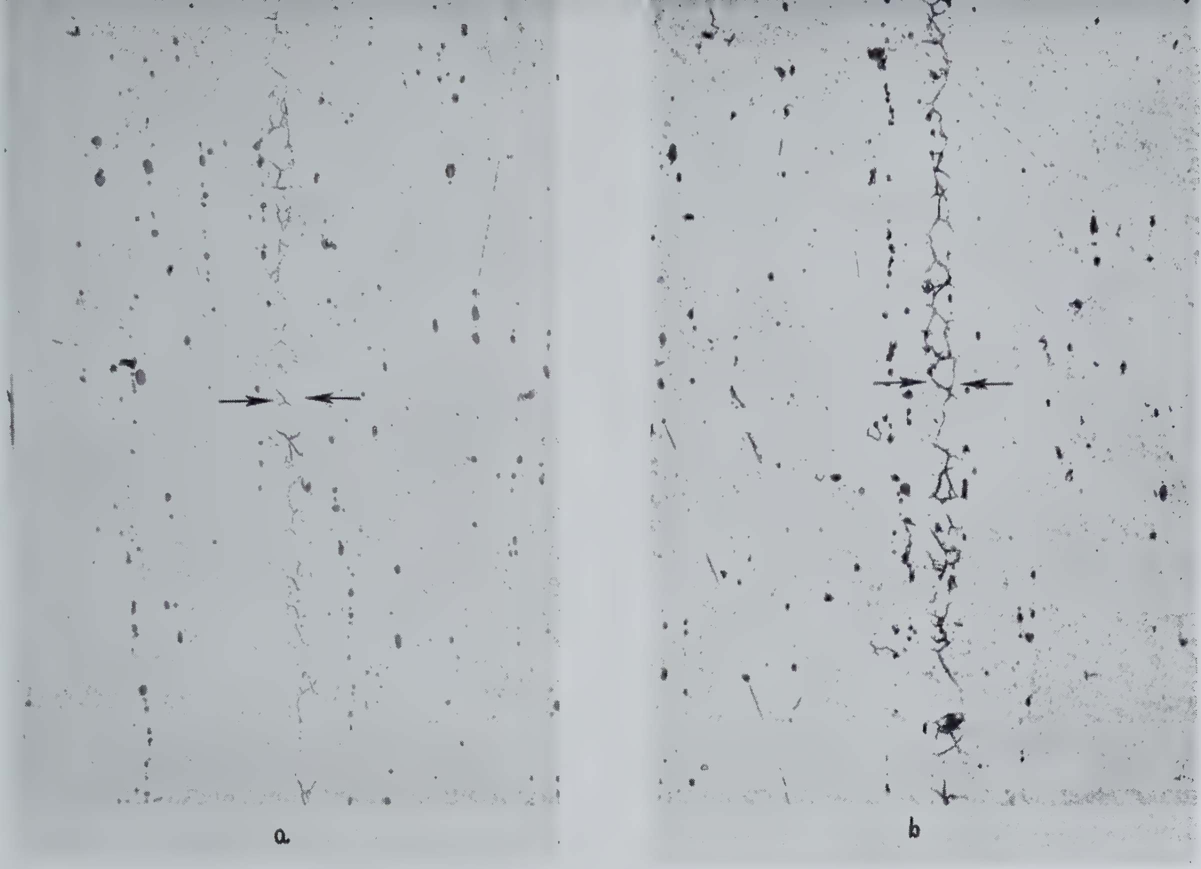

The precipitation region in two copper samples as viewed under a light microscope. The photographs were made and developed under identical circumstances so that the pictures represent the observed difference in the two precipitation regions. The magnification in each case was ×450 before publication. The precipitation region is the band of delineated grain boundaries lying between the arrows. (*a*) Shows the precipitation region of a sample bombarded with α-particles and aged *in vacuo* at 425°c for 252 hours. (*b*) Shows the precipitation region of a sample bombarded with α-particles and irradiated at 425°c in a reactor for 252 hours.

Fig. 3

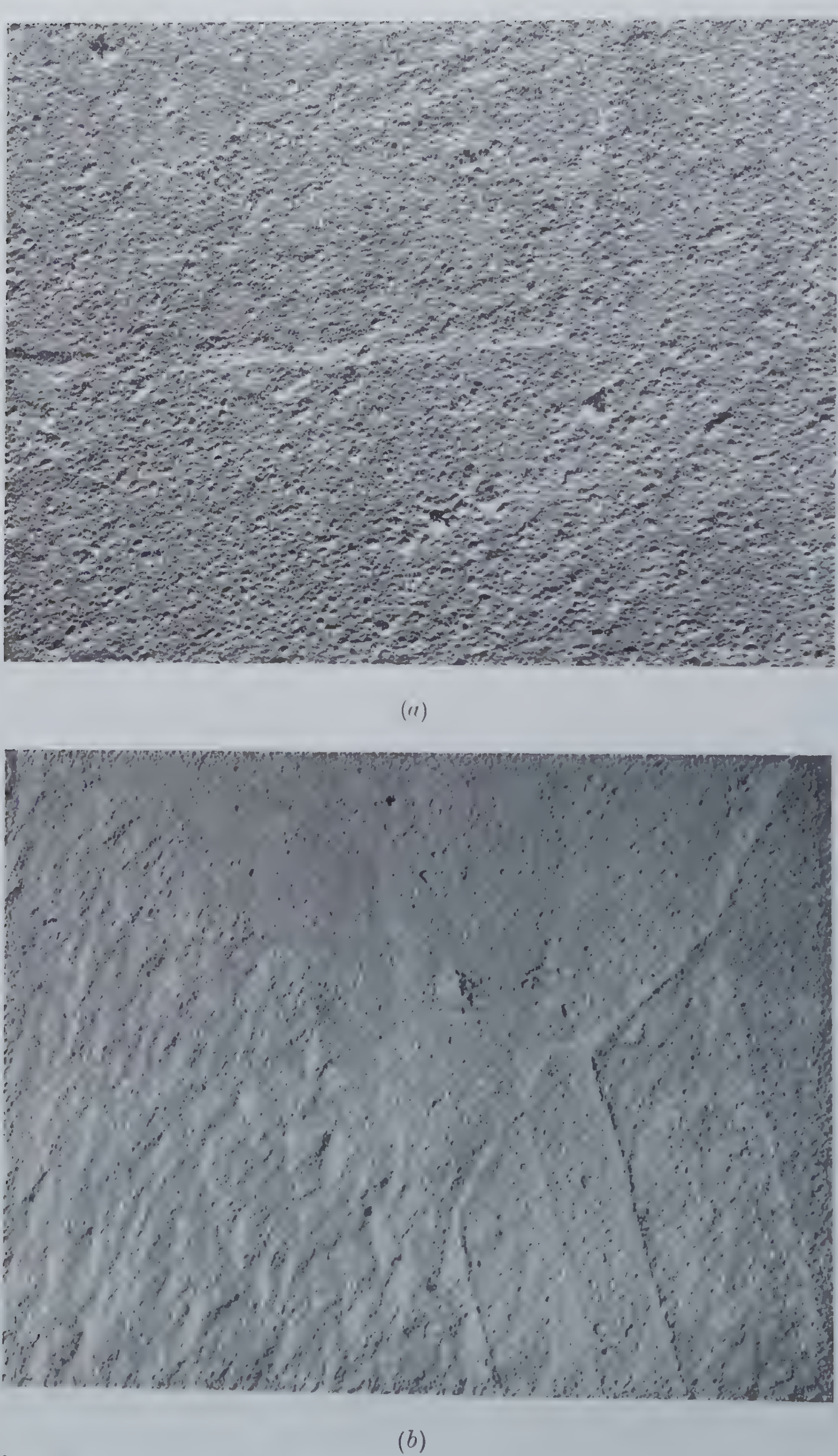

Electron micrographs of the two copper samples shown in fig. 2. Magnification is ×20 250. (*a*) The normal grain structure of the out-of-pile copper sample. (*b*) The normal grain structure of the in-pile copper sample.

Fig. 4

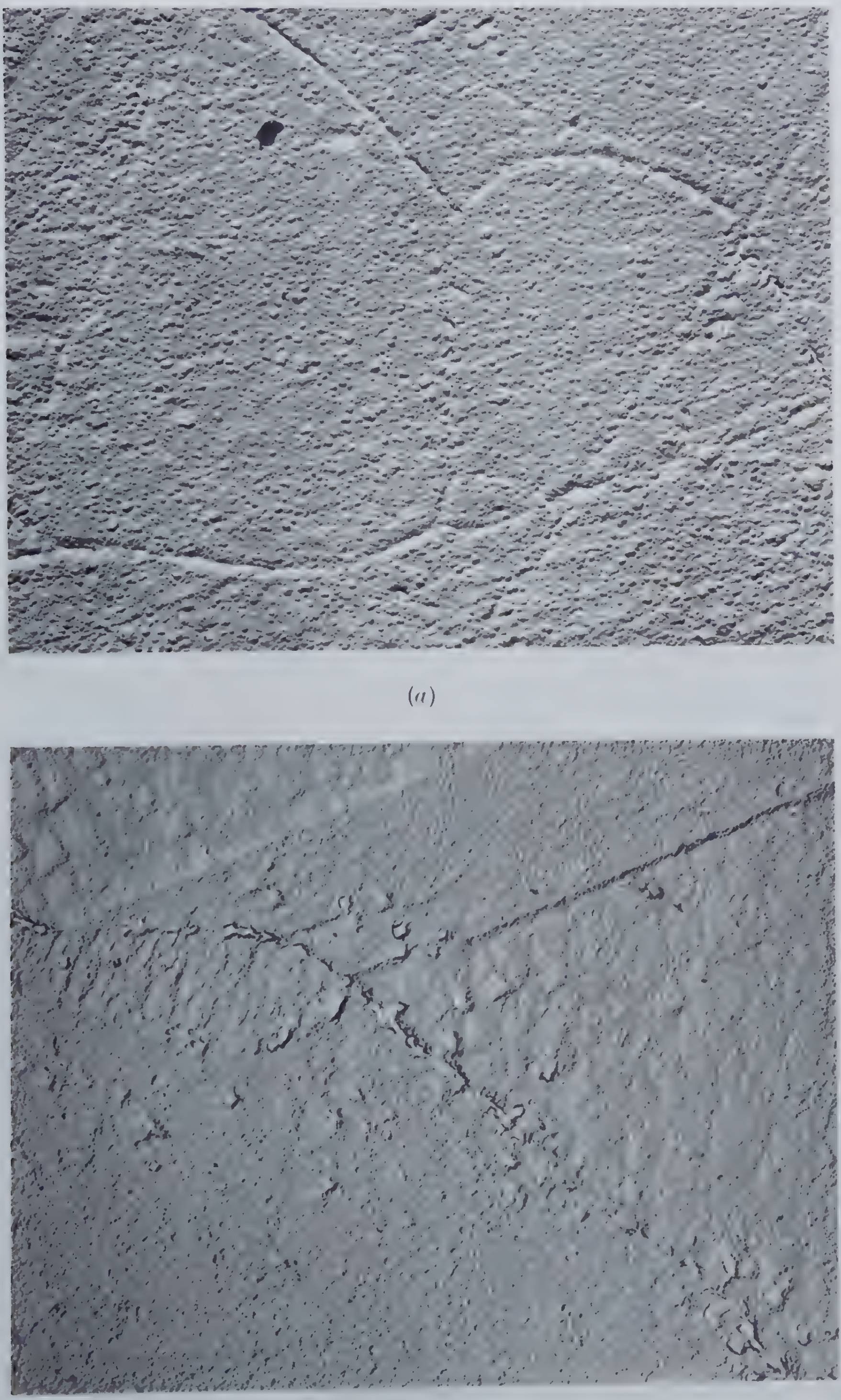

Fig. 4 (*continued*)

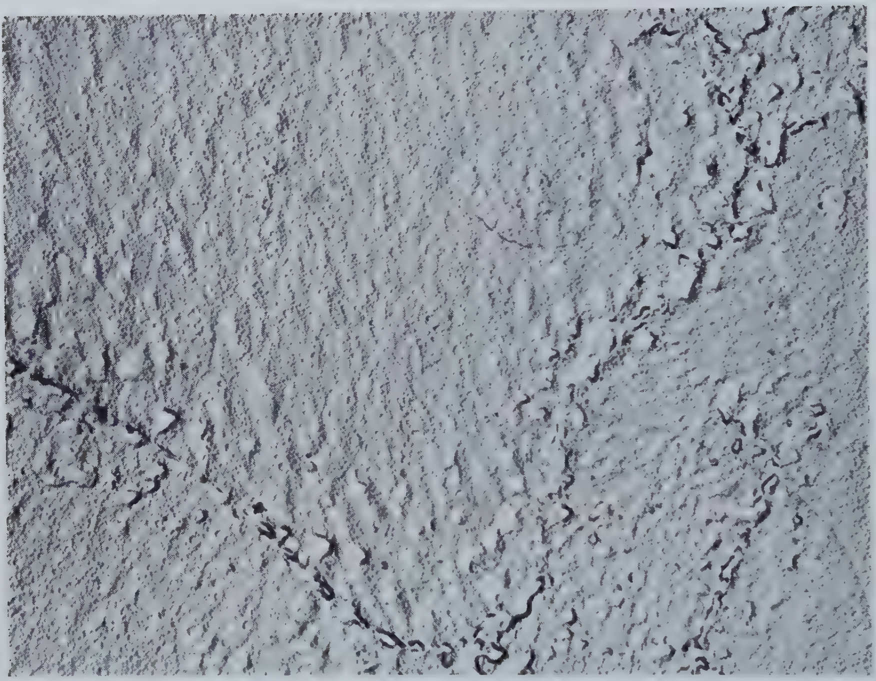

(*c*)

Electron micrographs of the precipitation region of the two copper samples. Magnification is ×20 250. (*a*) The grain structure of the precipitation region in the out-of-pile sample. (*b*) The grain structure of the precipitation region in the in-pile sample, showing an active grain boundary and one which is not active in supplying vacancies. (*c*) The grain structure in another portion of the precipitation region in the in-pile sample.

Fig. 1

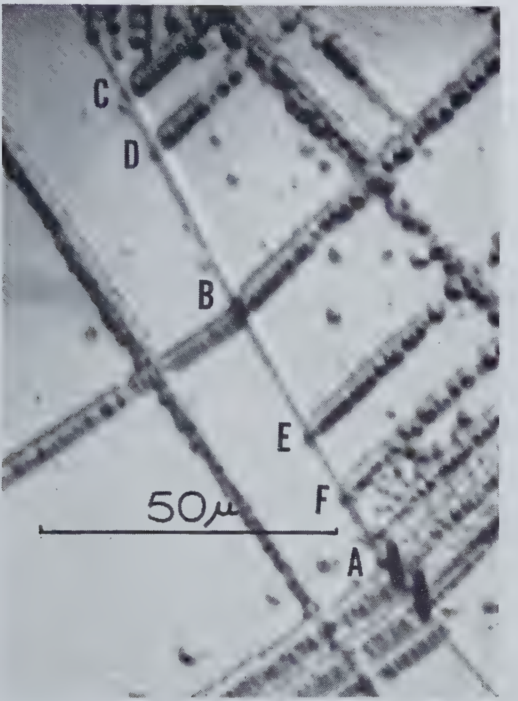

Cracks formed at grain boundary by piled-up groups of edge dislocations.

Fig. 2

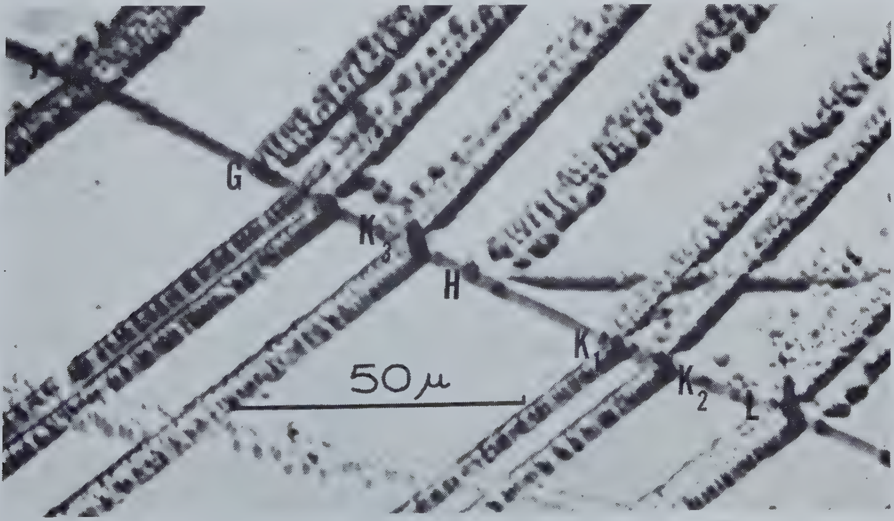

Cracks formed at grain boundary by piled-up groups of edge dislocations.

Fig. 3

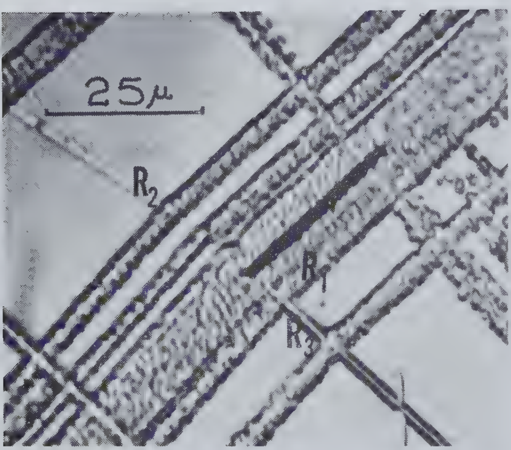

Crack propagating away from boundary on a {110} plane.

Fig. 6

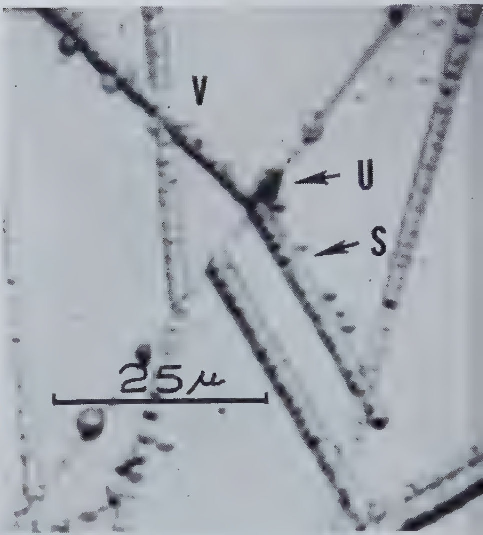

Crack formed at U by cooperation of dislo-cations in band V and from source S.

Fig. 4

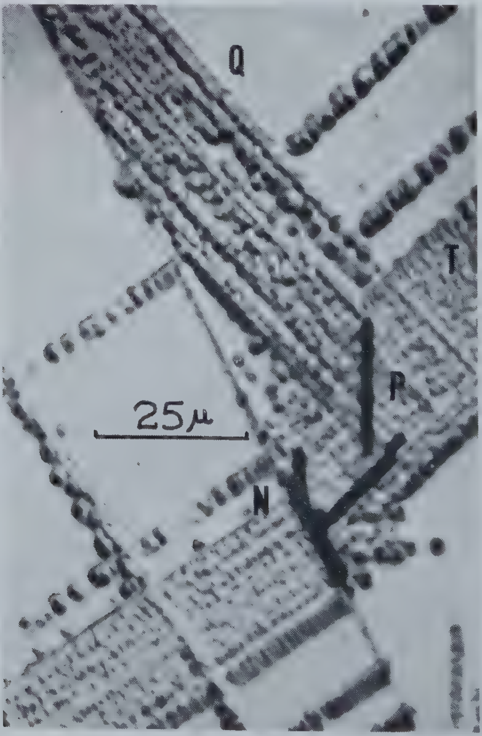

Crack at P possibly formed by interaction of dislocations in slip bands Q and T.

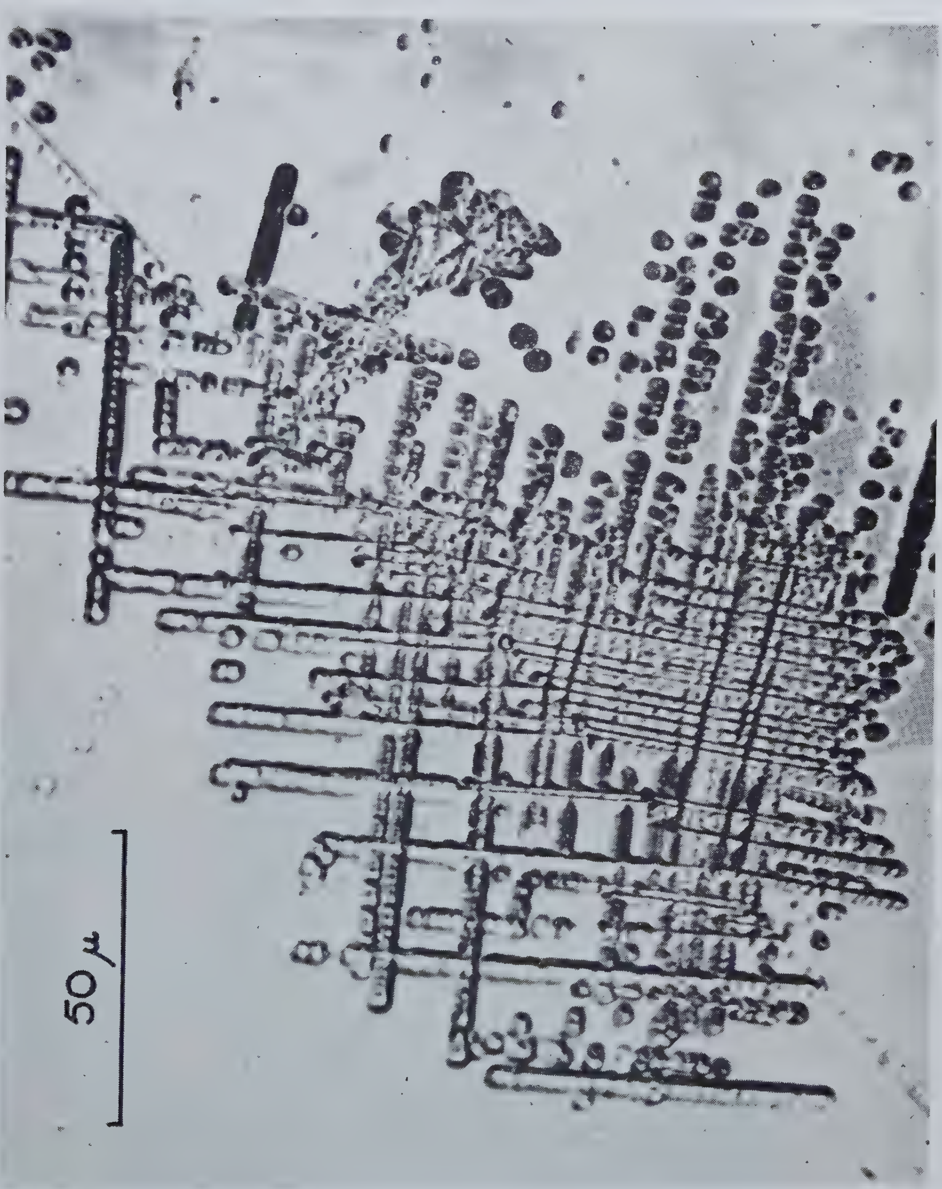

Fig. 5

Grain boundary acting as source of dislocations.

Fig. 1

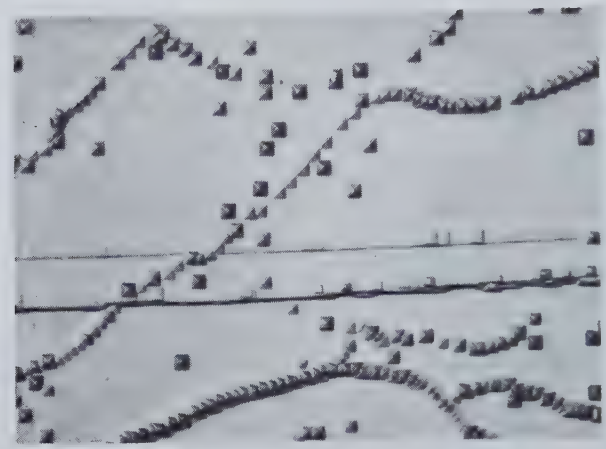

Etch pits on cleaved surface of undeformed crystal, showing pits at annealed-in dislocations and cleavage steps. (×260.)

Fig. 2

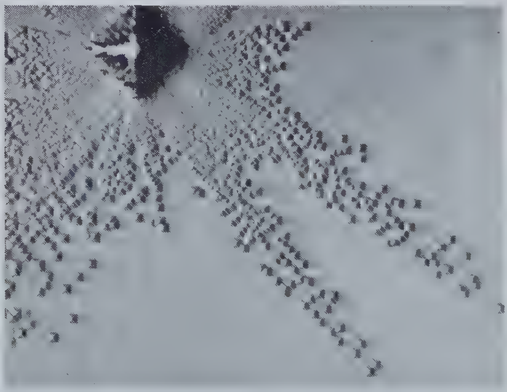

Part of rosette of etch pits on crystal indented, polished for 1 min and etched. (×410.)

Fig. 3

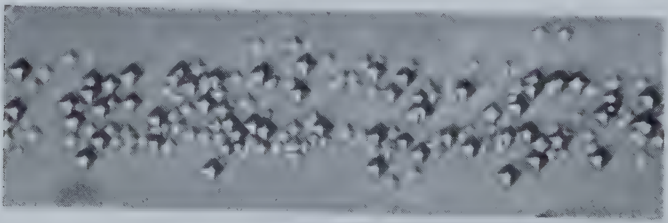

Normal and shallow etch pits in an edge slip band. (×650.)

Fig. 4

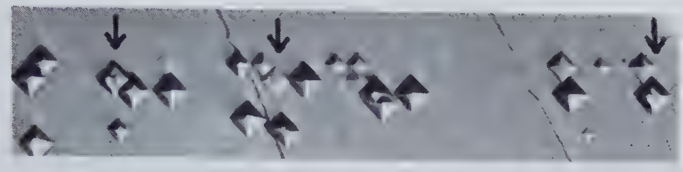

Pits showing intermittent etching in an edge slip band. (×580.)

Fig. 5

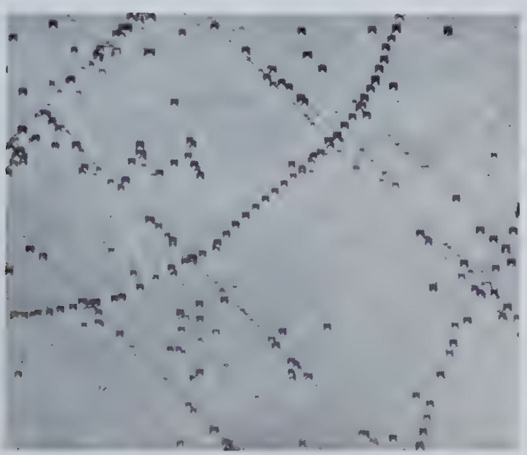

(*a*)

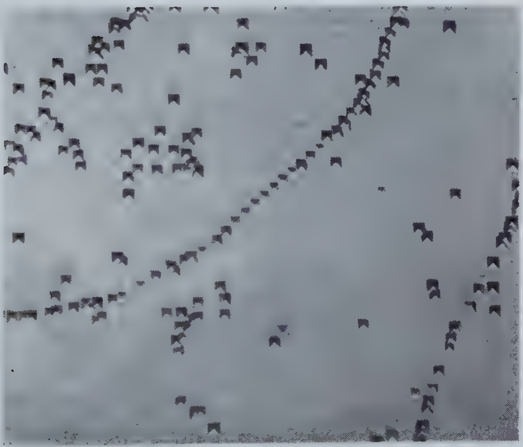

(*b*)

Etch pits on edge slip bands before and after annealing. (*a*) Deformed, cleaved, polished and etched. (*b*) Same region annealed 1 hr at 250°c, polished and re-etched. (×190.)

Fig. 6

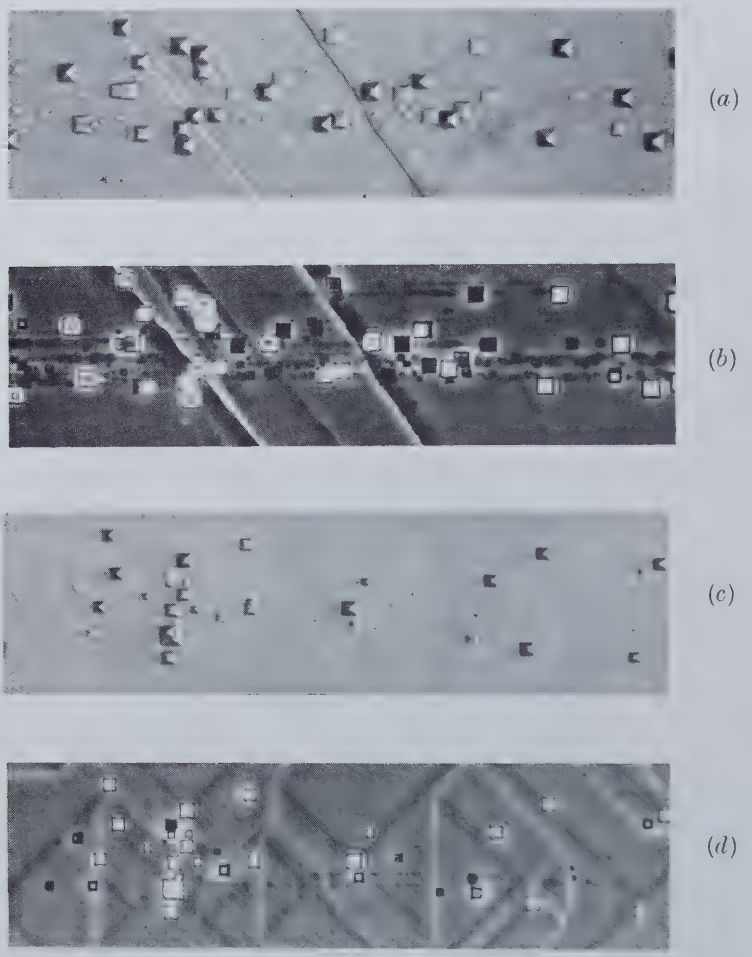

Etch pits on part of a screw slip band.
External surface: (a) oblique illumination, (b) phase-contrast.
Polished 1 min: (c) oblique illumination, (d) phase-contrast. (×540.)

Fig. 7

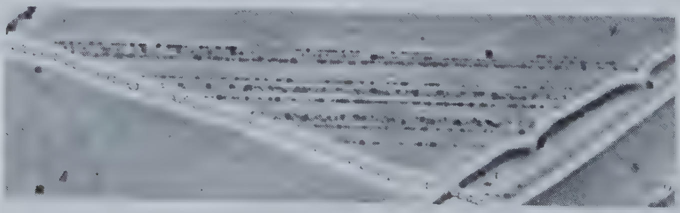

Streaks of pits formed by etching freshly cleaved surface of undeformed crystal. Phase-contrast. (×390.)

Fig. 8

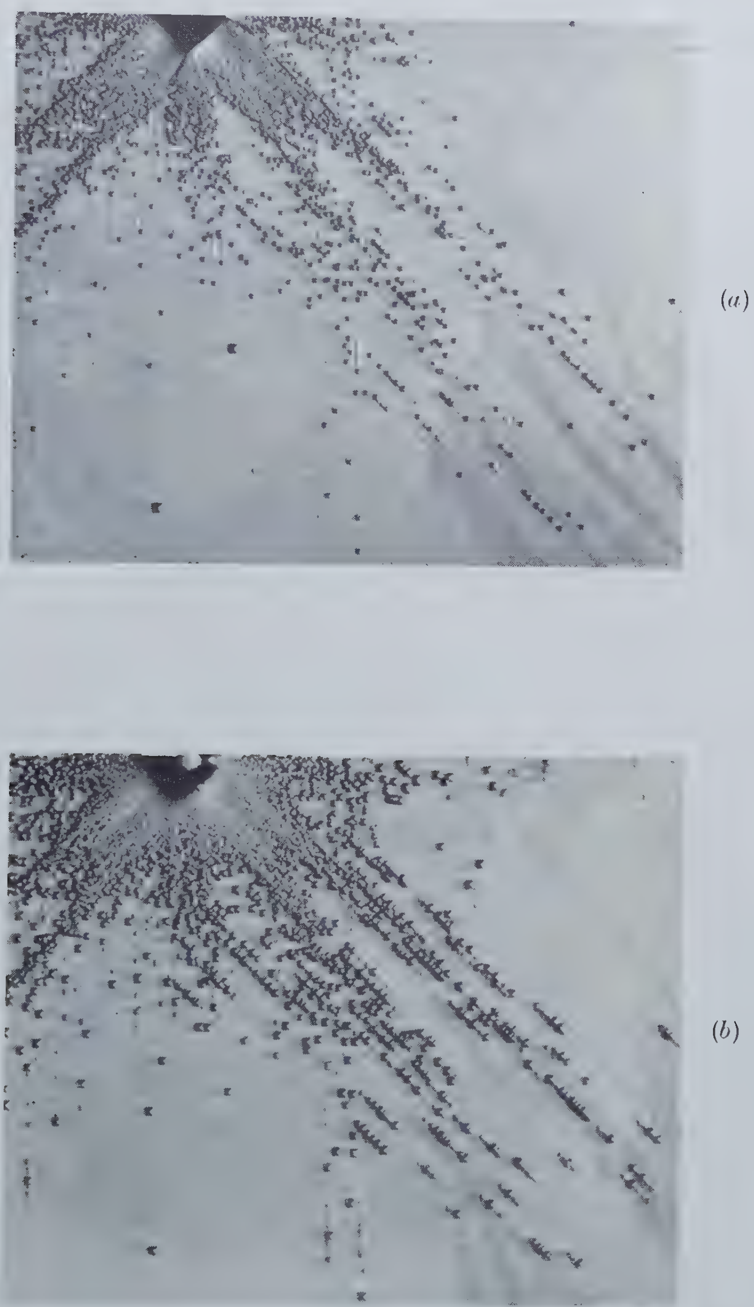

Part of rosette in crystal vibrated at 90 kc/s. (*a*) Polished, etched, indented, vibrated at strain amplitude of $2{\cdot}6 \times 10^{-4}$ and re-etched. (*b*) Same region polished 3 min and re-etched. ($\times$230.)

Fig. 9

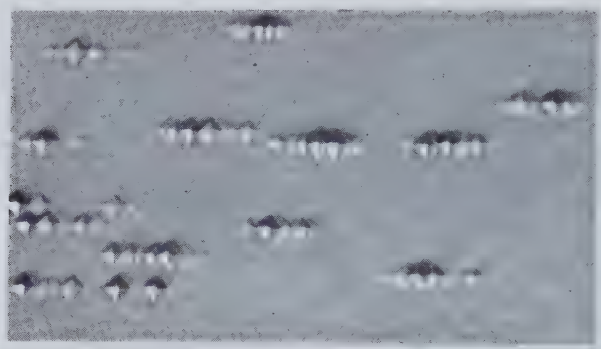

Pits associated with edge dislocations in crystal indented, vibrated at strain amplitude of $2{\cdot}0 \times 10^{-4}$, polished 3 min and etched. (×560.)

Fig. 10

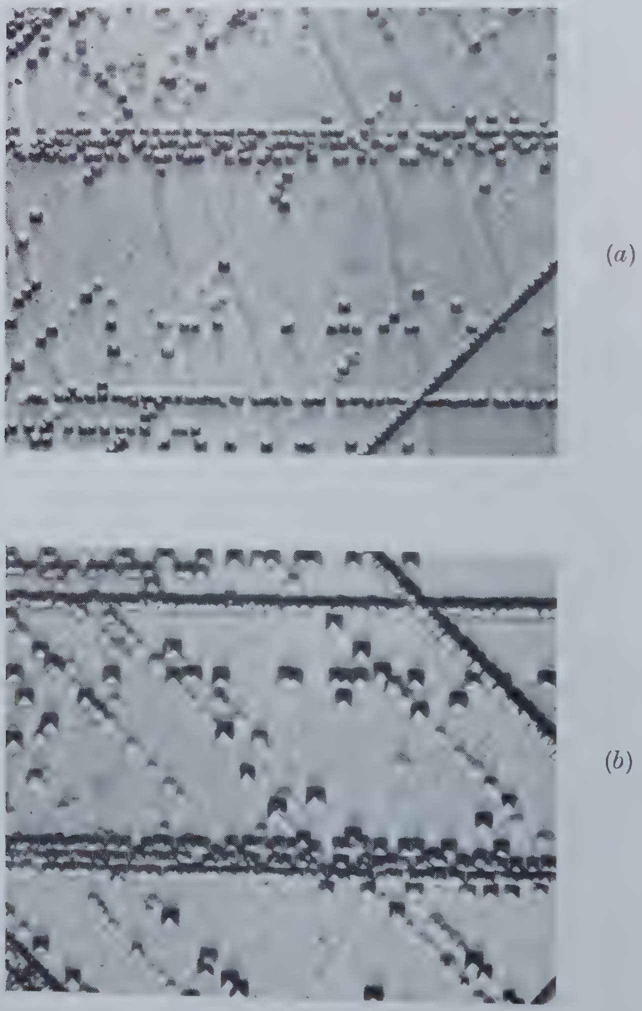

Etch pits in slip bands on matched cleavage faces of deformed LiF. (*a*) Etch W, (*b*) Etch H. Note poorly defined pits formed by H in edge slip bands (diagonal lines). (×550.)

Fig. 1

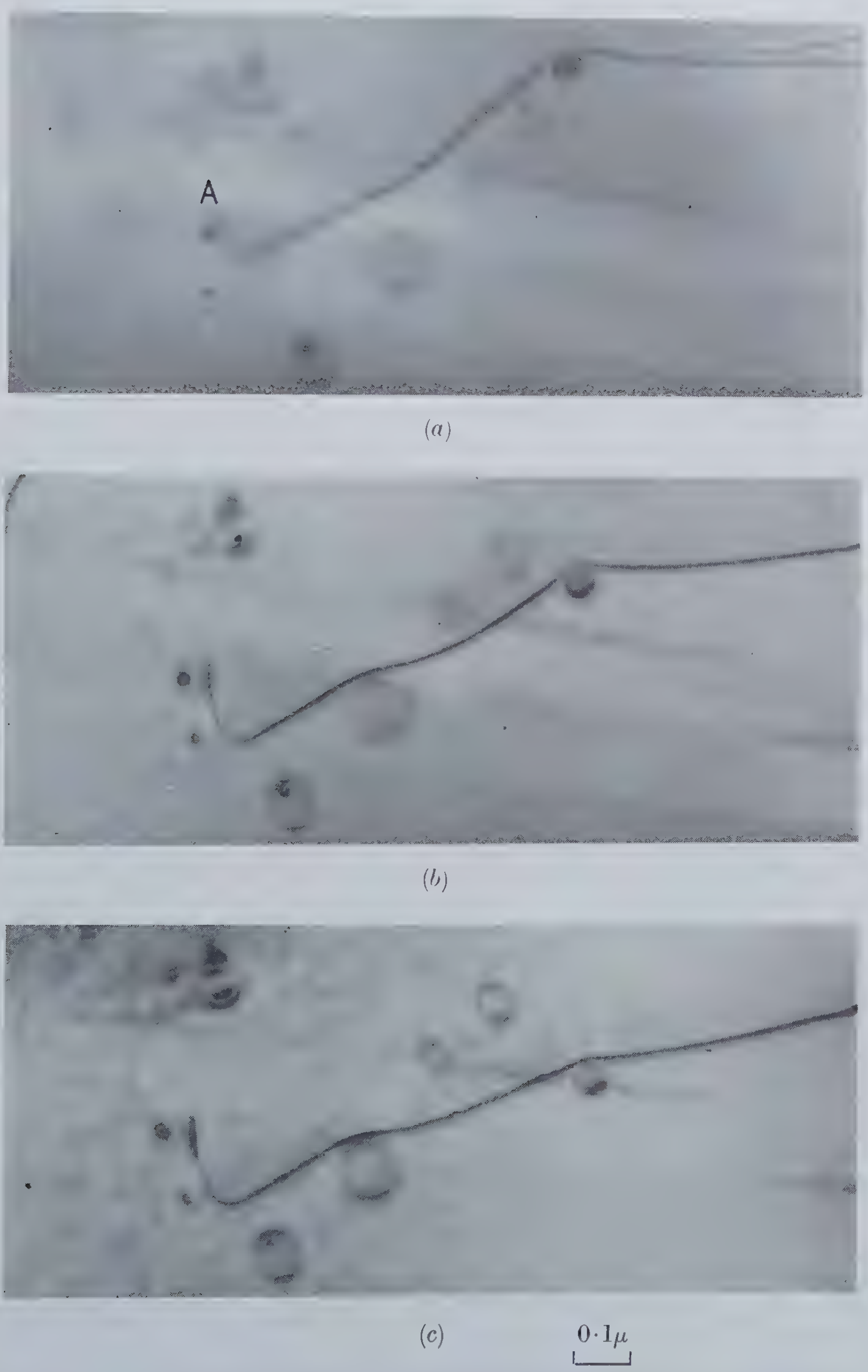

(a)

(b)

(c)

Sequence of transmission electron micrographs showing the 'conservative climb' motion of a dislocation loop with a [0001] Burgers vector due to its interaction with a moving edge dislocation with a $\frac{1}{3}[\bar{1}\bar{1}20]$ Burgers vector. The plane of the micrograph is parallel to the basal plane of the zinc platelet.

Fig. 1

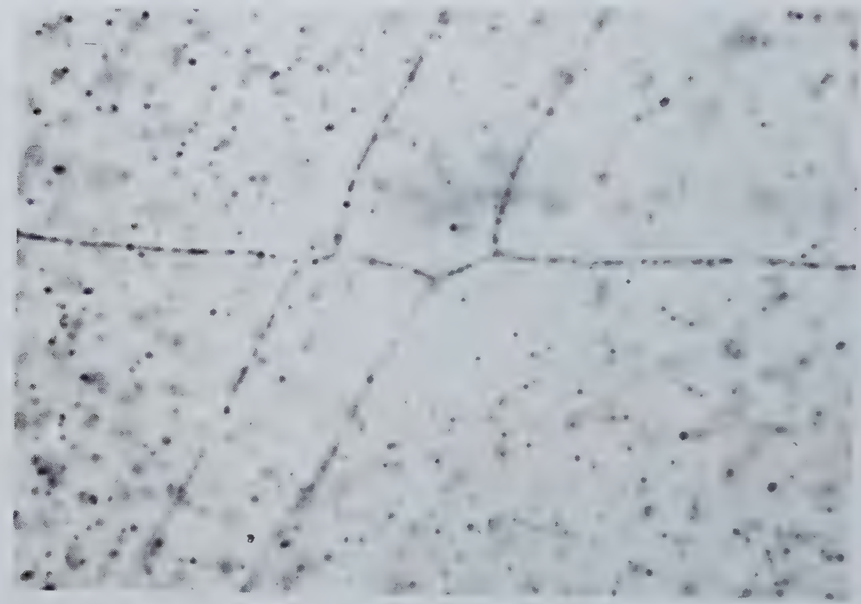

Interactions between dislocations with Burgers vectors at 120°. (×2100.)

Fig. 4

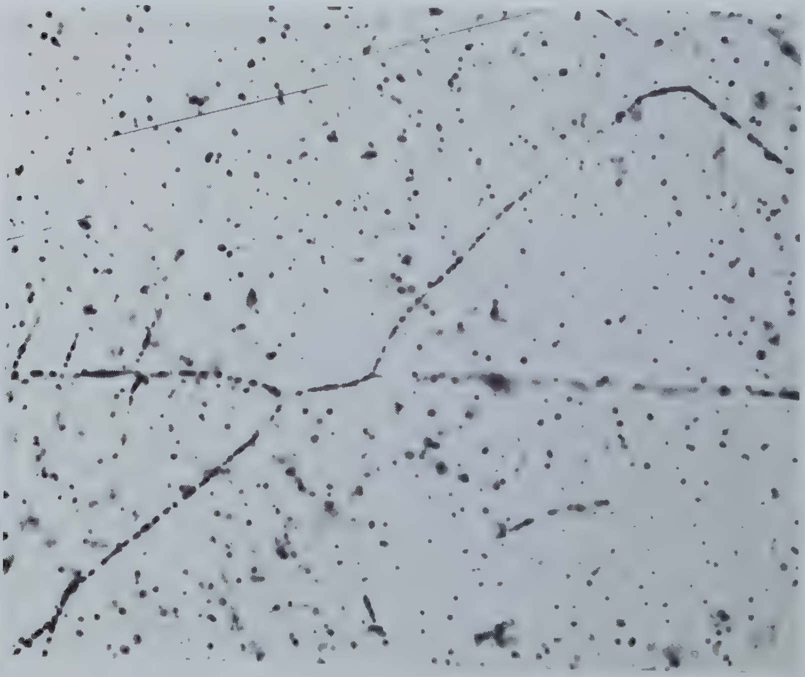

A group of interactions between dislocations with different Burgers vectors. (×1580.)

Fig. 1

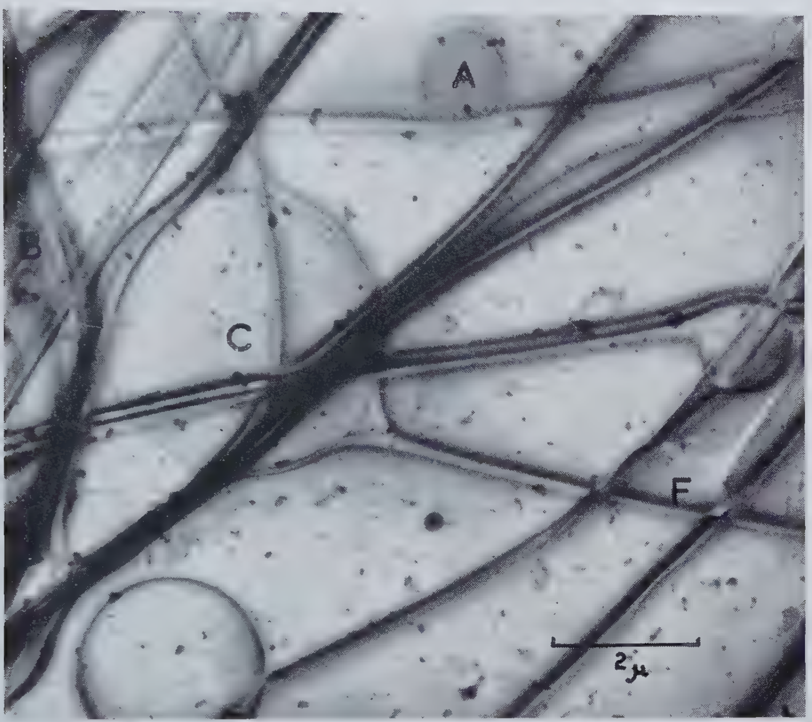

Bright field view showing vacancy loops and dissociated dislocations.

Fig. 2

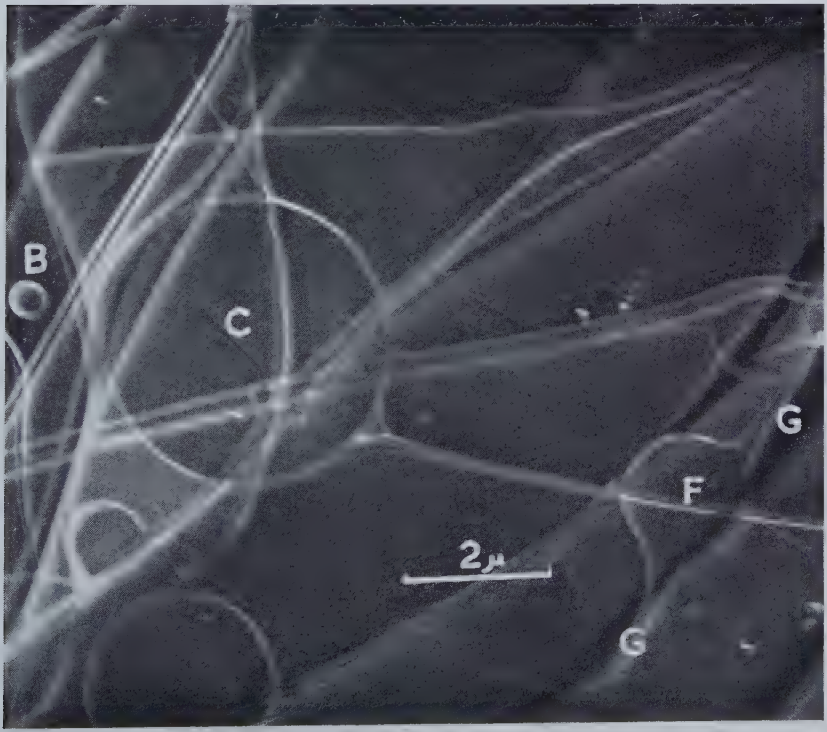

Dark field view of fig. 1 taken with $11\bar{2}0$ reflection.
Loop A has disappeared from contrast.

Fig. 3

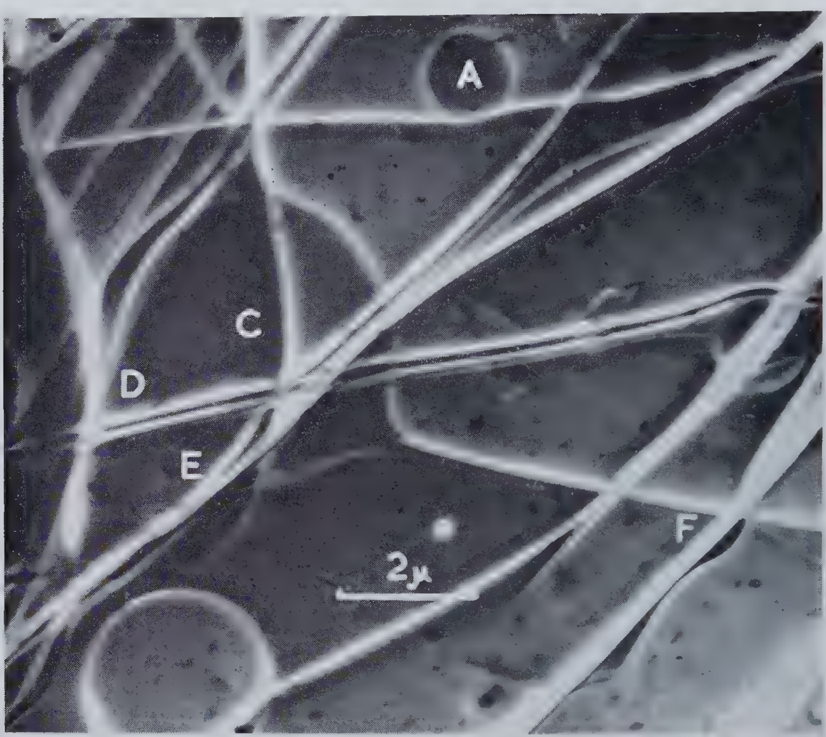

Dark field view of fig. 1 taken with another $11\bar{2}0$ reflection. Loops B and C and one side of loop F are out of contrast.

Fig. 5

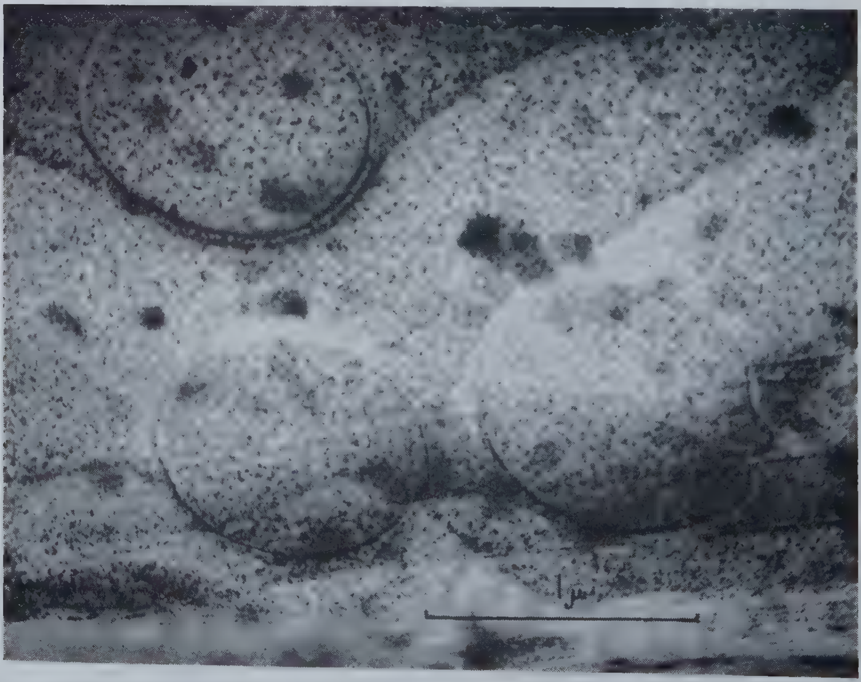

Interstitial loops in irradiated graphite with the specimen tilted about 30°.

Fig. 6

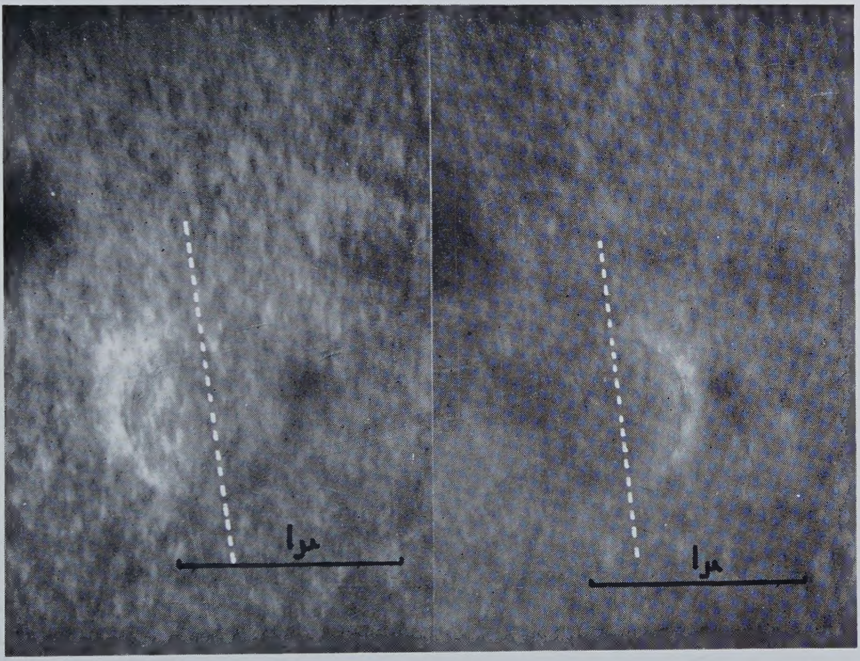

(*a*) (*b*)

(*a*) and (*b*). *Dark field* view of interstitial loop at slightly different reflecting conditions showing zero contrast along the diameter parallel to the reflecting plane (dotted line).

Fig. 1

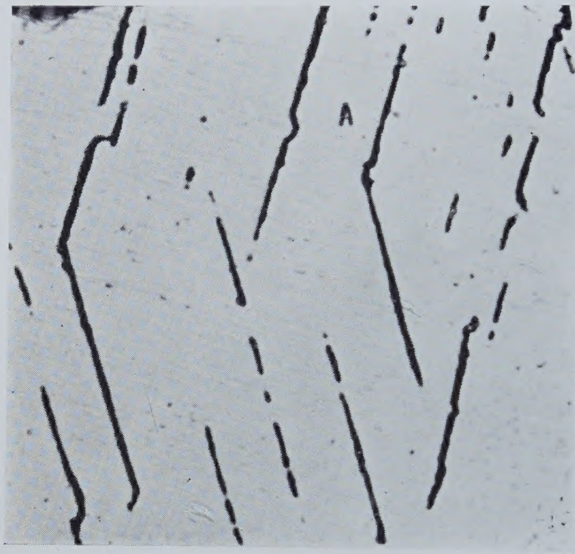

(*a*)

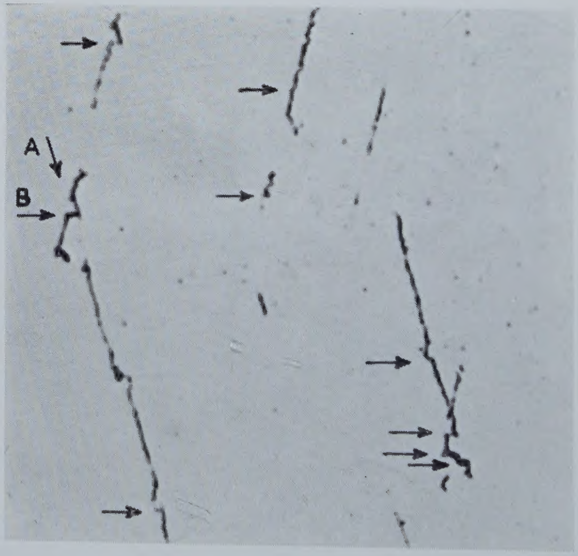

(*b*)

The occurrence of cross-slip in fatigued copper. (*a*) 3 microns removed by electropolishing. (*b*) A further 9 microns removed. (×340.)

Fig. 2

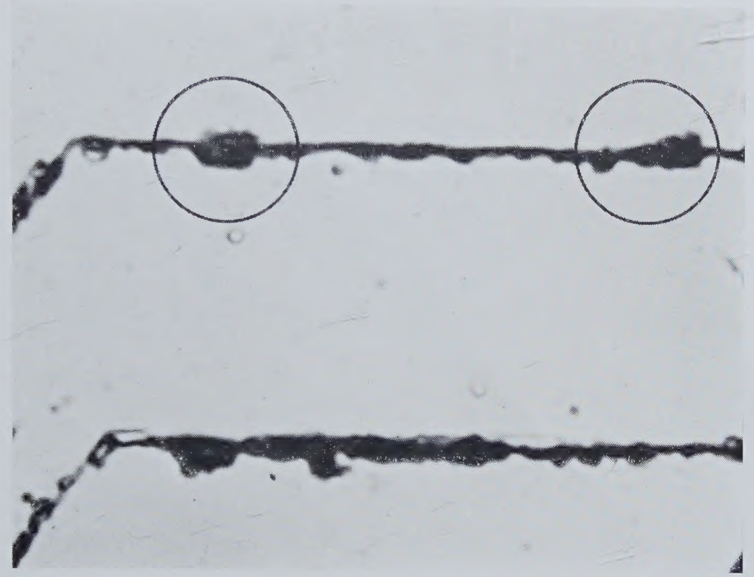

(*a*)

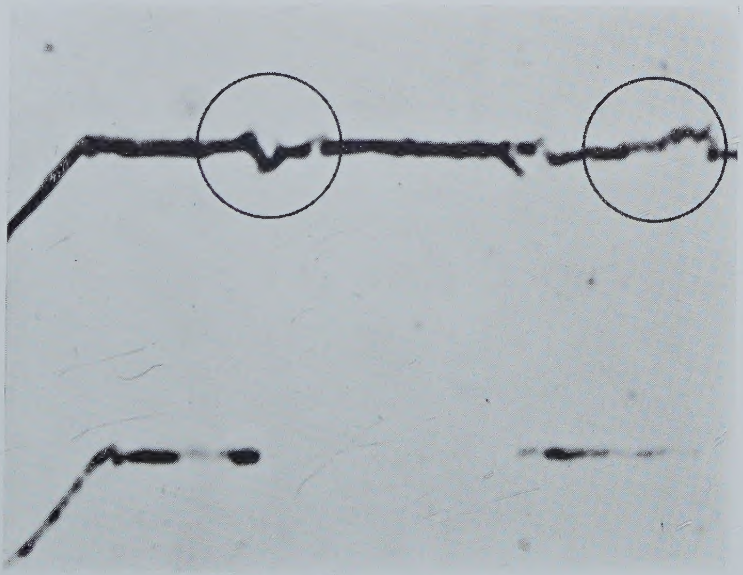

(*b*)

The correspondence between extrusions and cross-slip. (*a*) As fatigued. (*b*) 6 microns removed by electropolishing. (×1350.)